FIELD INVESTIGATION OF SUBGRADE NON-UNIFORMITY EFFECTS ON CONCRETE PAVEMENT

BY

HEMANT LAXMAN CHAVAN

THESIS

Submitted in partial fulfillment of the requirements
for the degree of Master of Science in Civil Engineering
in the Graduate College of the
University of Illinois at Urbana-Champaign, 2012

Urbana, Illinois

Adviser:

Professor Jeffery R. Roesler

ABSTRACT

The traditional method of designing concrete pavements is through the assignment of a single modulus of subgrade reaction (k-value) to the soil for the section under consideration. It is well known that soil under pavement is not a homogenous, elastic, and isotropic half-space but varies spatially due to variations in the soil geological properties, environmental factors, and construction methods. Few studies have attempted to characterize this heterogeneous behavior as non-uniform subgrade support, theoretically analyze its effect on slab responses, or its effect on concrete pavement performance.

This research has collected geotechnical data from two roadway sections in Michigan, MI I-94 and MI I-96, to characterize the effects of the foundation layer spatial non-uniformity on tensile stress changes in a concrete slab. For both the MI I-94 and MI I-96 roadway section, k-values were correlated from field Dynamic Cone Penetrometer (DCP) tests that were either deterministically or randomly assigned to a predefined area size. These spatial plots were discretized into various uniform area sizes to compare tensile stresses from a non-uniform support under a concrete pavement to a uniform support condition. The individual area sizes varied from 0.7x0.7 m^2 and 1.16x1.16 m^2. A 2-D finite element program was used to analyze the critical slab tensile stresses for multiple uniform and non-uniform conditions subjected to three axle configurations, loading paths, and temperature differentials.

The results for MI I-94 stress analysis showed that the deterministic assignment of k-value from the field did not result in any significant increase in critical tensile stresses compared to the uniform support assumptions even for varying individual area sizes. However, when the k-value of the foundation layer was randomly assigned to these individual areas, using a normal distribution, for a soft subgrade (k-value = 63 psi/in and standard deviation = 25.6 psi/in), the overall peak tensile stresses along the edge loading path increased by 31% and the average peak tensile stress increased by 37%. The greatest increase in tensile stresses relative to the uniform support condition occurred for individual support areas of 1.16x1.16 m^2. When the k-value was randomly assigned with a beta (B) distribution for a lower limit of 20 psi/in, there was no increase in the overall peak tensile stress in the slab relative to the uniform support condition. Although the section with stiffer soil (mean k-value = 397 psi/in), MI I-96, had a large range in measured k-values, it only increased the overall peak tensile stresses in the slab relative to

uniform support conditions by 11% when randomly assigned to 81 k-value areas and increased the tensile stress by 6% when the k-values were deterministically assigned.

The field data and theoretical analysis presented in this research has shown that non-uniform support conditions can lead to significantly higher slab stresses under certain geometric, loading, and slab support conditions. Non-uniform support along the edge of the slab especially very low support values near the location of maximum tensile stress substantially increased the slab tensile stresses. These tensile stresses are further increased under daytime temperature curling. Variability in the foundation stiffness had a larger impact on slabs supported by softer soils relative to stiff soils. For the inputs analyzed in this study, the size of the individual area of uniform support defined around 1 m^2 produced the greatest increase in tensile stress in the slab. Detection and treatment of areas of weak and variable support along the anticipated free edges of the slab are important to improving the performance of concrete pavements.

.

I would like to dedicate this thesis to the legacy of my grandfather. It's due to his vision and enterprising nature that has provided me the opportunity to fulfill my ambitions. I would like to thank my parents and siblings for their love and support throughout my time away from home.

ACKNOWLEDGEMENT

I would like to acknowledge my research adviser, Professor Jeffery R. Roesler, for giving me the opportunity to work with him, for providing support during my stay at the University of Illinois at Urbana-Champaign, and for his guidance throughout this project. His motivation and encouragement during the process of this thesis is of particular significance to me.

Special thanks to Professor David White and Dr. Pavana Vennapusa at Iowa State University for providing field data and valuable inputs throughout the course of this project. This study was developed for the Federal Highway Administration as part of FHWA DTFH 61-06-H-00011: WO18. Additionally, I would like to thank Alex Brand for all his technical help with this project. Acknowledgement is given to Applied Research Associates for providing the license for ISLAB2000 Version 1.1.

Table of Contents

Chapter 1: Introduction

1.1 Background

The soil properties and behavior can have a significant impact on the design of concrete slabs on grade. For elastic responses, a real soil has been idealized with two models neither fully representing the soil response: Elastic Solid (ES) and Dense Liquid (DL). In general, the DL model has been shown to characterize the soil responses better for a concrete pavement especially at joints and edges, whereas ES model has been more suitable to predicting soil behavior under a flexible (1). These models are shown schematically in Figure 1.

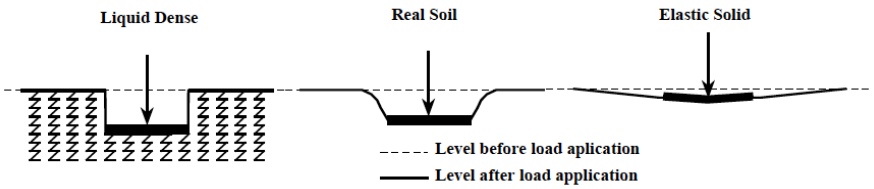

Figure 1: Soil behavior prediction models (1)

Westergaard (2) was one of the first researchers to consider the soil response into the theoretical analysis of rigid pavements. He introduced the term modulus of subgrade reaction, i.e., k-value, to describe the stiffness of the foundation layer support, as originally proposed by Winkler. The traditional method of designing concrete slabs is by assuming a uniform, single k-value for a particular section of the roadway.

The plate load testing (PLT) utilizes a rigid circular plate of 30 in. in diameter, and it is one technique to determine the modulus of subgrade reaction. Westergaard also suggested that the subgrade k–value could be backcalculated from deflections of the slab surface rather than from tests directly on the subgrade using the PLT (2). NCHRP 1-30 (3) lists many measurement and soil factors which affect the apparent k-value of a soil. The study also states that the soil k-value can also be empirically correlated to other soil strength tests such as the California Bearing Ratio (CBR) or R-value. These correlations

are not real accurate since, for example, CBR is a soil strength parameter whereas k-value represents stiffness of the soil dependent on many testing variables.

In order to better understand the subgrade effects on concrete slab responses, it is necessary to determine the soil stiffness variability. Variability in the geotechnical characteristics of the soil is dependent on the inherent geologic nature of the soil as well as environmental factors (4). Errors in the field data measurements also add to the variability of the assumed soil behavior (5)(6)(7)(8). Variability or non-uniformity in the soil stiffness is due to both internal and external factors which occur spatially (9). For example, the moisture content of the soil in the field is an important intrinsic factor affecting the strength and stiffness of the soil (10). Moisture content changes can occur due to saturated/unsaturated flow and from external effects such as wind, precipitation, or evaporation. Field investigations have showed that inadequate compaction (extrinsic factor) coupled with poor pavement drainage can lead to the accumulation of water at the pavement edges, which can result in softer or weaker pavement edges (11). These spatial moisture changes lead to a non-uniform subgrade support condition, i.e., areas of variable stiffness. A lower k-value can lead to increased deflection and tensile stresses in the slab thereby decreasing the pavement's fatigue life (9). The soft edges can be particularly detrimental as it can lead to corner breaks and/or premature cracking of the concrete slab. A few past studies have looked in to characterizing the effects of non-uniform support conditions or voids on slab responses (12)(13)(14) .

One of traditional mechanisms that effect stresses in pavement is the curling of the concrete slab due to differential temperature profiles, i.e., daytime or nighttime curling (15). Curling of the slab causes loss of support at different locations beneath the slab depending on the time of the day. The combined effect of an upward curled slab along with loss support can potentially lead to high deflection and pumping at the joint along the edges and the corners (16). Curled slabs placed on a subgrade with non-uniform stiffness areas will affect the pavement response.

Two-dimensional (2D) finite element (FE) programs have been used for many years to calculate slab responses for a slab on grade pavement system under a variety of input parameters (17)(18)(19)(20) and more recently, 3-D FE programs have been used to

predict slab responses. The advantage of using 3-D FE to determine the main inputs affecting slab responses under non-uniform subgrade conditions is having more complex soil response models and interaction of non-uniformity with small cracks at the top or bottom of the slab (21). This study used a simpler, 2-D finite element analysis program, ISLAB2000 Version 1.1 (22), to characterize the tensile stress changes in the concrete slab under different non-uniform subgrade support conditions taken from field measurements and under varying load configurations, loading paths and positions, and temperature differentials.

1.2 Problem Statement

Current concrete pavement design approaches use a single (uniform) k-value which is assigned to the roadway section as long as the soil properties are similar. The premature initiation of cracks in concrete pavement have been related to areas of weak support and therefore it is necessary to characterize the effects of local soil stiffness changes on slab tensile stress concentrations and slab cracking. This subsequent potential for premature failure should lead to concerns of better monitoring and controlling of the unbound layer construction process, such as through the implementation of intelligent compaction technology.

Laboratory shear tests conducted on soil specimens by simulating imperfect or more practical boundary conditions have shown that stress non-uniformities are produced at the center of the undrained soil specimen on account of increased pore water pressure (23). The pore water pressure build up can be from precipitation, depth of water table changes, evaporation, and freeze thaw cycles. Saturation of the subgrade may cause the pore water pressure to overcome the load carrying capacity of the soil, causing damage or erosion (24). Since the soil acts as a continuum body in the field, these changes in the material properties are continuously transitioning over a spatial area (25). The stress fields induced in the soil and concrete slab are then more non-uniform and must be considered either in the design or construction phase to increase pavement performance or reliability.

To combat foundation stiffness non-uniformity, chemical or mechanical stabilization techniques may be used but are not always cost-effective and their

application is heavily dependent on the geographic location and geological composition of the soil. Compaction of the subgrade is a traditional method of densifying and providing more uniform soil stiffness over a project through static, impact, gyratory, rolling, vibrating, and kneading mechanisms. Intelligent Compaction (IC) rollers spatially monitor these soil compaction mechanisms using global positioning systems in real time through the use of several types of drum sensors that indicate the relative soil stiffness (26). The IC machines return stiffness measurements of the soil every 0.1 to 0.5 m and this information can be used to actively adjust the roller drum operating characteristics to improve compaction (27). Previous IC studies have shown that spatial variation in stiffness, strength and permeability of the foundation layers exist (9)(28). The spatial resolution of the IC rollers measurement value has been reported to vary from 0.2 to 1.0 m (0.7 to 3.3 ft) (29). A non-uniform foundation layer support may increase localized deflections and can cause stress concentrations in the concrete pavement, which can lead to premature distresses and failures (30). A more fundamental understanding of how foundation layer non-uniformities affect concrete pavement responses will assist in better applying IC machines for the construction of support layers in concrete pavement.

1.3 Research Objective

The scope of this thesis is to analyze the effect of measured foundation data variability on concrete slab responses gathered from two field projects. Field data is used to identify the existence of the non-uniform stiffness areas and a 2-D finite element analysis program was used to determine the changes in concrete pavement tensile stresses due to the effects of subgrade stiffness non-uniformity. Both deterministic and statistical distributions of the soil stiffness variation were used based on the measured field data from recent interstate construction projects.

One main research objective of the study was to determine if subgrade non-uniformities significantly affect pavement responses over the traditional uniform foundation property assumption based on recent field data collection. For this study, the change in the slab's critical stresses were analyzed considering the following factors: size of the non-uniform area, relative stiffness change between adjacent non-uniform areas, varying loading configuration and loading path, and longitudinal position on the slab subjected to different linear temperature curling conditions. Knowledge of the critical

design variables and ranges of soil stiffness and non-uniform area size will lead to improved construction specifications for foundation layers by efficient use of IC technology and subsequently higher reliability in concrete pavement performance prediction. This study has only focused on non-uniform support on the potential for slab cracking due to tensile stress development and does not account for other concrete slab failure mechanisms such as support erosion.

Chapter 2: Non-uniform Foundation Support Literature Review

Research into the effects of subgrade non-uniformity on the pavement performance has not been extensive. With the introduction of IC technology for pavement construction, there is a greater need to understand how the non-uniformity of foundation layers affects the pavement responses. One of the first studies carried out was by Levey (4) who developed a methodology to assess pavement layer material variability on various pavement responses, i.e., not necessarily rigid or flexible pavements. Levey (4) developed a statistical process to randomly assign the elastic modulus of the top layer (mean of 105 psi and coefficient of variation (COV) =20%) and of layer 2 (mean of 104 psi and COV=40%) in the finite element program based on a normal distribution of the expected values of these properties. Levey found a COV of 16% in the maximum tensile stresses and a COV of 25% for surface deflection for the mean elastic moduli and COV above for layers 1 and 2.

Barenberg et al. (25) applied the same statistical process developed by Levey (4) to spatially assign paving material properties such as soil stiffness and concrete elastic modulus values to specific user-defined areas with the aim of analyzing pavement systems having non-uniform material properties. A finite element model for analysis of two-layered slabs on a Winkler type of support was selected to analyze stress, strains and deflections. These critical slab responses were completed for several load locations (edge and corner). The critical strain results showed that location of the critical strain did not always occur under the loading position, which validates the presence of corner breaks due to edge loading. Barenberg et al. (25) reported an overall low sensitivity of the pavement responses to the varying subgrade stiffness (range of 11-197 psi/in.) with a constant slab elastic modulus. For example, for a COV of 30% in the k-value assignment, an increase of approximately 11% and 2% in tensile strain was observed from the uniform support (single k-value) to the worst case k-value distribution for edge and corner loadings, respectively. The best and worst support conditions were created by placing the strongest and weakest $4ft^2$ area of k-values around the critical load location.

The responses of varying the slab elastic modulus under a uniform k-value support condition were more critical. For 30% COV in data set of slab elastic modulus assignment, an increase of approximately 25% and 38% in strain was observed from the best condition to the worst for edge and corner loading cases, respectively. Ironically, Barenberg et al. (25) noted that application of moving load over a non-uniform pavement system along with increasing the size of non-uniform area would develop a better understanding of critical responses, which were two recommendations addressed in this research.

As part of a larger study, White et al. (30) assessed the effect of a non-uniform subgrade support on critical pavement responses for long term pavement performance. A spatial grid pattern of the subgrade engineering properties was developed based on in-situ field tests from 12 sites. The influence of spatial variability of the subgrade on the pavement was analyzed through ISLAB2000. The modulus of subgrade reaction was estimated using the following equation from Bowles (31) where ES is the soil stiffness (psi) and B is the plate diameter, which is assumed to be 30 in.

$$k_s = \frac{E_S}{B(1-\mu^2)} \qquad 2.1$$

The Poisson's ratio, μ, was assumed in this estimation to be 0.35, which was representative of the soil layer. The results of the analysis showed that the maximum principal stresses and deflections were reduced in the pavement under a uniform subgrade thereby increasing the slab's fatigue life. Specifically, one of the test sections had an 8.0% and 36.8% increase in COV for stresses and deflections, respectively, when changing from a uniform support condition to a non-uniform support. This limited study demonstrated the possibility that subgrade non-uniformity can lead to a reduced fatigue life. Further research effort was clearly needed to quantify the required area size of the non-uniformity that produce the critical responses, understand the effects of different loading positions and paths on tensile stresses produced (only the wheel paths were analyzed), and inclusion of various temperature curling states, i.e., allowance for boundary condition change at certain slab positions.

Based on the results of White et al. (30), which reported the criticality of the spatial non-uniform foundation stiffness, a sensitivity analysis was recently carried out by Brand et al. (32) This new study was based on developing idealized subgrade support cases, as shown in Figure 2, by arbitrarily assigning deterministically soft and stiff k-values to user-defined areas of a uniform support. A single slab geometry was considered, measuring 12 x 15 ft^2, with soft subgrade areas defined as 50 psi/in and stiff areas of 500 psi/in. The axle types that were used in this analysis included single, tandem, and steer-drive axles and the slab was subject to three linear temperature differentials of +20°F, -20°F, and 0°F. The axle types traversed longitudinally in 10 inch increments to simulate a moving axle load along the different subgrade support cases for each temperature curling condition.

The primary finding of the Brand et al. (32) stress analysis showed that tandem axles with soft edges (case 3 in Figure 2) during daytime curling was the critical combination of input variables. The soft edge cases resulted in 34% and 63% increase in tensile stresses (no temperature differential and -20°F, respectively) relative to the uniform soft subgrade support condition. The uniformly stiff support (case 2) performed similarly to stiff edges (case 4) concluding that type of edge support has an important bearing on slab response. The tensile stress magnitude of the random non-uniform subgrade support cases was primarily linked to the location of the soft areas relative to the area of expected maximum tensile stress of the slab. The idealized analysis work by Brand et al. (32) demonstrated that extreme spatial differences in subgrade stiffness can cause potential cracking damage in the concrete slab.

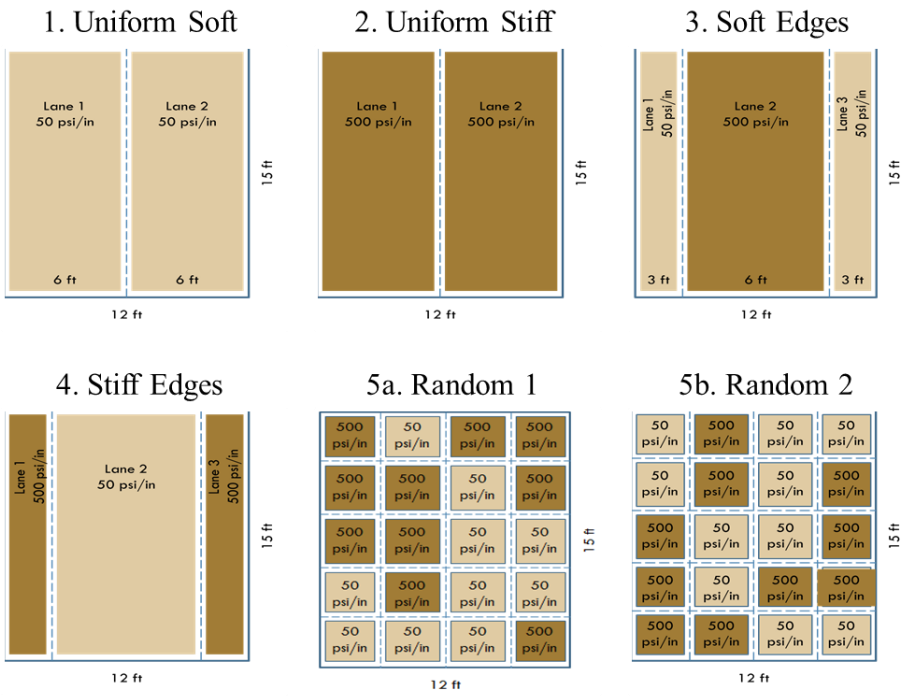

Figure 2: Subgrade non-uniformity cases used for finite element sensitivity analysis (32)

These past analyses of concrete slab responses under non-uniform pavement support have shown that slab fatigue life can be reduced due to an increase in slab tensile stresses. These past studies have been theoretical in nature, and with the recent availability of field data from White et al.(34), there is potential to identify if measured spatial non-uniform support will lead to significant changes in the calculated slab tensile stresses.

Chapter 3: Field Studies of Variation in Foundation Support

3.1 MI I-94: Field Data of Support Condition

3.1.1 Test Site Overview

Field measurements and data analysis conducted by the research team from Iowa State University formed the basis for the evaluation of the practical effects of subgrade non-uniformity. The non-uniformity of the subgrade was primarily quantified in terms of the spatial variation of modulus of subgrade reaction (k-value). The Michigan Department of Transportation (MDOT) was reconstructing a section of I-94 in St. Clair and Macomb Counties, Michigan, between mile posts 23.0 and 6.1, due to poor ride quality. Based on AASHTO pavement design guide (AASHTO 1993), the new pavement structure would consist of a 11-in. thick jointed Portland Cement Concrete (PCC) slab, 16 in. open graded drainage course (OGDC) placed over the subgrade with a geotextile separation layer to be placed at the interface of the subgrade and OGDC.

Although IC equipment was utilized for this MI I-94 construction project, it was not used as part of the spatial test bed field data collection to characterize the effect of non-uniform subgrade support on the stresses in the concrete pavement. In order to rapidly assess spatial variability, in-situ test data obtained from static PLT and DCP were correlated. The modulus of subgrade reaction (k-value) was obtained from PLTs carried out along the length of test bed 3a with measurements located at every 50 feet between stations 839+50 and 866+00. The PLTs were conducted on top of the newly constructed OGDC base layer to determine the static (composite) k-values. DCP tests at the same station locations were run in accordance with ASTM D6951-03 to determine the dynamic penetration index (DPI). From the DPI profiles, the California Bearing Ratio (CBR) was calculated from the following equation from ASTM D6951-03 (33)

$$CBR = \frac{292}{DPI^{1.12}} \qquad 2.1$$

Intensive in-situ tests over a 7x7 m^2 spatial grid area were also carried out on test bed 1b (TB 1b), as shown in Figure 3, in order to analyze spatial stiffness of the foundation layer over a small area.

Figure 4a shows the test bed 3a up on which PLT was carried out whereas Figure 4b shows the coordinates of the test bed 3a having 121 individual field testing locations. These 121 test locations and spacing of each test for TB 1b on the MI I-94 section are shown in Figure 5. The DCP tests were conducted through the OGDC base layer and into the subgrade layer.

Figure 3: DCP test being carried out on an OGDC layer on test bed 1b (34)

(a)

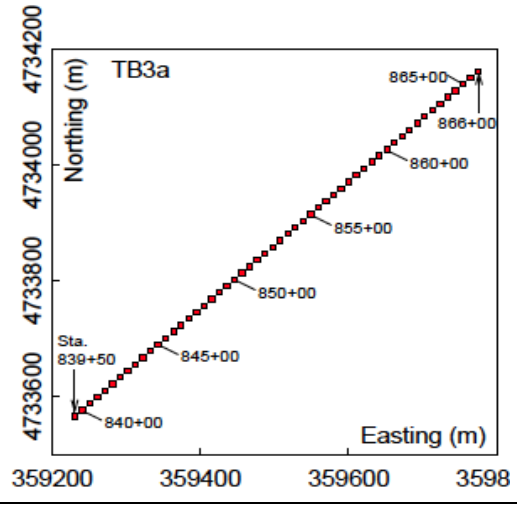

(b)

Figure 4: (a) Test bed 3a (TB3a) site location with OGDC base layer and (b) coordinates of each PLT and DCP test location (34)

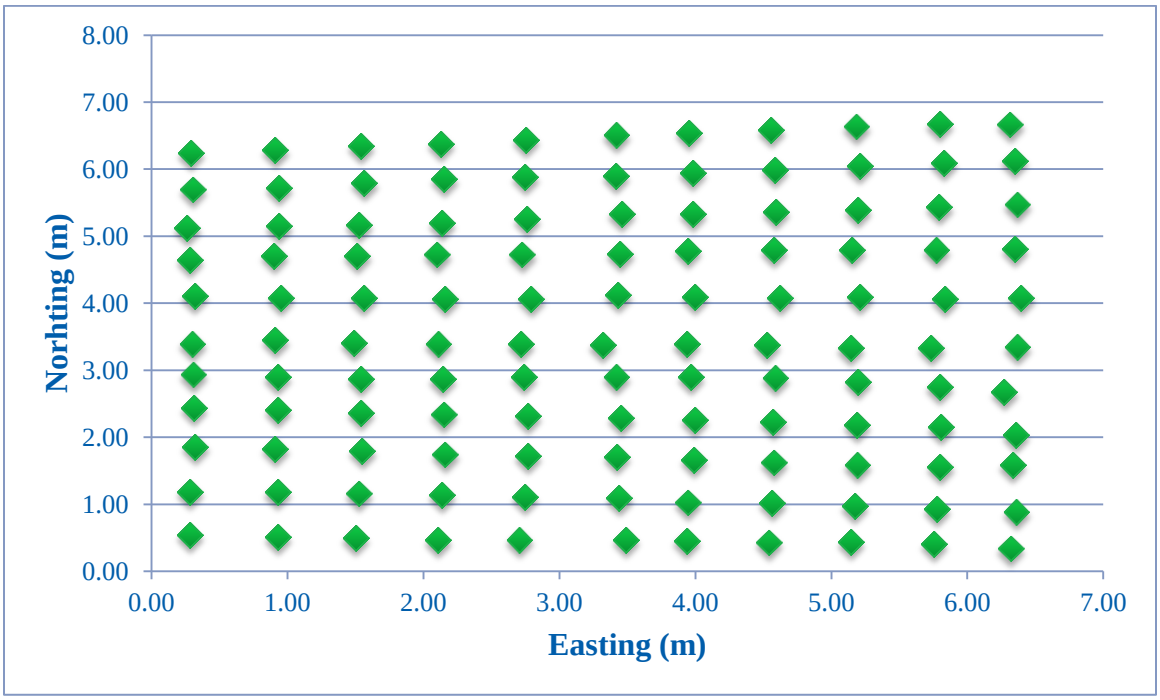

Figure 5: MI I-94 DCP test locations on TB 1b.

All PLTs in the field were performed with a 12 in. diameter plate. A 30 in. diameter plate is prescribed by AASHTO (1993) to carry out PLT and determine the

foundation k-value. The measured k_{comp}, which is the modulus of subgrade reaction for both the soil and OGDC base layer, were corrected for the discrepancy in the plate size using a theoretical relationship proposed by Terzaghi (35) for granular materials.

$$k = k_1 \left[\frac{B+B_1}{2B}\right]^2 \qquad 2.2$$

where k= modulus of subgrade reaction using 30 in. diameter plate, k1 = modulus of subgrade reaction using a 12 in. diameter plate, B_1= 300 mm and B = 720 mm.

3.1.2 Development of Support Stiffness Correlation Equation

The next step of the analysis involved correlating the simple field test (DCP) to the required input value for finite element analysis (k-value). Only the DCP penetration results in the subgrade layer were utilized in the DPI to CBR correlation from equation 2.1. Correlation equations from literature were first investigated between k-value and CBR. The following equation was developed by the Federal Aviation Agency (FAA) based on their Advisory Circular (AC) 150/5320-6E (36):

$$k = \left[\frac{1500\,CBR}{26}\right]^{0.7788} \qquad 2.3$$

The FAA AC states the values obtained from this equation are approximate in nature, i.e., values are not exact or unique. Another correlation is based on charts developed by Hall et al. (3) for NCHRP 1-30. These relationships are also empirical in nature with a range of k-value that varies with the soil type. The upper, middle, and lower curves in Figure 6 show the range of k-values for a particular CBR value.

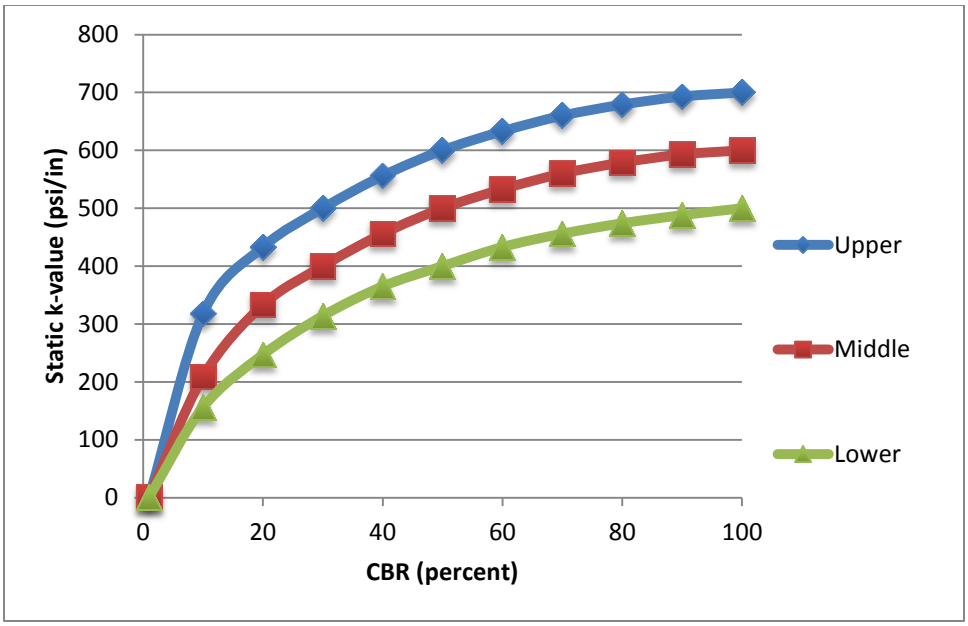

Figure 6: Approximate relationship of k-value (3)

The third correlation equation is from the AASHTO design guide (37) as shown in equations 2.4 and 2.5 where M_r is modulus of soil.

$$M_r = CBR \times 1500 \quad (2.4)$$

$$k = \frac{M_r}{19.4} \quad (2.5)$$

Two other theoretical linear relationships based on empirical data from Lysmer et al. (38) and Department of the Army and the Air Force (39) are:

$$k = 6.5 \times CBR \quad (2.6)$$

$$k = 20 \times CBR \quad (2.7)$$

Since the MI I-94 TB 3a had DCP and k-value measurements, a correlation equation could be developed, which could then be used to calculate the k-values from the 7x7 m^2 TB 1b. The existing field data from the MI I-94 site was used to develop a DCP-CBR to k-value correlation equation, which would give more realistic values of subgrade stiffness of the site under investigation. CBR values obtained from DCP tests and k-value obtained from PLT at TB 3a are listed in Table 1.

Table 1: CBR and k-value field data for Test bed 3a

k-value (psi/in)	CBR Subgrade (%)
166	5.3
150	7.0
175	6.9
81	6.2
100	5.7
145	6.2
91	4.0
59	7.9
173	7.3
104	8.4

The FAA equation 2.3 was re-calibrated based on the field data from Table 1 to generate the following equation:

$$k = 23.532 \times CBR^{0.7787} \qquad 2.8$$

The 121 field-correlated CBR to k-value from equation 2.8 is listed in the appendix. The use of this correlation equation is an approximation of the subgrade k-values given the results of the DCP-CBR. As conducting 121 PLTs on an intensive plot such as TB 1b was not practical, the use of a correlation equation was the best alternative based on the available field data.

3.1.3 Discretization of Spatial Plot

In order to determine if the actual field-measured foundation variability produces changes in the critical slab tensile stresses, TB 1b data was used to theoretically analyze a certain slab geometry, load configuration and load path, and temperature condition. Based on the above soil CBR to composite k-value correlation analysis, discretized spatial plots for the foundation layer for Test bed 1b were created for 2-D finite element analysis. As shown in Figure 7 the test grid of 121 data points (called Case 121) was over a 7x7 m^2 square plot and is based on assigning the field data locations in Figure 5 for the subsequent 2-D finite element analysis. The spacing of each uniform foundation area was approximately 0.7 x 0.7 m^2 with the corner areas approximately 0.35 x 0.35 m^2.

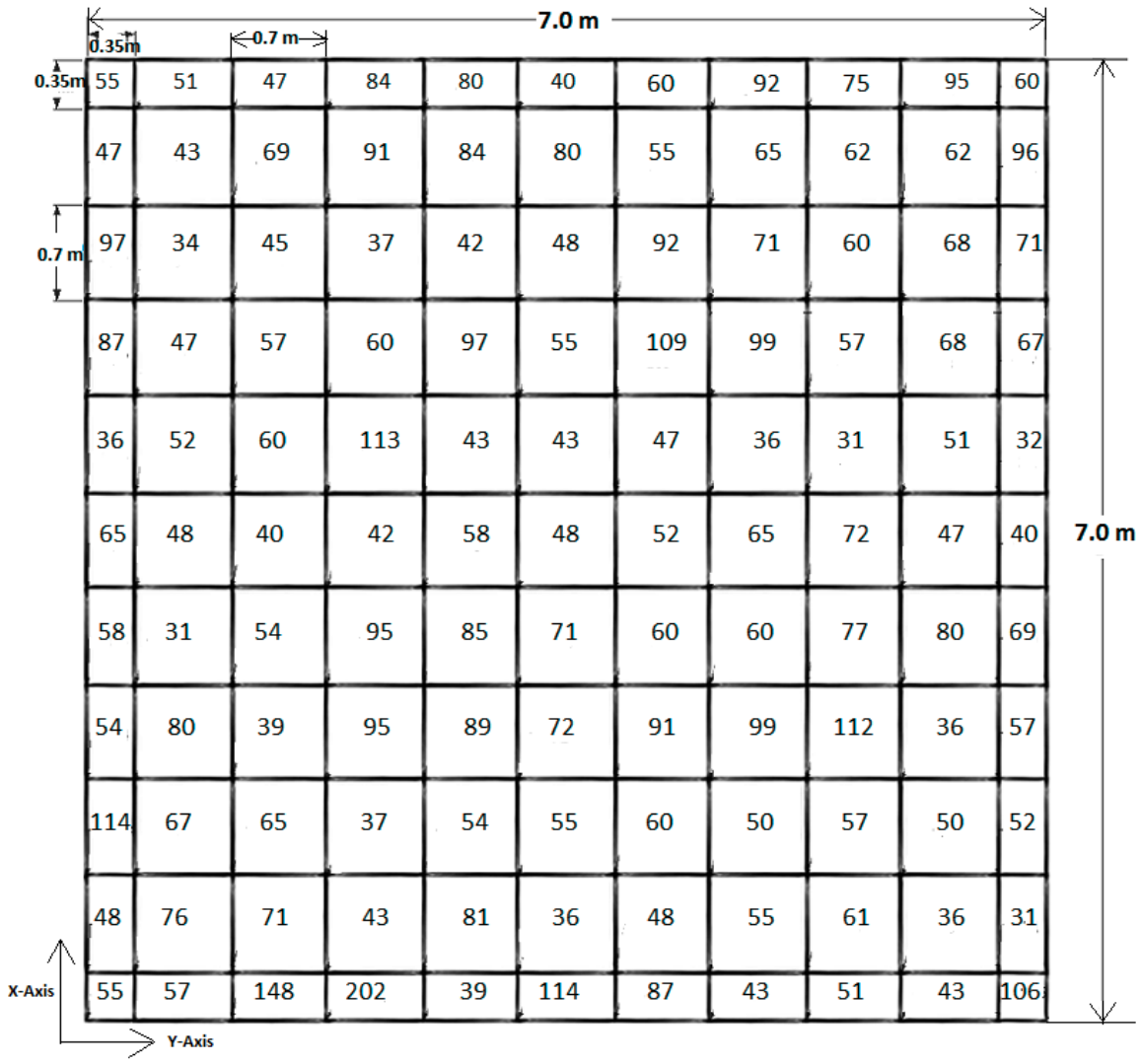

Figure 7: 121 correlated k-value (psi/in) areas (Case 121)

The range of the k-values for Case 121 was 32-202 psi/in with a mean of 63 psi/in and a standard deviation of 25.6 psi/in. This case represents practical field conditions and is quite different than the arbitrary deterministic distributions assumed by Brand et al. (32) of 50 and 500 psi/in. However, the range between the minimum and maximum value of k-value for this 7x7 m^2 was still a factor of 6 versus 10 for Brand et al. (32). In the study by Barenberg et al. (25), the range of the k-values assumed was from 11 to 197 psi/in having a factor of approximately 20 with a mean of 90 psi/in and standard deviation of 30.1 psi/in. Figure 8 represents the uniform case with a single k-value (called case 1) which is derived by averaging all 121 k-values from case 121.

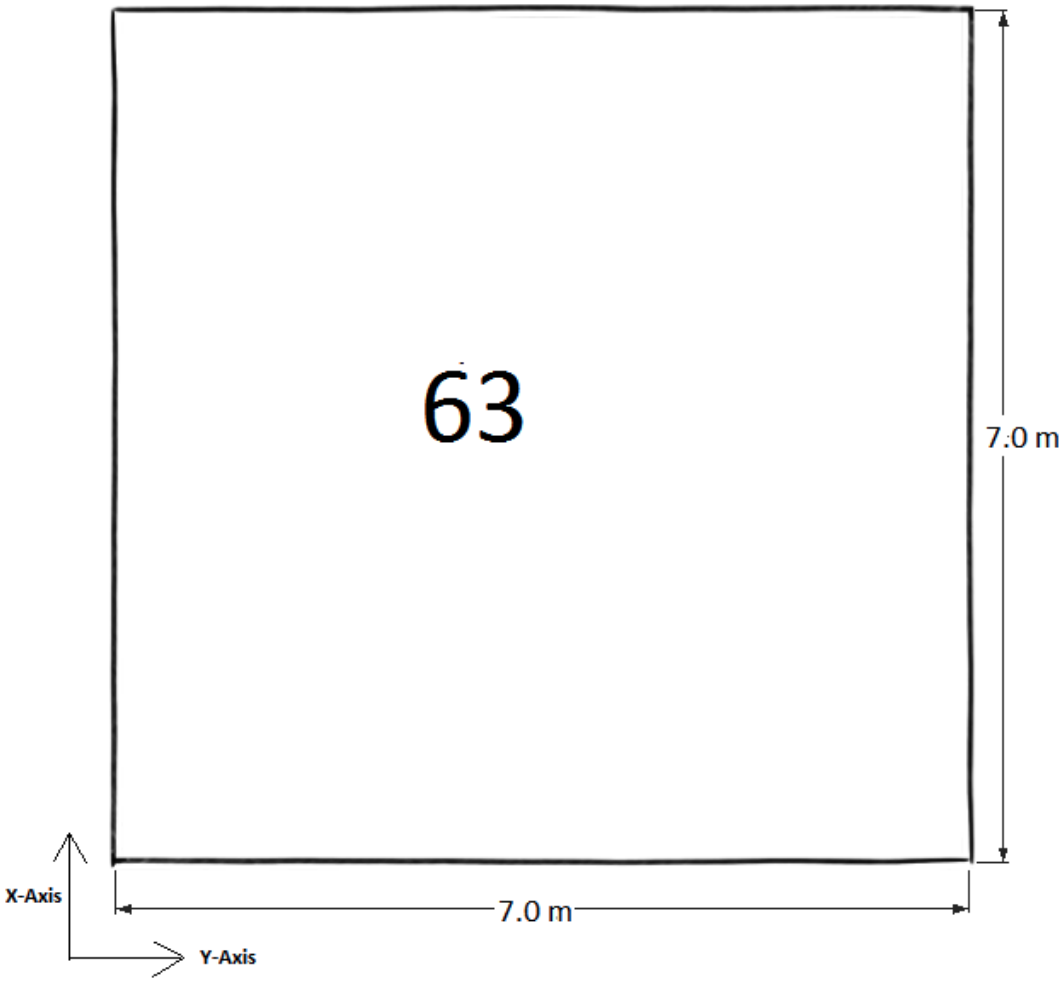

Figure 8: Case 1 with the mean k-value (psi/in) for the 121 data points collected.

An additional non-uniform support case was analyzed for MI I-94 to investigate the size of the non-uniform areas and its effect on the tensile stress change relative to the uniform (1 k-value) and 121 k-value cases. As shown in Figure 9, this case used a weighted average to produce k-value areas of 1.16 x 1.16 m^2 for a total of 36 k-values for the 7x7 m^2 area. Due to the weighted average approach to create the 36 k-value areas, the range of k-values was only 39 to 116 psi/in or a factor 3 difference. Although the mean remained at 63 psi/in, the standard deviation reduced to 14.1 psi/in compared to 25.6 psi/in for case 121, and inherently this averaging technique reduced the variation of stiffness support.

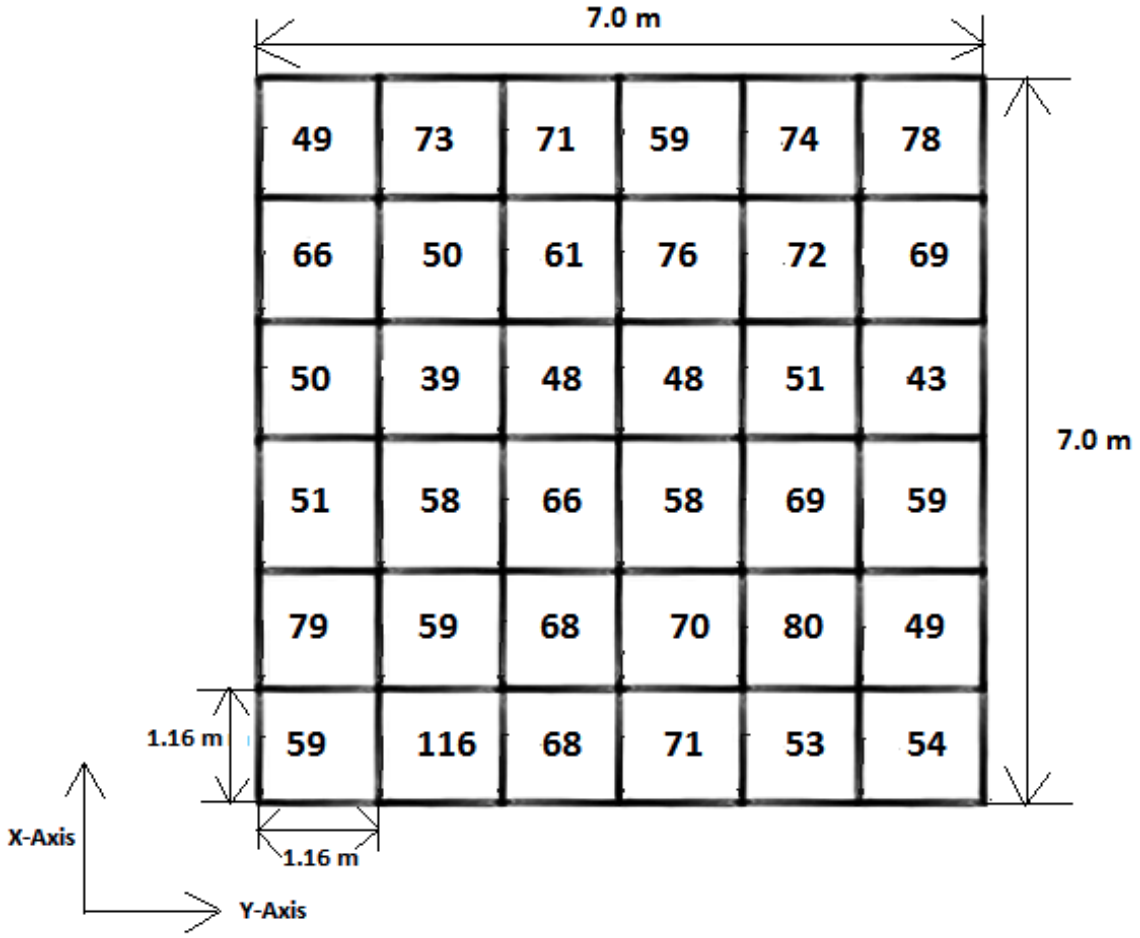

Figure 9: 36 discretized k-value areas (Case 36) of 1.16x1.16m^2 area each

3.1.4 Analyses Inputs and Factor Levels

Two dimensional finite element analysis with ISLAB2000 (22) was employed for calculating the critical tensile stresses in the concrete slab for the variety of inputs and non-uniform support conditions. The x-y location and magnitude of tensile stresses developed at the top or bottom of the concrete slab was recorded for each case and axle position. Table 2 lists the pavement input parameters used in the analysis:

Table 2: Input Parameters for ISLAB 2000 Analysis

Slab Size	23 ft. x 23 ft. (7m x 7m)
Slab Thickness	8 in.
Elastic Modulus	4.0x106 psi
Poisson Ratio	0.15
Coefficient of Thermal Expansion	5.5x10-6/°F
Unit Weight	0.087 psi/in
Tire Pressure	90psi
Aspect Ratio (b/a)	1
Element Size	2x2 in^2
Wheel Spacing	96 in.
Axle Spacing (Tandem Axle)	48 in
Axle Spacing (Steer-Drive Axle)	96 in.
Single Axle	18 kip
Tandem Axle	36 kip
Steer Drive	54 kip
Joint Load Transfer Efficiency (LTE)	70%

In contrast to the theoretical analyses conducted by Brand et al. (32) with a single slab, the field measured foundation support was done over a large area, approximately 7x7 m^2 and required a total of 4 slabs of 3.5x3.5 m^2 as shown in Figure 10. The analysis matrix consists of five different loading paths (lateral offsets) that traverse the slab longitudinally: right lane edge (RE), middle of the lane (M), left lane edge (LE), right lane wheel path (RW) and left lane wheel path (LW), as shown in Figure 10. Based on the study by Brand et al (32) for extreme changes in k-value (i.e., 50 to 500 psi/in), the axle loading along the longitudinal edge with soft support produced the most critical tensile stresses. Case RE would be the movement of the axles along the right free edge whereas Case LE is along left free edge. Case M represents movement of the axles at the exact center of the two lanes which would not be expected to produce the overall greatest tensile stress of all loading paths. Finally, Cases RW and LW represents wheel path loading (lateral offset of approximately 15.75 in.) in either the right or left lane, respectively.

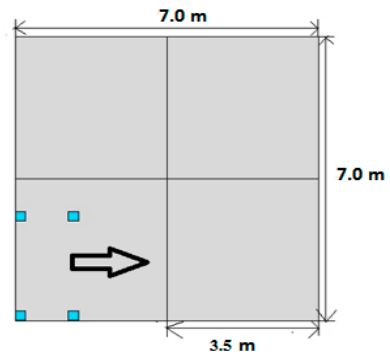

a) Case RE: Right Lane Edge

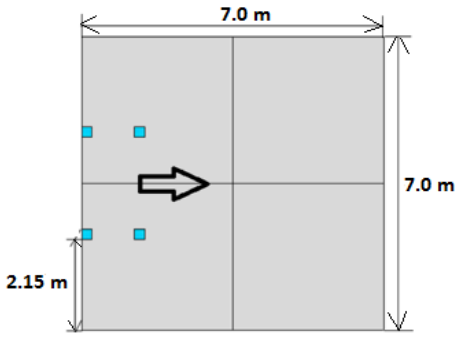

b) Case M: Middle of Lane

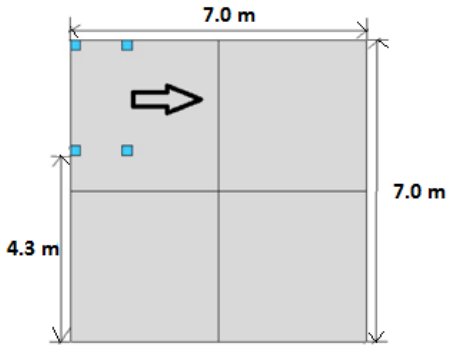

c) Case LE: Left Lane Edge

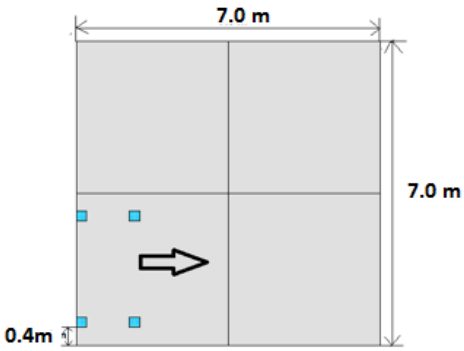

d) Case RW: Right Lane Wheelpath

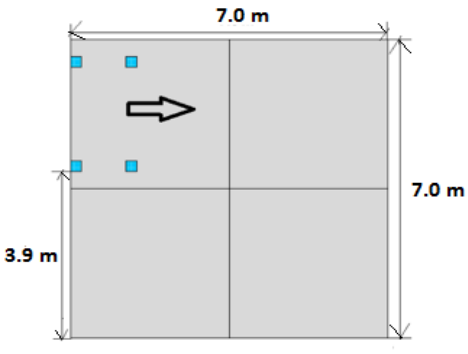

e) Case LW: Left Lane Wheelpath

Figure 10: Five load paths (lateral offsets) analyzed for all 3 axle configurations and subgrade uniformity on four slab assembly

The following three axle configurations were traversed in the longitudinal direction to determine the critical load location and tensile stress magnitude: single axle, tandem axle and steer-drive axle as shown in Figure 11. The loaded area was 10-in. by 10-in. After the first analysis point at the free edge of the transverse joint, the longitudinal position of the axles were traversed at 20-in. intervals for the single axle and until the front axles of the tandem and the steer-drive cross the opposite transverse free edge. The single axle requires a total of fourteen load positions, the tandem axle requires twelve, and the steer-drive axle requires seven load positions to traverse the 275 in. (7m) slab sections. The last single axle position analyzed was 260 in. while for the tandem axle it was 210 in. (210+48 inch = 258 in.).

Three temperature conditions were considered: no temperature differential, positive (+20°F) linear temperature differential and negative (-20°F) linear temperature differential. The joint load transfer efficiency was selected to be 70% at the joints in both the x and y coordinate directions. The other input variables listed in Table 2 such as slab thickness, concrete elastic modulus, slab size, and coefficient of thermal expansions were not changed even though they may have an effect on the magnitude of the stress sensitivity due to the changes in spatial foundation properties. Note that the standard axes used in ISLAB2000 and in this analysis are inverted from the normal Cartesian coordinate system.

The objective of assessing five different lateral offsets or loading paths, shown in Figure 10, was to identify the most critical loading location and critical tensile stress position in the slab for the measured foundation variability. The critical slab stresses are an interaction between the axle type, loading path and location on the slab, the relative location of the non-uniform soil support areas, size of the non-uniform area, and curling condition.

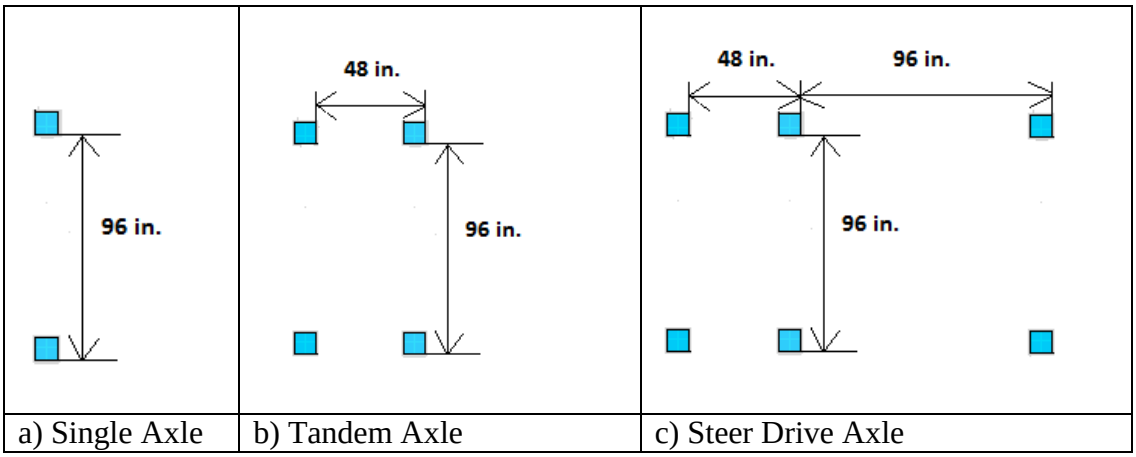

a) Single Axle	b) Tandem Axle	c) Steer Drive Axle

Figure 11: Single, Tandem, and Steer-Drive axle configurations used for stress analysis

3.1.5 ISLAB2000 Background

Numerical modeling to characterize the slab response to non-uniform support data has been carried out with the 2-D finite element analysis program, ISLAB2000. A mesh size of 2x2 in^2, shown in Figure 12, was chosen to ensure convergence of the outputted stresses and deflections. The pavement response recorded for this study was the maximum tensile stress at either the bottom or top of the slab at each load location. For certain cases, this critical tensile stress was a result of load plus temperature curling. With ISLAB2000, it is possible with daytime curling (+20°F) or nighttime curling (-20°F) that gaps beneath certain nodes exist prior to mechanical loading with the axle.

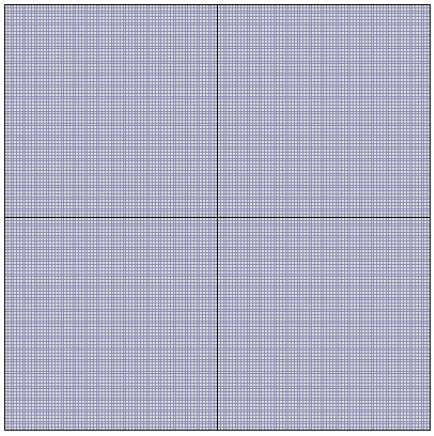

Figure 12: 2 x 2 in^2 mesh resolution for ISLAB 2000 analysis

3.1.6 Tensile Stress Analysis Nomenclature

Table 3 gives the nomenclature of the cases analyzed for the 121 discrete k-value locations, 36 k-values based on weighted average of 121 k-values, and one mean k-value based on the 121 measurement points. In all subsequent plots, the legend describes what cases are being plotted in terms of the loading path and number of discrete k-value areas under the 4 slab assembly.

Table 3: Case Nomenclature for Finite Element Analysis Runs

Case RE121	RE: Right Lane edge; 121: 121 k-values
Case RE1	RE: Right Lane edge; 1: 1 k-value
Case RE36	RE: Right Lane edge; 36: 36 k-values
Case M121	M: Middle of Slab; 121: 121 k-values
Case M1	M: Middle of Slab; 1: 1 k-value
Case M36	M: Middle of Slab; 36: 36 k-values
Case LE121	LE: Left Lane edge; 121: 121 k-values
Case LE1	LE: Left Lane edge; 1: 1 k-value
Case LE36	LE: Left Lane edge; 36: 36 k-values
Case RW121	RW: Right Lane wheelpath; 121: 121 k-values
Case RW1	RW: Right Lane wheelpath; 1: 1 k-value
Case RW36	RW: Right Lane wheelpath; 36: 36 k-values
Case LW121	LW: Left Lane wheelpath; 121: 121 k-values
Case LW1	LW: Left Lane wheelpath; 1: 1 k-value
Case LW36	LW: Left Lane wheelpath; 36: 36 k-values

The 121 k-value (Case 121) was considered first and subjected to the five loading paths and three axle configurations (single, tandem and steer-drive axle) at three temperature differentials (+20°F, 0°F, -20°F). In all plots, “S” represents single axle, “T” represents tandem axle and “D” represents steer-drive axle while 0F, 20F, and -20F are the respective temperature differential used in that particular case.

3.2 MI I-94: Deterministic Assignment of k-values from Field Measurements

3.2.1 Stress Analysis for Right Edge (RE) Loading Case

Figure 13 shows the results of the maximum tensile stresses recorded at the each longitudinal position for case RE121 (right edge with 121 areas with discrete k-values) for single, tandem, and steer-drive axle combinations and three temperature differentials. For case RE121, critical tensile stress regions were observed at similar locations in the two slabs but not identical since the distribution of measured spatial k-values were not symmetrical (see Figure 7). The difference in maximum tensile stresses is less than 10% despite the significant difference in local k-values at both mid-slab locations (from 43 to 202 psi/in in one location along the edge in Figure 14). The peak tensile stress recorded for all RE121 cases was for a single axle configuration during daytime curling conditions. The reason for this behavior was the discretized k-value areas were relatively small, i.e., 0.7x0.7 m^2. with low k-values near mid-slab, coupled with the single axle producing a highly concentrated tensile stress especially under positive temperature. The drop in tensile stresses in Figure 13 around 137.5 in. from the initial load position was the location of the transverse joint and thus there was a reduction in tensile stresses due to a high joint LTE of 70%. The red areas in Figure 14 show areas with non-uniform adjacent stiffness area and the orange area represents the location of the peak tensile stress for case RE121.

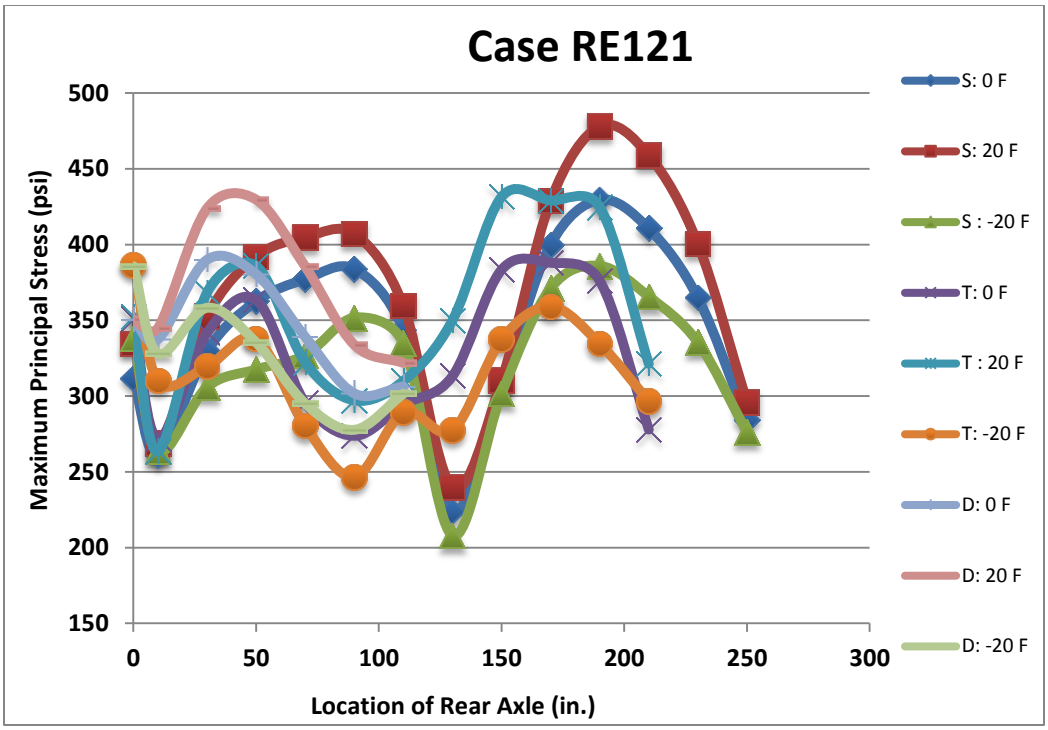

Figure 13: Maximum principal (tensile) stress at each axle position for Case RE121

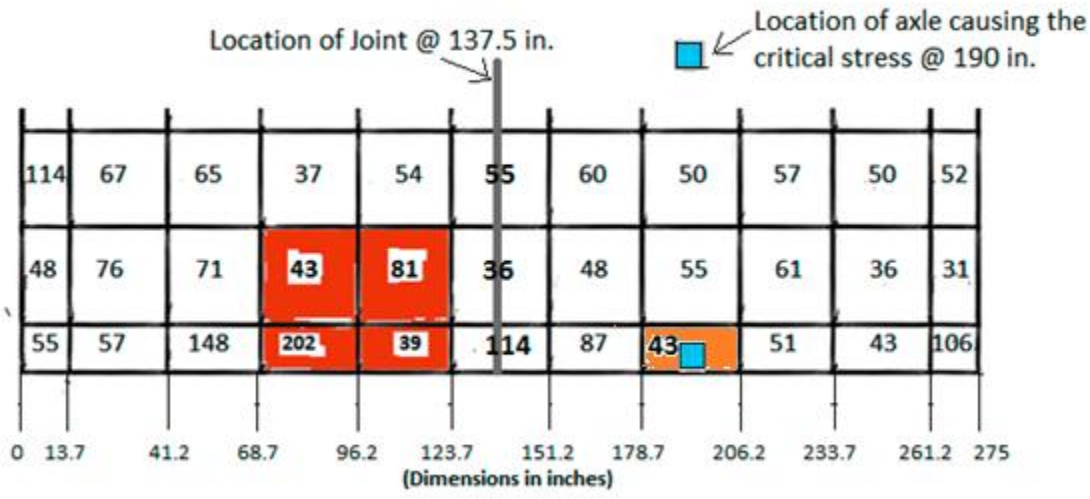

Figure 14: Local variation in k-values along right hand edge of the slab for case RE121

Similarly, the maximum tensile stresses at each longitudinal position for cases RE1 and RE36 are shown in Figure 15 and Figure 16. Although, the peak tensile stresses for the three discretized support cases at the right edge is similar (within 5% of each

other) the standard deviation of the range of k-values for case 121 and case 36 reduces from 25.6 to 14.1 psi/in on account of weighted averaged k-values for the latter case. This reduces the variation in the stiffness of the subgrade support and hence case 36 would not be an important parameter for critical stress development for the other loading location cases. The magnitude of the peak tensile stresses for case 121 is 478 psi, 470 psi for case 36, and 463 psi for case 1. For these cases, a decrease in the peak tensile stress corresponded to an increased size of the pre-defined, uniform k-value area. The peak tensile stress occurred at the mid-slab edge, i.e., 190 in. from the initial loading location, for all three discretized support conditions.

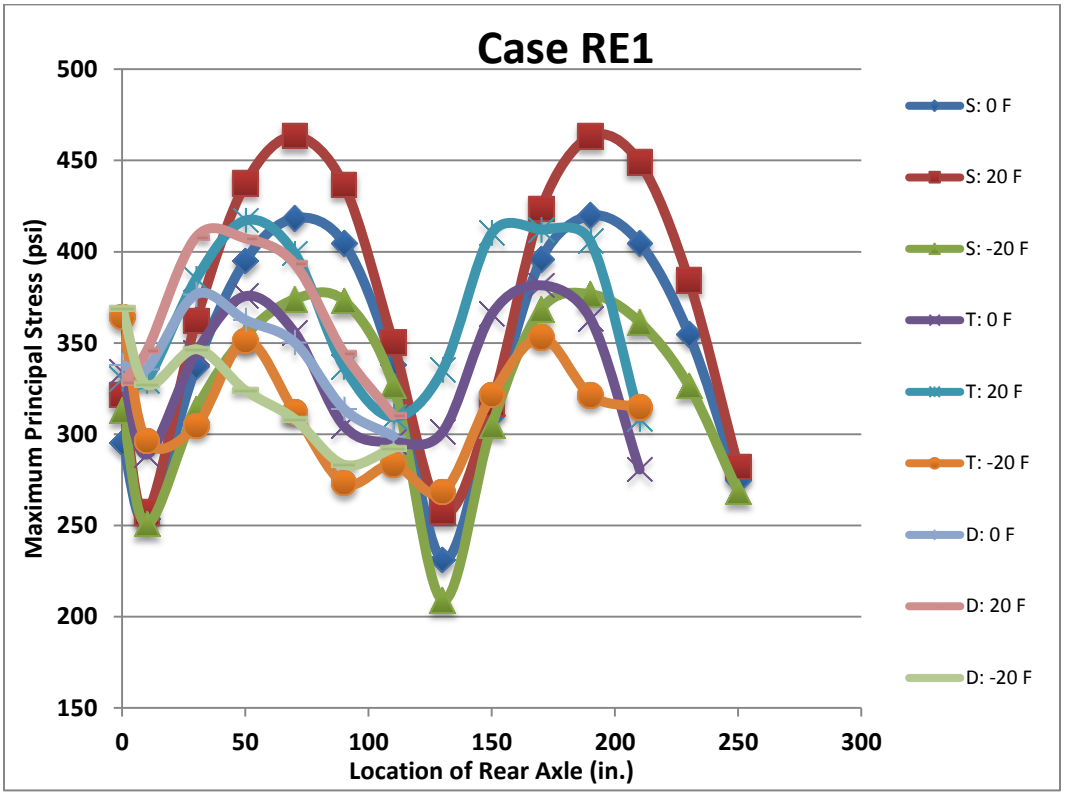

Figure 15: Maximum principal (tensile) stress at each axle position for Case RE1

The peak tensile stresses in Figure 13 and Figure 16 correspond to soft areas under the slab for cases 121 and 36, respectively. The k-values at the location of the peak tensile stress were 43 psi/in and 53 psi/in, respectively, which are lower than the 63 psi/in for the uniform support case. Hence, the peak tensile stresses for each support type corresponded to the magnitude of the local k-values at the expected peak stress location.

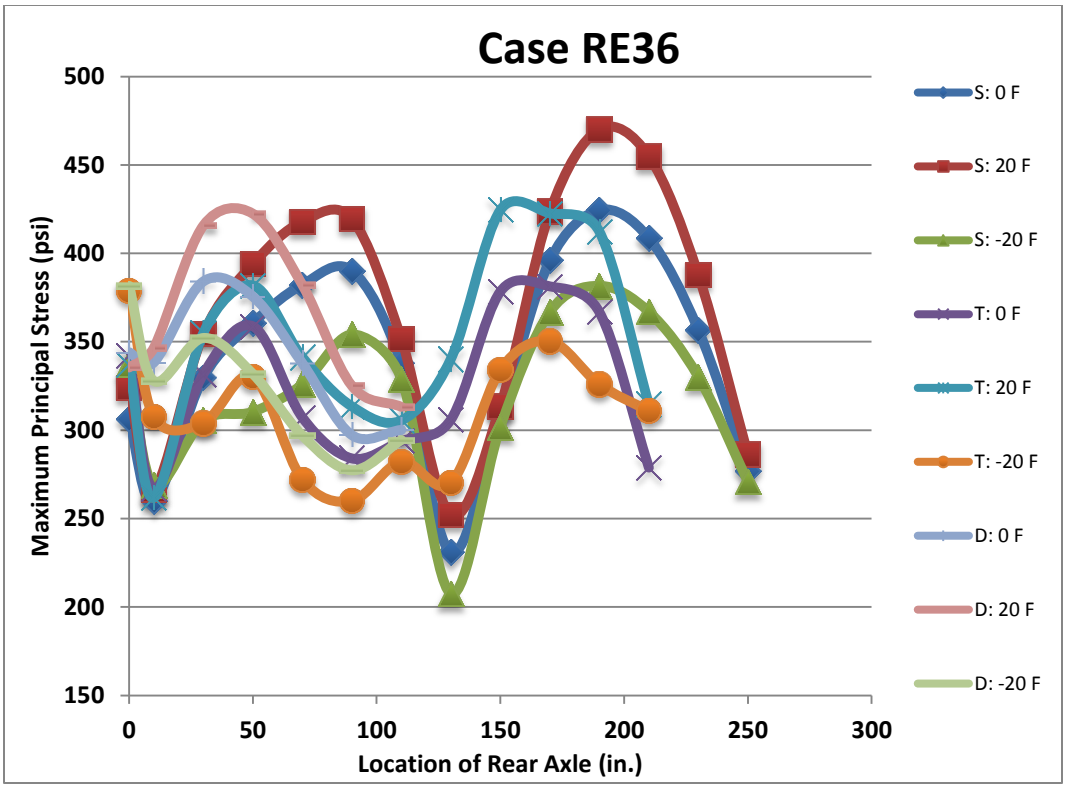

Figure 16: Maximum principal (tensile) stress at each axle position for Case RE36

Figure 17 compares the peak tensile stresses produced by the combination of axle configuration and temperature loading for cases RE1, RE36, and RE121. For each individual axle type, the overall peak tensile stress occurred during positive temperature differential condition. The tandem axle and steer-drive axle at nighttime curling condition produced the peak tensile stresses at the top of the slab for the three support conditions. A summary of the maximum tensile stresses and their respective location (x,y,z) are given in Table 4. “t” and “b” represents the location of the critical stress either at the top or bottom of the slab.

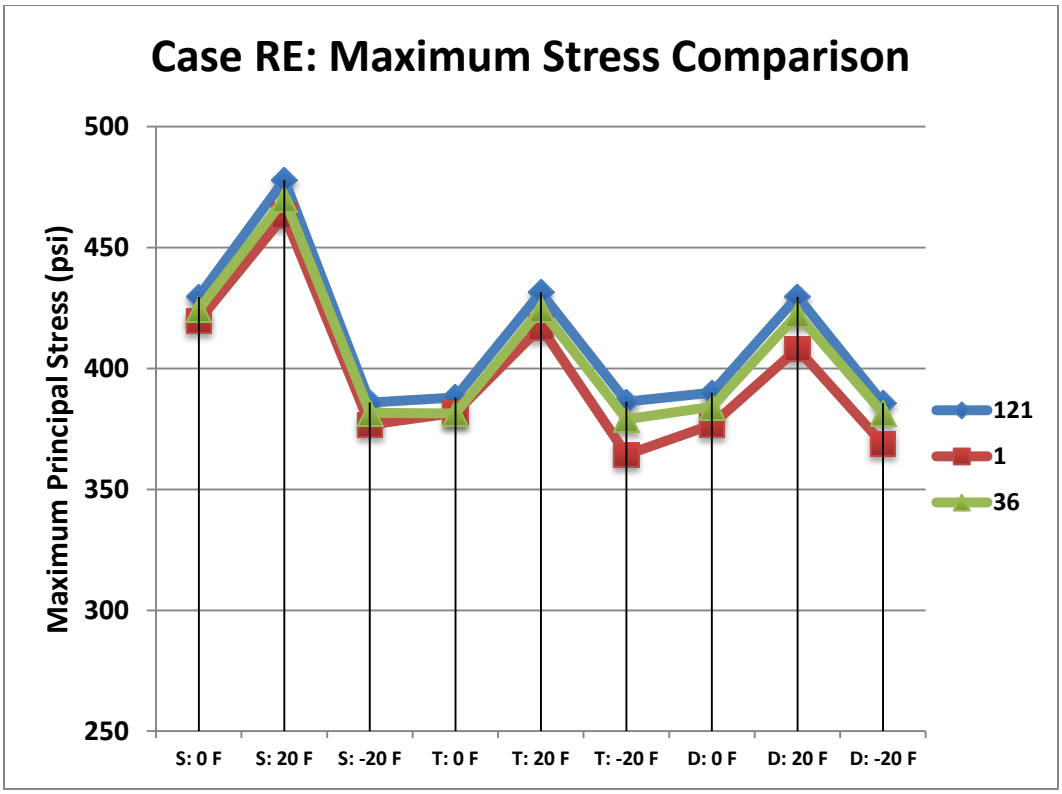

Figure 17: Comparison of the critical tensile stresses for Case RE for each input factor level and the three non-uniform support conditions

Table 4: Summary of peak tensile stress for each subcase for RE loading location

Axle and Temperature Differential	Case RE121 Peak Stress (psi)	Location (x,y,z)	Case RE1 Peak Stress (psi)	Location (x,y,z)	Case RE36 Peak Stress (psi)	Location (x,y,z)
S: 0 F	430	(0,195,t)	420	(0,195,b)	424	(0,195,b)
S: 20 F	478	(0,195,t)	463	(0,195,b)	470	(0,195,b)
S: -20 F	386	(0,195,t)	377	(0,195,b)	382	(0,195,b)
T: 0 F	388	(0,175,t)	382	(0,175,b)	381	(0,223,b)
T: 20 F	431	(0,203,t)	417	(0,55,b)	424	(0,203,b)
T: -20 F	386	(45,0,t)	364	(42,0,t)	379	(45,0,t)
D: 0 F	390	(0,179,b)	377	(0,179,b)	384	(0,179,b)
D: 20 F	430	(0,199,b)	408	(0,179,b)	422	(0,199,b)
D: -20 F	386	(45,0,t)	369	(44,0,t)	382	(45,0,t)

The most notable finding in Figure 17 and Table 4 is the peak tensile stress for all cases changes very little as the subgrade support goes from uniform (single k-value of 63

psi/in) to non-uniform (121 k-values). The difference between the average peak tensile stress for case 121 (non-uniform) and uniform case 1 (uniform) was 3.6%. Several reasons for this difference are the size of each uniformly defined area was only 0.7m by 0.7m and the range of k-value was only 6 as compared to Brand et al. (32) which used a predefined area of 0.9m (3ft) and only two discrete k-values of 50 and 500 psi/in. Furthermore, to assign k-value for case RE36, a weighted average of Case RE121 values were used which additionally reduced the range in expected k-values to a factor of 3.

Several other observations from Figure 17 are that the single axle loading for this support assumption produced the highest tensile stresses for no curling and daytime curling and the nighttime curling condition produced the lowest tensile stresses for all axle types. These findings were slightly different than Brand et al. (32), which found the tandem axles were the dominant axle in the majority of cases analyzed. This reinforces that determination of the critical axle type depends on the distribution and size of the non-uniformity area, slab geometry, and load location.

3.2.2 Stress Analysis for Left Edge (LE) Loading Case

Case LE121 represented the movement of the axles along the left edge of the slab similar to RE121 with 121 k-values, as shown in Figure 18. The distribution of stresses for case LE121 is similar to case RE121 in Figure 13, with the critical tensile stresses occurring near the center of each slab. The single axle configuration with daytime curling produced the peak tensile stress like case RE121. The critical tensile stress was found at the bottom of the slab. Similarly, the maximum tensile stresses at each longitudinal position for cases LE1 and LE36 are attached in the appendix in Figures B1 and B2. The maximum tensile stresses for LE1 were the same as RE1 while case LE36 had similar trends and findings as RE36. A summary of the peak tensile stresses for the left edge loading path can be seen in Table 5.

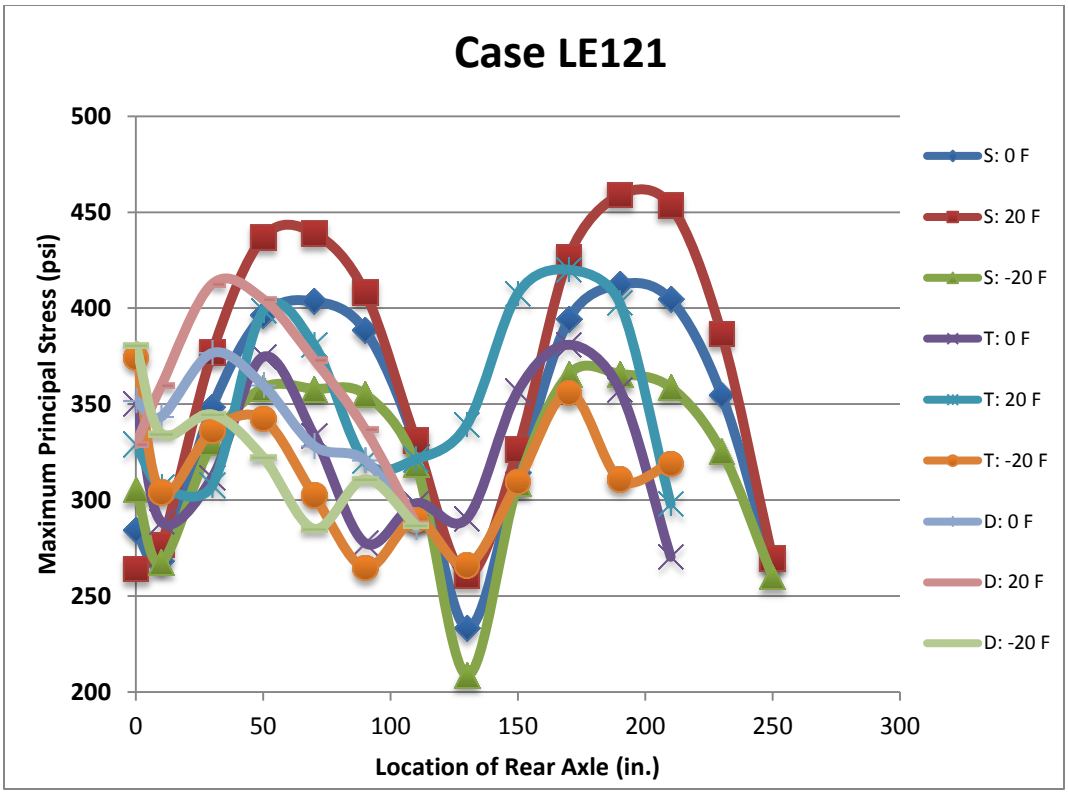

Figure 18: Maximum principal (tensile) stress at each axle position for Case LE121

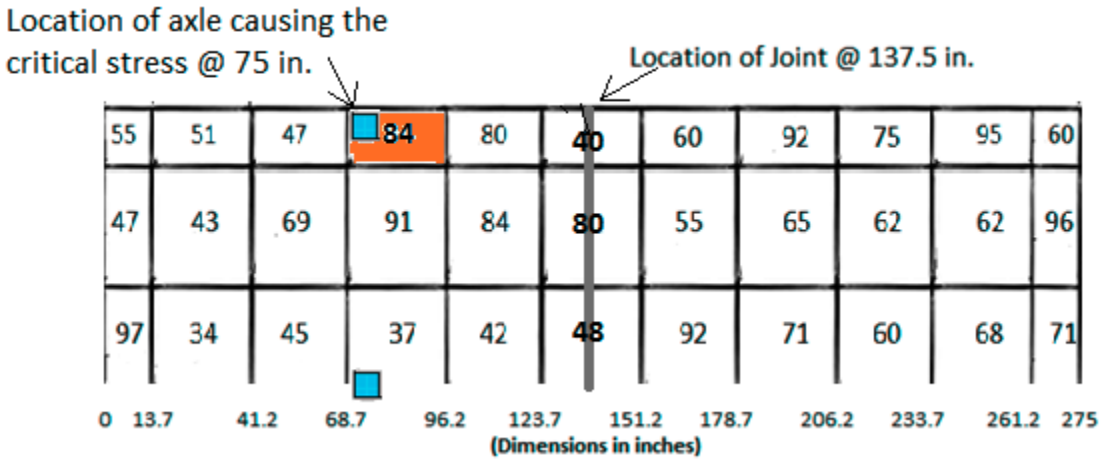

Figure 19: Local variation in k-values along left edge of the slab for case LE121

Figure 19 shows the location of the axle causing the peak tensile stress for LE121. The overall peak tensile stress (463 psi) occurred under the uniform support condition case (LE1) as seen in Table 5. However the overall peak tensile stress for each of the support condition are within 1%. From Figure 20 it can be seen that case LE121 with

discretized area of 0.7 x 0.7 m^2 and case LE36 with discretized area of 1.16 x 1.16 m^2 had a similar magnitude of tensile stress relative to the uniform support assumption (case LE1). Therefore, the size of the non-uniform area or number of discretized areas did not play a role in the tensile stress changes (0.8% decrease in average peak tensile stress was observed when moving from a non-uniform subgrade support to a uniform subgrade support). This can be attributed to the distribution of k-values being closer to mean (63 psi/in) along the left lane edge case, as seen in Figure 19.

To calculate the mean k-value along the edge for cases RE and LE only the k-values along the respective edges, i.e., two corner stiffness areas with size 0.35x 0.35 m^2 and the remaining stiffness areas of 0.35x0.70 m^2 at each edge location were selected. The mean of the k-values at the left hand edge was 67 psi/in with a standard deviation of 17.8 psi/in while the right hand edge had a higher mean of 86 psi/in but the standard of deviation was almost 50 psi/in. From Figure 21 and Figure 22 it can be seen that k-values have wider distribution for RE compared to LE, hence, the higher critical stress at RE compared to LE is due to higher variation in the adjacent k-values. In Table 5, the k-value at the overall peak tensile stress location for case 121 was 84 psi/in which is higher than the uniform support k-value of 63 psi/in. Even though the peak tensile stress for case LE121 occurs at higher k-value (almost 30 psi/in difference), this tensile stress was comparable to case LE1 on account of the variation in the adjacent area stiffness.

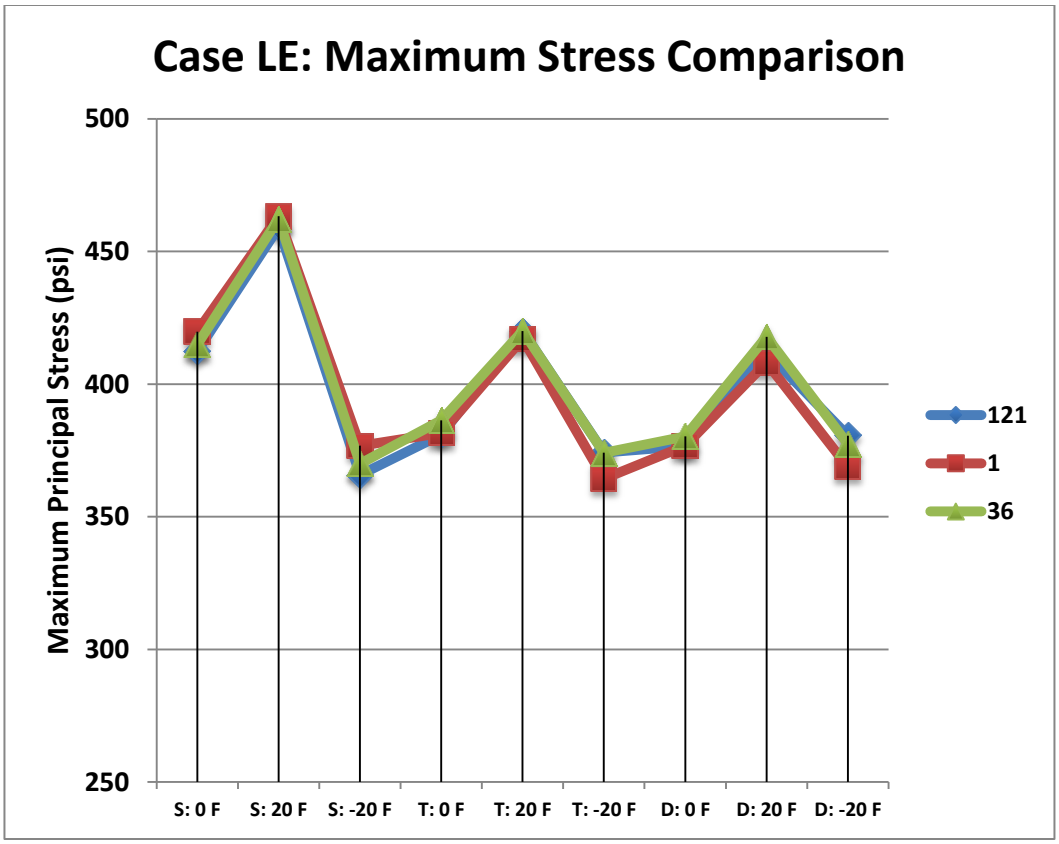

Figure 20: Comparison of the critical tensile stresses for Case LE for each input factor level and three non-uniform support conditions

Table 5: Summary of Peak Tensile Stress for each Subcase for LE Loading Location

Axle and Temperature Differential	Case LE121 Peak Stress (psi)	Location (x,y,z)	Case LE1 Peak Stress (psi)	Location (x,y,z)	Case LE36 Peak Stress (psi)	Location (x,y,z)
S: 0 F	412	(275,195,b)	420	(275,195,b)	415	(275,195,b)
S: 20 F	459	(275,195,b)	463	(275,75,b)	462	(275,195,b)
S: -20 F	366	(279,195,b)	377	(279,195,b)	370	(279,175,b)
T: 0 F	381	(275,175,b)	382	(275,175,b)	386	(275,175,b)
T: 20 F	420	(275,175,b)	417	(275,55,b)	420	(275,175,b)
T: -20 F	374	(229,0,t)	364	(233,0,t)	374	(229,0,t)
D: 0 F	377	(275,179,b)	377	(275,179,b)	380	(275,179,b)
D: 20 F	412	(275,179,b)	408	(275,179,b)	418	(275,179,b)
D: -20 F	381	(229,0,t)	369	(231,0,t)	377	(229,0,t)

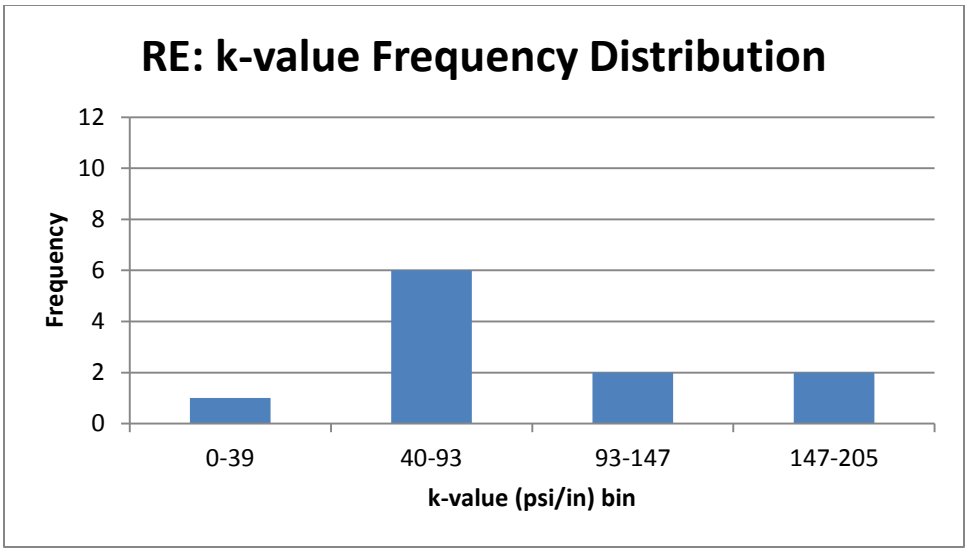

Figure 21: k-values along the right hand edge for case RE121 of MI I-94 roadway

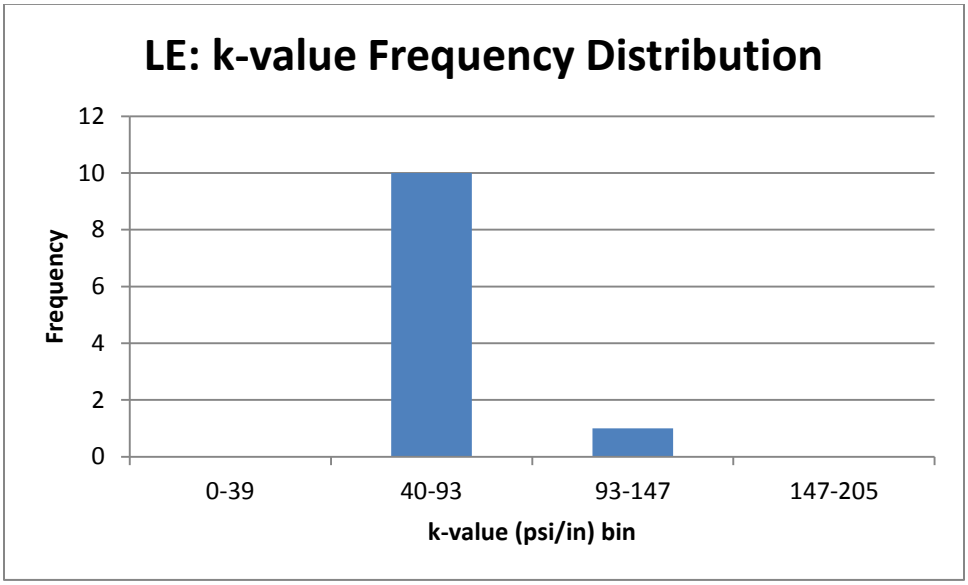

Figure 22: k-values for case LE121 of MI I-94 roadway

3.2.3 Stress Analysis for Middle of Lane (M) Loading Case

For the middle of the lane cases with the axle straddling the longitudinal joint (case M), the same analysis matrix was applied. The results for Case M121 in Figure 23 show the maximum tensile stress patterns at different longitudinal positions are significantly different than case RE in Figure 13. The maximum tensile stresses are much higher at the initial transverse joint relative to the RE case. Positive temperature differentials produced the highest tensile stresses for all three axle types. When the rear

axle of the tandem and steer-drive axle reached around 90 in., a large tensile stress increase was observed, which was related to local variation in k-value (36 to 113 psi/in over 90 in.) as shown in Figure 24. This behavior again confirms the importance of local non-uniformity on the slab's tensile stresses. Although the highest tensile stresses are observed at the initial transverse edge, this location would not have controlled if there was an adjacent slab to offer load transfer to the transverse free edge. The interior loading locations had lower tensile stresses as compared to free edge loading case RE. For case M, the mean of the k-value covers all the k-value areas that the width the axle will cover through its longitudinal traverse from the initial loading location to the end of the slab. Since the interior loading location is not as critical as the edges, the slab should not have the same response sensitivity to changes in the local k-values. The mean k-value of the loading locations was 63 psi/in with a standard deviation of 20.3 psi/in. From Figure 26 it can be seen that case M has a higher frequency distribution of k-values within one standard deviation of the mean and hence does not behave in the same non-uniform way as the free edge RE case. The interior loading path coupled by the presence of a contraction joint are contributing factors to lower tensile stresses along the middle of the slab loading path compared to the edge loading path.

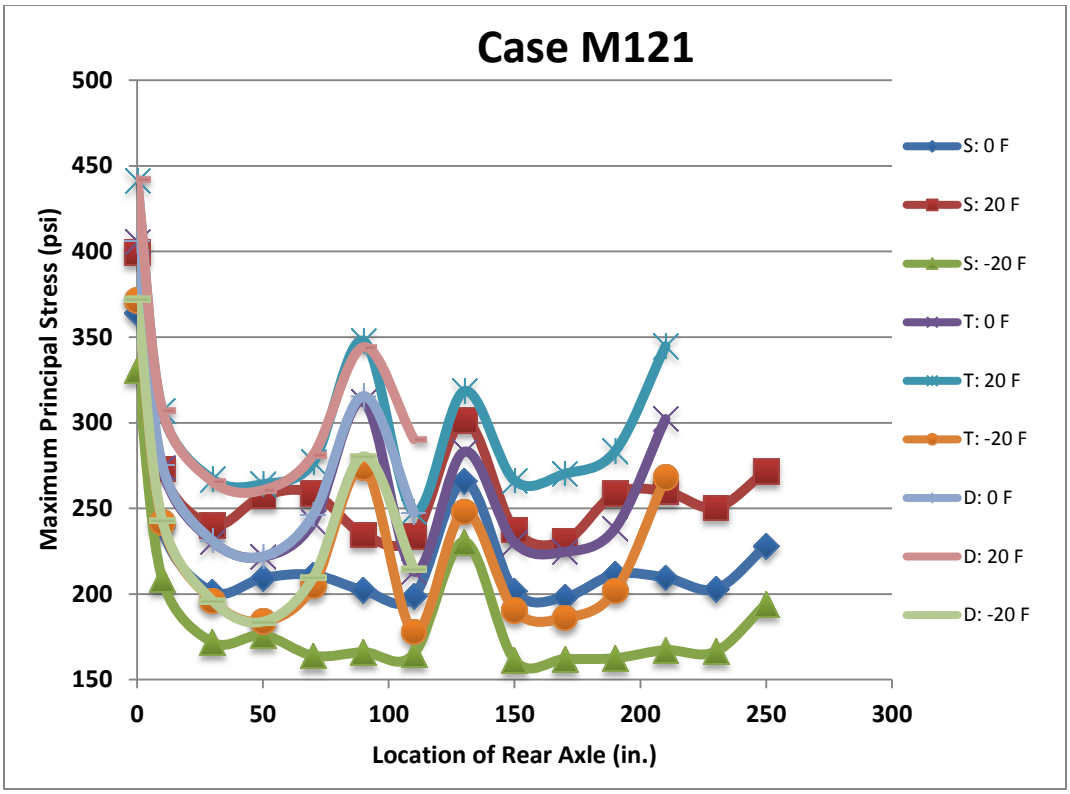

Figure 23: Maximum principal (tensile) stress for Case M121 versus axle position

As expected, the middle loading path with a single k-value (M1) or 36 discrete k-values (M36) produced similar peak tensile stresses to M121 as shown in Figure 25 with a slight decrease in average peak tensile stress from non-uniform to a uniform subgrade support of 0.8%. All the critical stresses in Figure 25 are at the bottom of the slab with negative temperature curling causing the lowest tensile stresses for each axle configuration. The maximum tensile stresses at each longitudinal position for cases M1 and M36 can be seen in Figures B3 and B4 in the appendix.

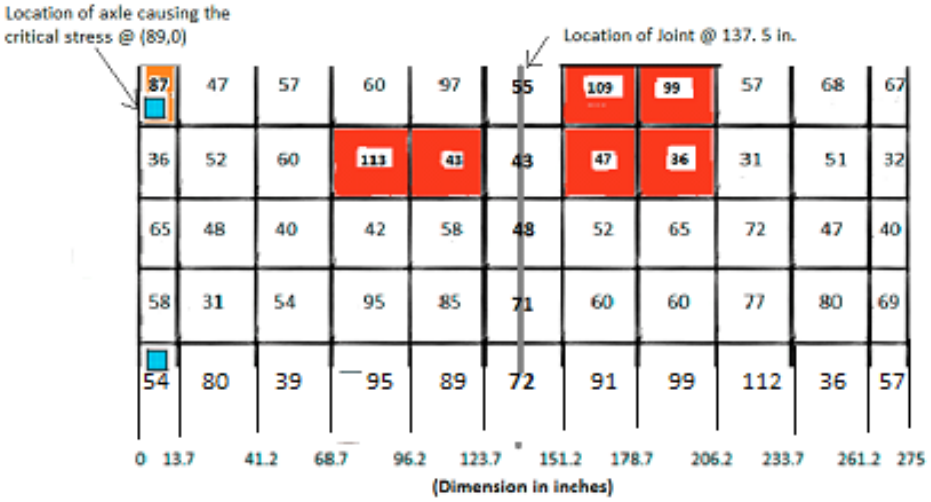

Figure 24: Local variation in k-values along interior of the slab for Case M121

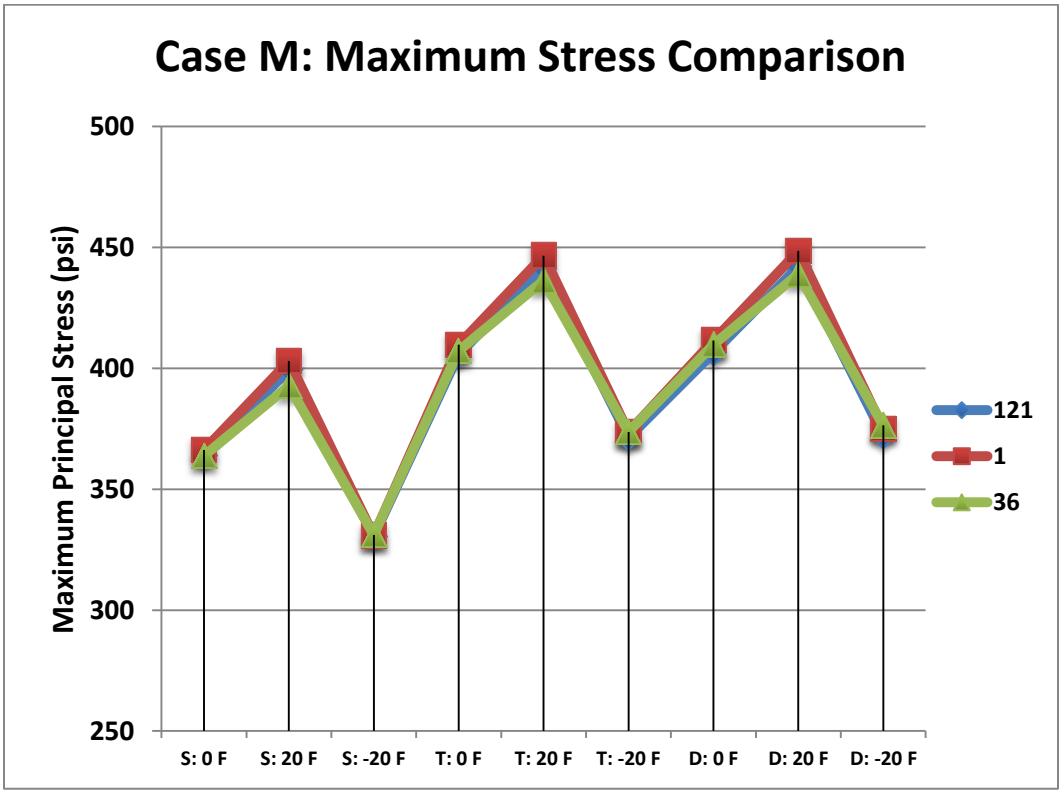

Figure 25: Comparison of the peak tensile stresses for Case M for each input factor level and three non-uniform support conditions

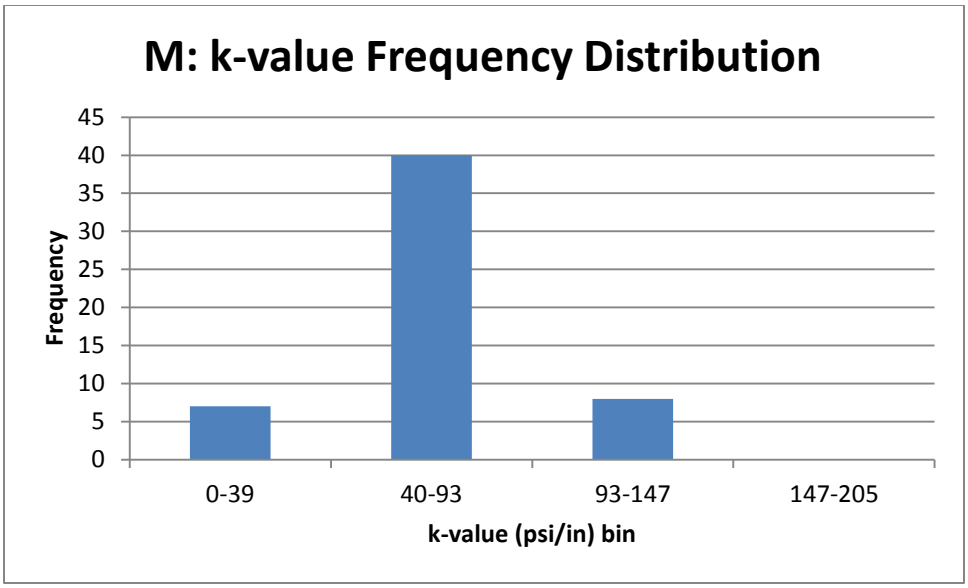

Figure 26: k-values for case M121 of MI I-94 roadway

Figure 27 compares the peak stresses of the three loading locations (RE, LE, M) with the three axle types and temperature differentials. The distribution stresses for the two edges, RE and LE, follow a similar pattern for each case with the RE cases having a higher variation of subgrade stiffness relative to LE. As seen in Figure 27, RE produced the most critical tensile stresses for each variable combination with the maximum tensile stress occurring with single axle during daytime curling. However, the difference between the maximum tensile stresses between RE and LE was only 3%. Although for M loading, tandem and steer drive axles developed the most critical tensile stresses, these stresses are located at the free transverse edge, which are greatly reduced in the presence of joint load transfer. The longitudinal edge loading had a 19% increase in peak tensile stress between case RE and case M. The most important finding so far was the effect of discretization of the non-uniform subgrade stiffness areas. There was not a significant difference between the overall peak tensile stress of uniform and non-uniform support condition with a maximum of 3.2% for the most critical location (RE121 for S: 20F) and the difference of 3.6% in average peak tensile stress. One reason for this is the change in adjacent k-values at the critical loading location (case RE121) was 2, i.e., k-value of 87 and 43 psi/in from Figure 14, while Brand et al. (32) had a factor of 10 (50-500 psi/in) for change in k-values, which produced a tensile stress change of 32%.

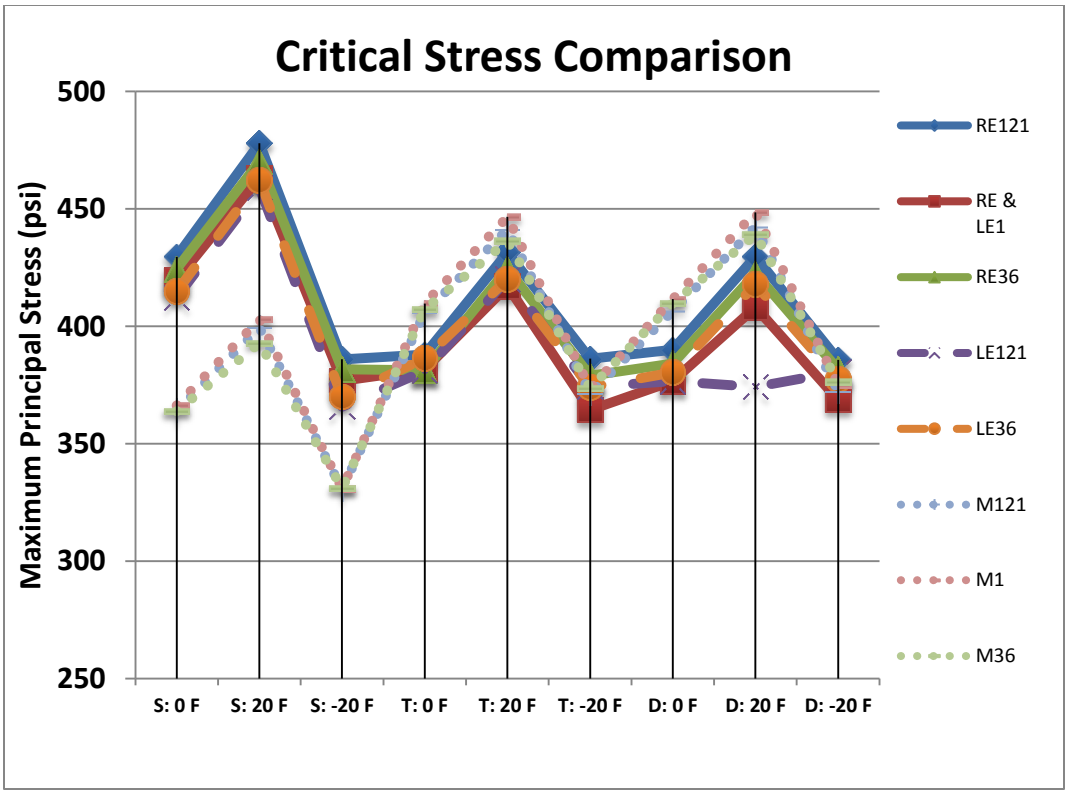

Figure 27: Comparison of peak tensile stresses for RE, LE and M for each combination of support condition, axle type and temperature differentials

3.2.4 Stress Analysis for Right Wheelpath (RW) and Left Wheelpath (LW) Cases

Two additional analyses were carried out, Cases RW121 and LW121, representing longitudinal movement of the axles in the right and left wheel paths, respectively. Figure 28 and Figure 29 show intuitively that lower tensile stresses result when axles are not traversing along the free edge of the pavement, i.e., there is a significant drop in peak tensile stresses relative to Cases LE and RE in Figure 27. Cases RW121 and LW121 show also some similar trends in maximum tensile stresses for the different axle configurations, temperature differentials, and longitudinal position, as seen in Figure 28 and Figure 29, but there are some minor differences depending on the changes in local support stiffness. This tensile stress behavior is due to the interior slab loading location along with the distribution of k-values under the outer wheel at the various axle loading locations in the wheel path being closer to the overall mean k-value of 63 psi/in. The mean was calculated by including all the k-value areas loaded by the

right or left wheel as the axle traversed longitudinally along the RW and LW. The RW case has a mean k-value of 60 psi/in and standard deviation of 18.1 psi/in, while LW has a mean of 67 psi/in and standard deviation of 19.8 psi/in compared with case RE with a mean of 86 psi/in and a standard deviation of 50 psi/in. The distribution of k-values under for RW121 and LW121, shown in Figure 32 and Figure 33, respectively, suggests the frequency distribution of the majority of the k-values are close to the uniform support k-value of 63 psi/in and within one standard deviation from the mean resulting is similar tensile stress development.

The single axle and positive temperature differential combination produced the overall peak tensile stress for both RW121 and LW121 cases. The location of the overall peak tensile stress developed when the axle was at 190 in. from the first loading location, which is approximately mid-slab of the second concrete slab. The overall peak tensile stresses for RW121 and LW121 are approximately 35% lower than the RE121 overall peak tensile stress with only 2% difference between the overall peak tensile stress of RW121 and LW121

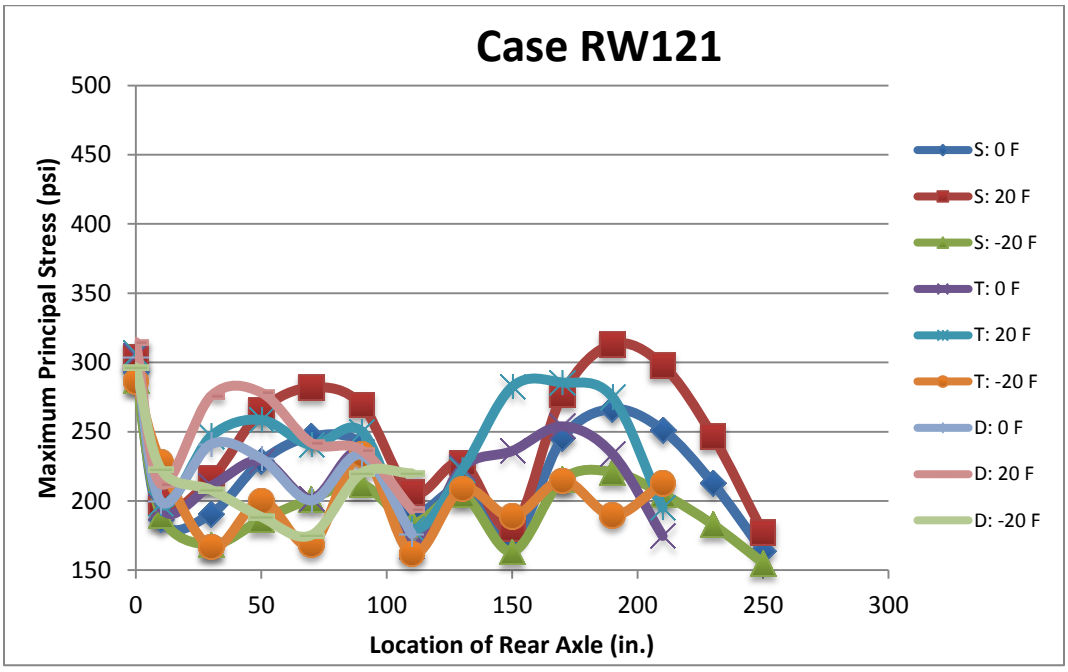

Figure 28: Maximum principal (tensile) stress for Case RW121 versus axle position

The maximum tensile stresses at each longitudinal position for cases RW1, RW36, LW1, and LW36 are shown in the appendix. A summary of the tensile stress analysis for all three distribution of k-values (1, 36, and 121 support areas), shown in Figure 30 and Figure 31, demonstrated that 0.7 x 0.7 m^2 uniform areas (121 k-values) produced the highest slab tensile stresses for all but one loading configuration and temperature curling condition. The average peak tensile stresses increased by 5.3% and 3.5%, respectively, for the right wheelpath and left wheelpath when going from fully uniform support to 121 support values. The overall peak tensile stress difference between uniform support and non-uniform 121 support for RW and LW was 2% and 1%, respectively. The effect of the non-uniformity of support on slab stresses in these cases are not significant enough to cause premature cracking failures if it is ignored as the critical tensile stress of 313 psi for RW121 and 307 psi for LW121 are almost half of the typical concrete flexural strength of 650 psi. For the wheelpath loading positions, all peak tensile stresses in Figure 30 and Figure 31 were located at the bottom of the slab.

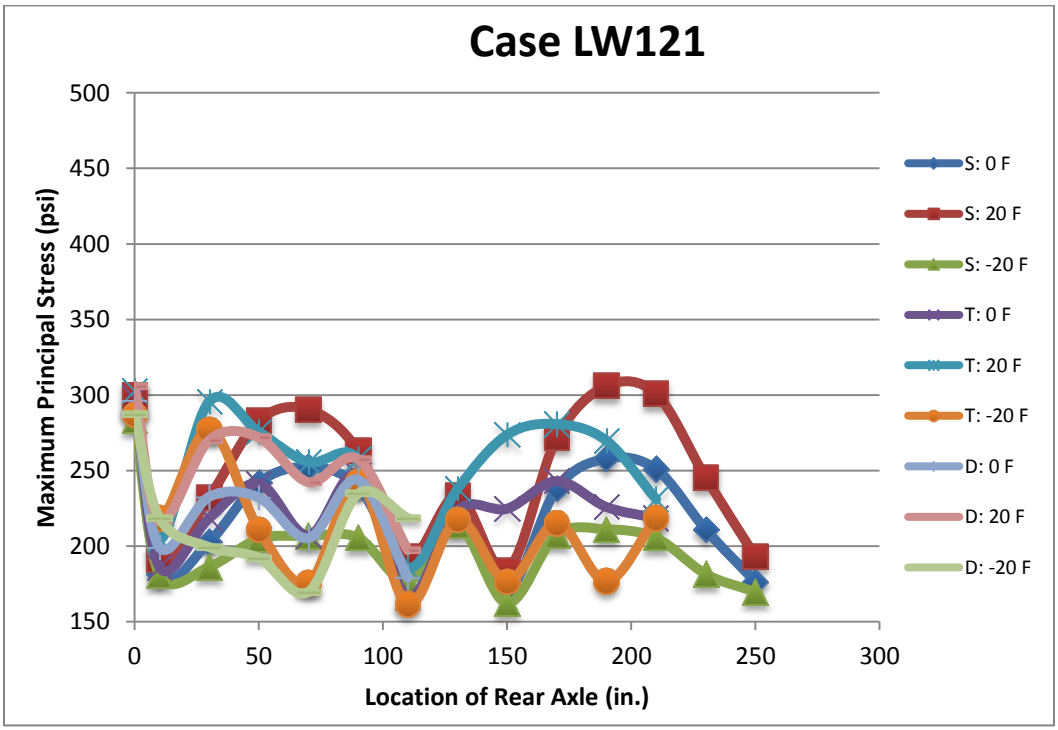

Figure 29: Maximum principal (tensile) stress for Case LW121 versus axle position

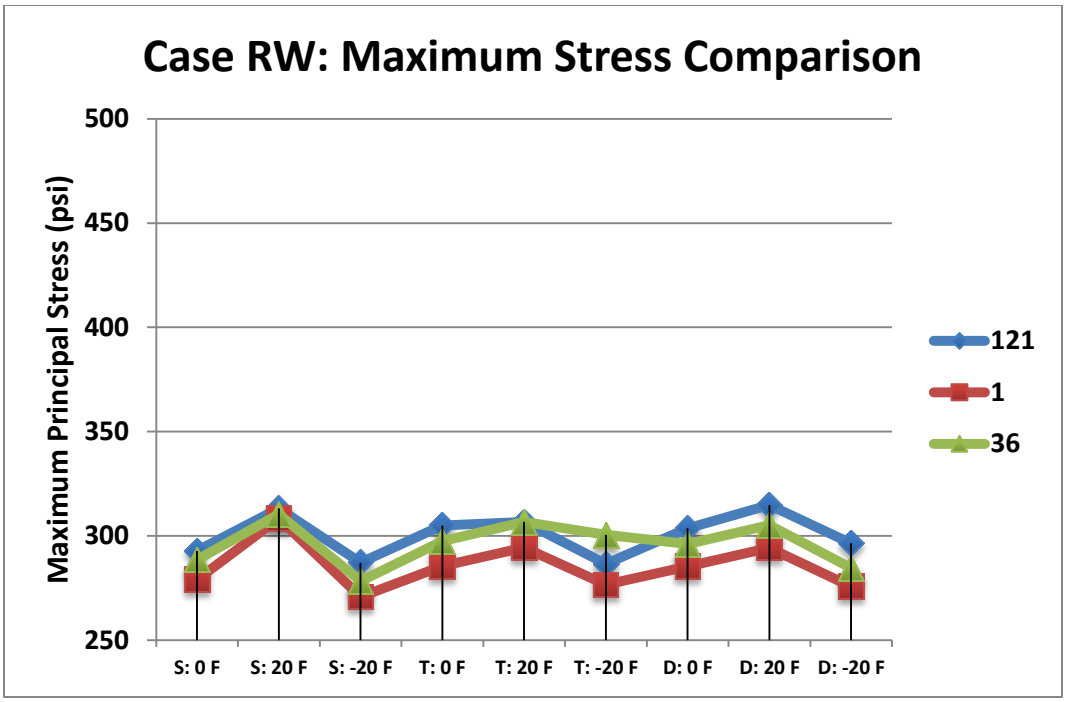

Figure 30: Comparison of the peak tensile stresses for Case RW for each input factor level and the 3 levels of non-uniform support

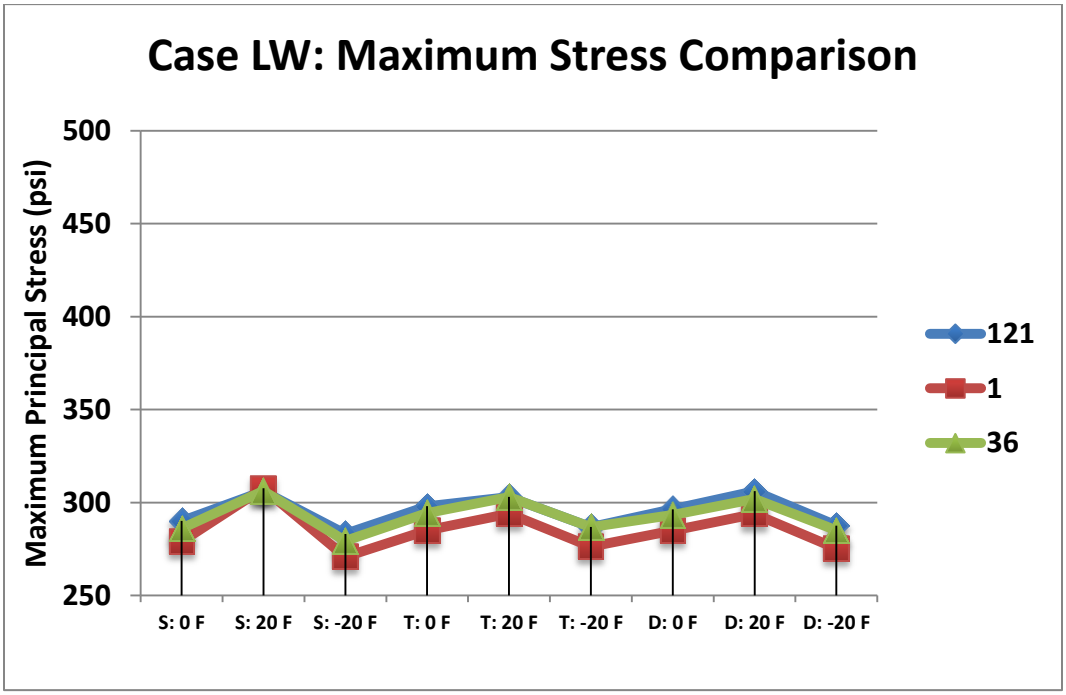

Figure 31: Comparison of the peak tensile stresses for Case LW for each input factor level and the 3 levels of non-uniform support

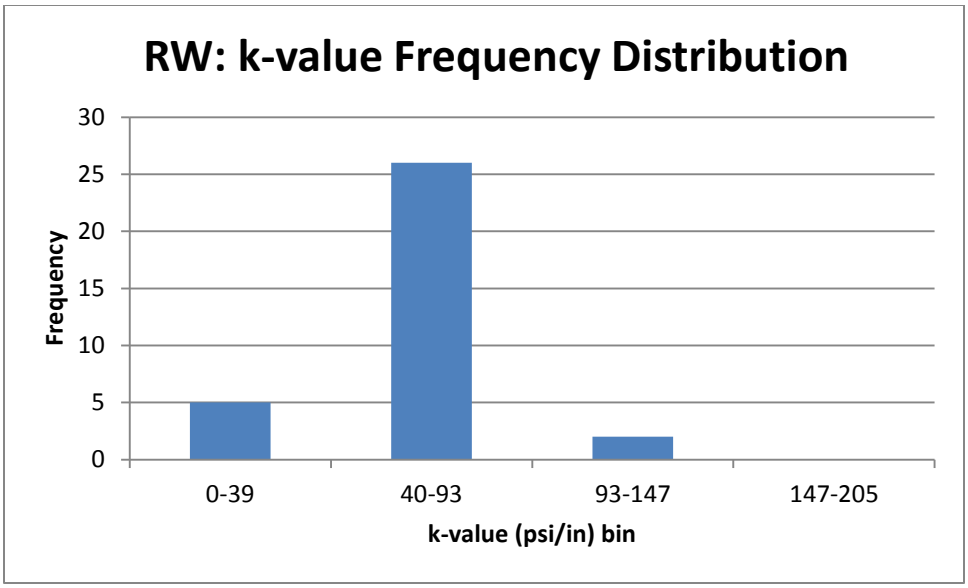

Figure 32: k-values for case RW121 of MI I-94 roadway

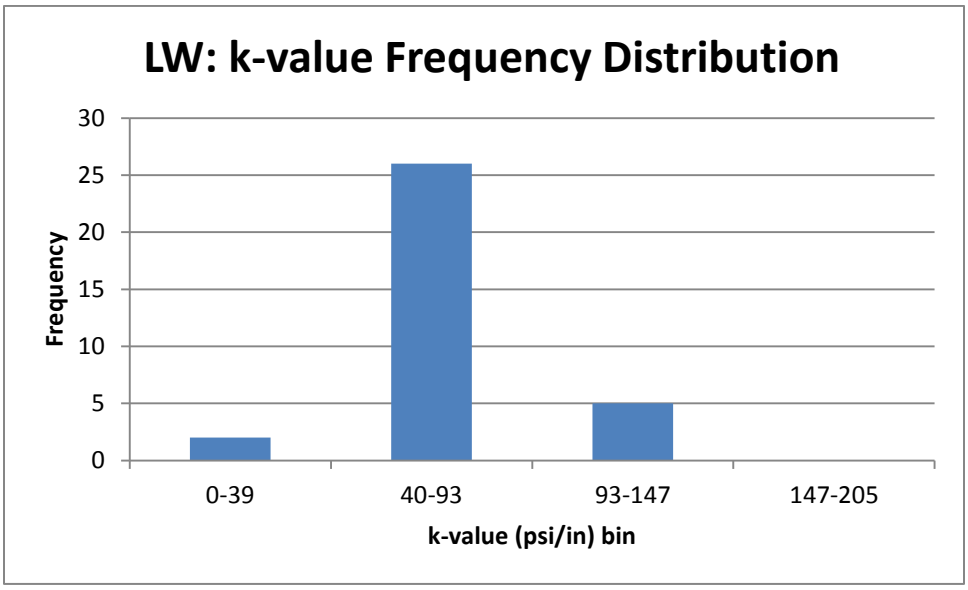

Figure 33: k-values for case LW121 of MI I-94 roadway

3.2.5 Summary of MI I-94: Deterministic Assignment of k-values from Field Measurements

Based on the analysis of the MI I-94 deterministically assigned spatial field data, several conclusions can be made regarding the effect of subgrade non-uniformity. From Figure 34, the loading paths, case RE followed by case LE, produced the largest tensile stresses. The change in tensile stresses from the uniform subgrade case was the highest

with the 121 discrete k-value areas in particular for Cases RE and RW. However, Table 6 shows that the tensile stress increases from the uniform support condition for all loading paths were not at the significance level found by Brand et al. (32). In fact, in several loading paths (Cases M and LE) the uniform case had higher peak tensile stresses due to the spatial distribution of the k-value under the slab relative to the expected critical load location. Overall, the range in k-values was less than a factor of 7 (31 to 202 psi/in), which was less than the Brand et al. (32) study of 10. Furthermore, the Brand et al. study had much greater local variation in the k-value since only two discrete k-values were used, i.e., 50 and 500 psi/in. These initial findings with the field data

The field measurements and analysis did confirm Brand et al. (32) findings that the support condition along the longitudinal edge was the most critical tensile stress location and should be the zone most controlled if intelligent compaction is going to be efficiently used. Finally, the local variation in k-value relative to the critical load location, e.g., cases RE versus LE, affects which loading path has the overall peak tensile stress.

Table 6: Change in average peak tensile stress between non-uniform (121 k-values) to uniform (single k-value) for each loading path

Loading Path	**Change in Average Peak Tensile Stress**
Case RE (Right Lane Edge)	3.6% (Increase in stress)
Case M (Middle of Lane)	0.8% (Decrease in stress)
Case LE (Left Lane Edge)	0.8% (Decrease in stress)
Case RW (Right Lane Wheelpath)	5.3% (Increase in stress)
Case LW (Left Lane Wheelpath)	3.5 % (Increase in stress)

One reason for the lack of significant change in tensile stress moving from uniform support (1 k-value) to non-uniform support (121 k-value), besides a relatively lower standard deviation in k-value in the field measurement, is the definition of the size of the non-uniform area. For the same k-value distribution, as the non-uniform area decreases, its effect on slab tensile stresses decreases as well; likewise as the non-uniform area approaches the size of the slab, the slab stresses tend to the uniform support tensile

stresses. The discretization of larger non-uniform area of 1.16x1.16 m^2, e.g., 36 k-values, was thought to be a more critical size as noted in Brand et al. (32), but failed to develop the most critical tensile stresses. Further review revealed that the 36 k-value cases were developed by weighted average of adjacent k-values from case 121 and thus the extreme k-value values were eliminated when converting the measured 121 k-values to 36 k-values. Therefore, the technique to create the other non-uniform support cases inherently reduced their tensile stress sensitivity. Figure 34 shows that the critical tensile stresses produced by RW and LW were considerably lower (approximately 33% less than RE) then edges or middle of lane cases and hence can be deemed as non-critical in nature primarily on account of their interior loading location. As mentioned earlier, the high critical stress of case M is due to the presence of a free transverse edge loading condition.

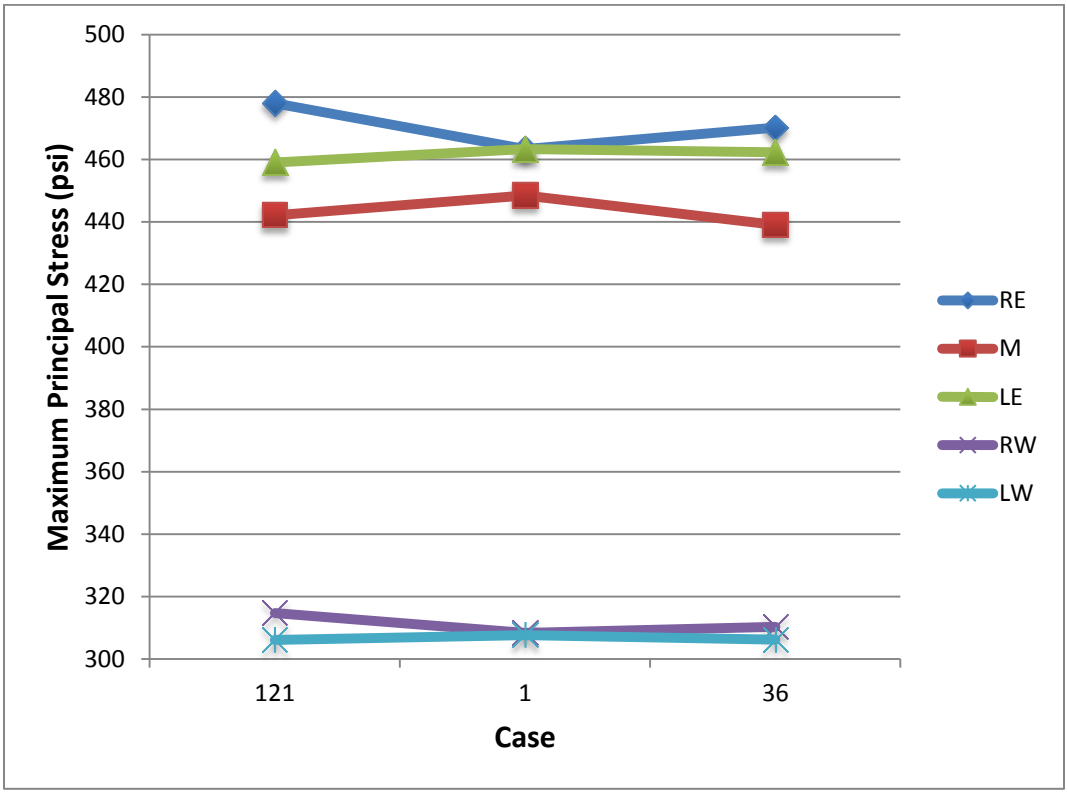

Figure 34: Comparison of peak tensile stress for each loading path with three subgrade support conditions

As noted above, the spatial distribution and range of k-values was a factor in the peak tensile stress for each case. The percentage frequency distribution of k-values for cases 36 and 121, shown in Figure 35, demonstrated a 27% greater occurrence for case

36 in the bin 56-80 which represents the k-values closer to the mean. Case 121 distribution was created for a mean of 63 psi/in, standard deviation of 25.6 psi/in and range of 31 to 202 psi/in whereas case 36 had a mean of 63 psi/in, standard deviation of 14 psi/in and range of 39 to 116 psi/in. It is obvious that Case 36 had the same mean and lower standard deviation since it was defined based on creating uniform discrete areas of 1.16m x 1.16m by weighted average of the 121 k-values measurements.

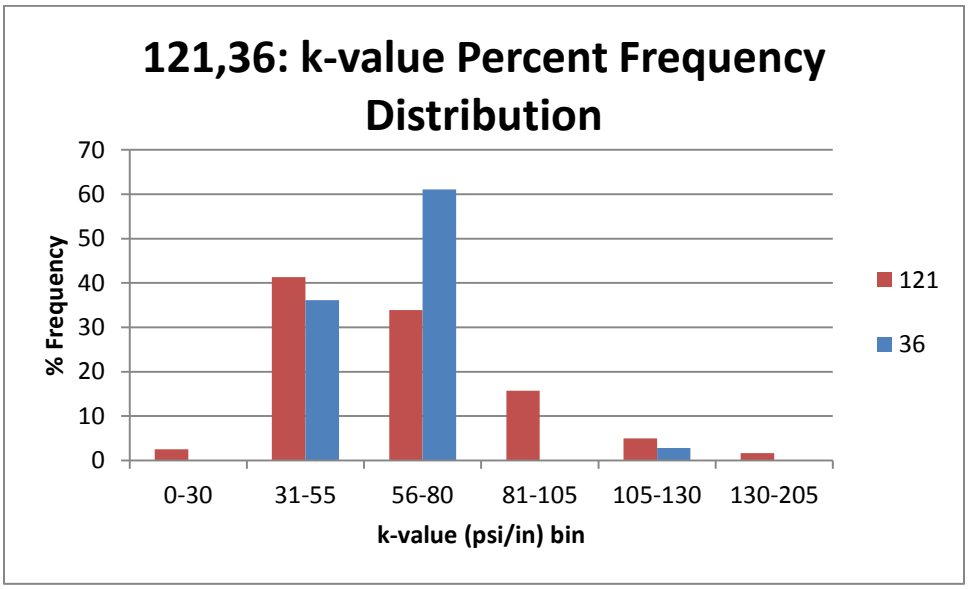

Figure 35: Percent frequency distribution of k-values for cases 36 and 121

Table 7: Location and magnitude of critical tensile stress for each factor level analyzed

Case	Single Axle			Tandem Axle			Steer Drive Axle		
	0 F	20 F	- 20 F	0 F	20 F	- 20 F	0 F	20 F	-20 F
RE121	429 (0,195,b)	478 (0,195,b)	385 (0,195,b)	387 (0,175,b)	331 (0,203,b)	386 (45,0,t)	389 (0,179,b)	429 (0,199,b)	385 (45,0,t)
RE1	419 (0,195,b)	463 (0,175,b)	376.7 (0,195,b)	381 (0,175,b)	417 (0,55,b)	364.3 (42,0,t)	376.7 (0,179,b)	408.0 (0,179,b)	368.7 (44,0,t)
RE36	424 (0,195,b)	470 (0,195,b)	381 (0,195,b)	381 (0,223,b)	424 (0,203,b)	378 (45,0,t)	384 (0,179,b)	422 (0,199,b)	381 (45,0,t)
LE121	412 (275,195,b)	458.9 (275,195,b)	365 (275,195,b)	380 (275,175,b)	420.0 (275,175,b)	374 (229,0,t)	376 (275,179,b)	412 (275,179,b)	380 (229,0,b)
LE1	419 (275,195,b)	463 (275,95,b)	376 (275,195,b)	381 (275,175,b)	417 (275,55,b)	364 (233,0,t)	376 (275,179,b)	408 (275,179,b)	368 (231,0,b)
LE36	414 (275,195,b)	462 (275,195,b)	369 (275,175,b)	386 (275,175,b)	420 (275,175,b)	374 (229,0,t)	380 (275,179,b)	417 (275,179,b)	377 (229,0,b)
M121	363 (89,0,b)	399 (89,0,b)	330 (89,0,b)	405 (89,0,b)	441 (89,0,b)	371 (89,0,b)	406 (89,0,b)	442 (89,0,b)	372 (89,0,b)
M1	366 (89,0,b)	403 (89,0,b)	330 (89,0,b)	409 (89,0,b)	446 (89,0,b)	373 (89,0,b)	411 (89,0,b)	448 (89,0,b)	374 (89,0,b)
M36	363 (89,0,b)	392 (89,0,b)	331 (89,0,b)	407 (89,0,b)	436 (89,0,b)	373 (89,0,b)	409 (89,0,b)	438 (89,0,b)	376 (89,0,b)
RW121	292 (117,0,b)	313 (20,195,b)	287 (117,0,b)	304 (117,0,b)	306 (117,0,b)	286 (117,0,b)	303 (117,0,b)	314 (117,0,b)	296 (117,0,b)
RW1	279 (117,0,b)	308 (20,75,b)	270 (117,0,b)	285 (117,0,b)	294 (117,0,b)	276 (117,0,b)	285 (117,0,b)	294 (117,0,b)	275 (117,0,b)
RW36	288 (117,0,b)	310 (20,195,b)	278 (117,0,b)	297 (117,0,b)	306 (117,0,b)	300 (117,0,b)	296 (117,0,b)	305 (117,0,b)	284 (117,0,b)
LW121	290 (157,0,b)	306 (255,195,b)	283.0 (157,0,b)	297 (157,0,b)	302 (157,0,b)	286 (157,0,b)	296 (157,0,b)	306 (157,0,b)	287 (157,0,b)
LW1	279 (157,0,,b)	307 (255,175,b)	270 (157,0,b)	285 (157,0,b)	294 (157,0,b)	276 (157,0,b)	284 (157,0,b)	293 (157,0,b)	275 (157,0,b)
LW36	286 (157,0,b)	306 (255,195,b)	279 (157,0,b)	294 (157,0,b)	302 (157,0,b)	286 (157,0,b)	293 (157,0,b)	301 (157,0,b)	285 (157,0,b)

t: Top of slab; b: Bottom of slab

Table 7 shows the location of the peak tensile stress for each factor level and loading path. The positive temperature differential was the most critical temperature loading case for all axle types. As expected, edges were the most critical loading locations with right hand edge location having slightly higher magnitude in the peak tensile stress than left hand edge due to a greater variation in k-values along the loading path. For the right and left edge, the peak tensile stresses were located at the mid-slab edges. The single axle was the critical axle configuration both the edge cases (RE and LE) and middle of lane (case M), whereas steer-drive and tandem axles were critical for the wheel path (cases RW and LW). Single axle generated tensile stresses along the edge were more sensitive to local variations in k-values. Relative to the uniform support case with the mean k-value of the field measurements, the non-uniformity in subgrade support did not produce significant tensile stress changes (maximum of 3.2% along the critical loading path) as seen in Brand et al. (32) which showed 32% change in peak tensile

stresses for an arbitrary, pre-defined non-uniform support compared to a uniform support condition.

3.3 MI I-94: Random Assignment of Support Condition to Arbitrary Pre-Defined Discrete Areas

The initial approach of assigning k-values correlated from field DCP measurements did not suggest overwhelmingly that non-uniformities could produce premature slab cracking. In order to further refine the stress analysis, a statistical process to randomly assign k-values to the same spatial grid patterns used for the previous section's deterministic analyses was implemented. The main assumption for this analysis was that each user-defined area, when spatially connected forms a non-uniform support, has a probability distribution similar to the measured field data. Thus each user-defined area is independently assigned a k-value and does not depend on adjacent areas. A random function generator for a normal distribution was used to assign these k-values to the pre-defined spatial grid. The mean and the standard deviation of the correlated k-values from the MI I-94 data (case 121) was used as inputs to produce the normal distribution shown in Figure 35, which shows the possibility of assignment of k-values below 0 psi/in. Therefore, a set of non-uniform support cases related to the actual measured stiffness distribution on MI I-94 would be produced to determine their effect on the slab's peak tensile stresses. Figure 37 and Figure 38 show 7x7 m^2 non-uniform support areas with 121 and 36 randomly assigned k-values without bias, respectively. For the initial analysis, any randomly generated value less than zero is assigned a k-value of 1 psi/in. This low to no support condition could be interpreted as a void, area of localized erosion, or soft spot.

For this analysis, the slab geometry and ISLAB2000 input parameters from Table 2 are the same as the previous section including the axle types, loading locations and temperature differential. The nomenclature for the analyses is update to add the prefix 'R-' for random k-value assignment, e.g., Case R-121. For the randomly assigned non-uniform support case with 36 k-values (1.16x1.16 m^2 uniform area size), five independently generated sub-cases, shown in Figure 38 were developed since the

randomly assignment of two k-values by Brand et al. (32) clearly demonstrated that high and low tensile stresses could be generated for a particular case depending on the location and variation of the support relative to the potential maximum stress location. The areas marked in red are areas of large changes in support stiffness. As seen in Table 8, all options had similar mean k-values and standard deviations with the maximum mean k-value only 10% different and standard deviation difference of only 20%. Based on preliminary ISLAB2000 runs for each sub-case along the edge loading path, option IV was selected for the full stress analysis due to the changes in support changing greatest in the region of maximum tensile stress. Figure 39 represents the loading case R-36 with areas of potential critical stresses highlighted as an indicator.

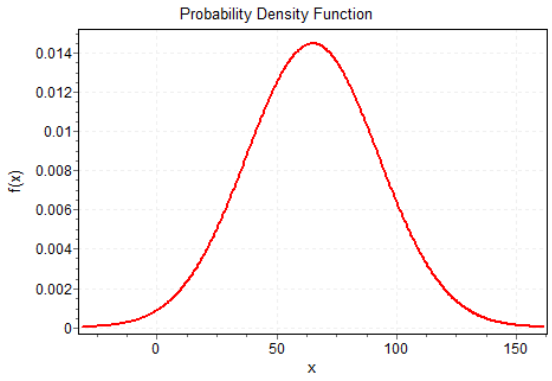

Figure 36: Theoretical distribution curve for randomly assigned k-values for a) case R-121 and b) case R-36

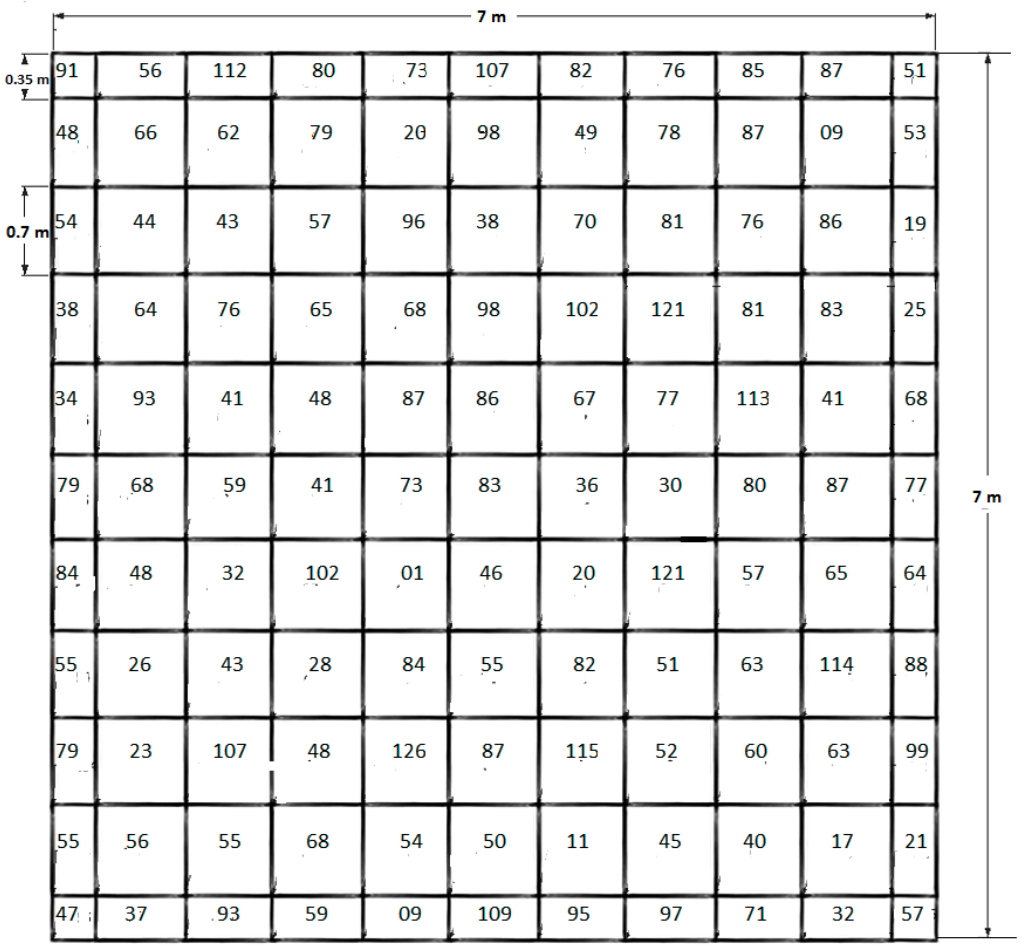

Figure 37: Spatial distribution of k-values for Case R-121

Table 8: Spatial k-value data for five sub-cases of Case R-36

Case R-36	Range	Mean	Standard Deviation
Option I	01 to 126	64	27.5
Option II	23 to 115	67	24.6
Option III	01 to 143	67	30.5
Option IV	03 to 114	61	29.3
Option V	07 to 126	63	26.3

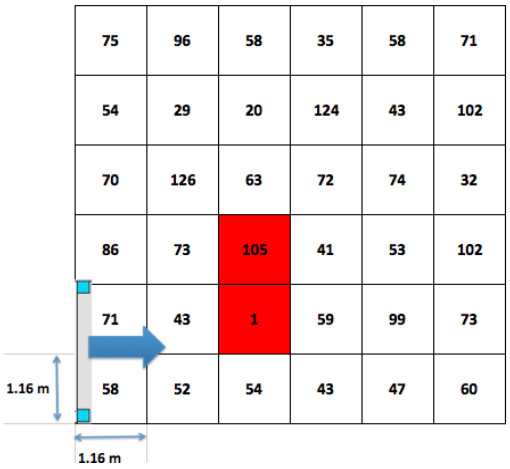

a) Option I

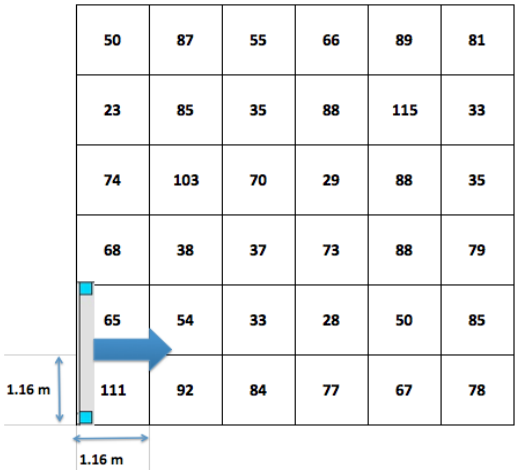

b) Option II

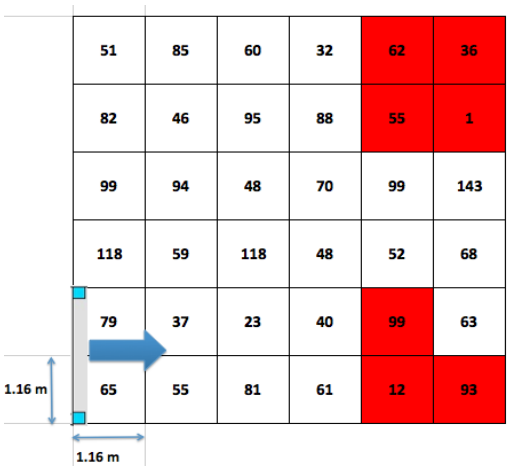

c) Option III

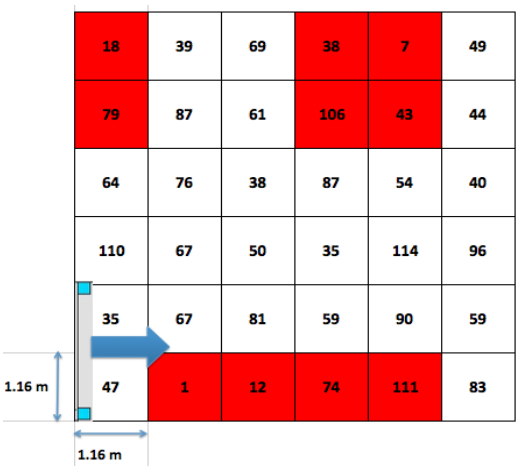

d) Option IV

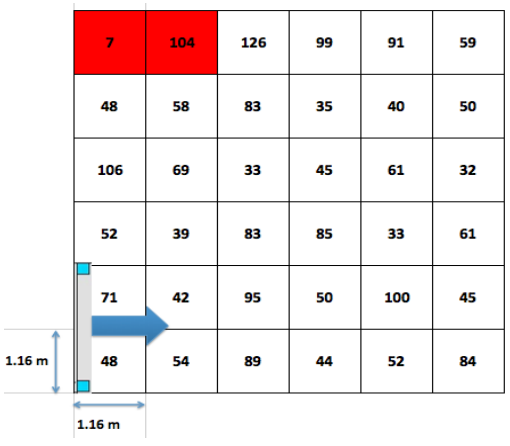

e) Option V

Figure 38: Spatial distribution of k-values for five sub-cases of R-36

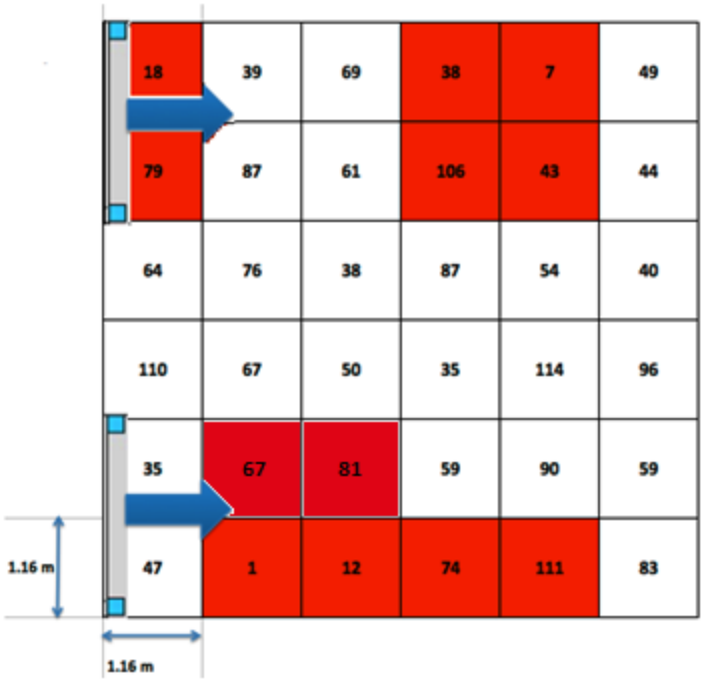

Figure 39: Spatial Distribution of k-values with axle loading on RE and LE for option selected for Case R-36 Option IV

3.3.1 Stress Analysis of Randomly Assigned Support Condition for Right Edge (R-RE) and Left Edge (LE) Cases

The critical tensile stress at each longitudinal position for Cases R-RE121 and R-LE121 that are shown in Figure 40 and Figure 41 have similar magnitudes in stresses compared to case RE 121 and LE 121. In the case of R-RE121 the maximum tensile stress of 479 psi/in is similar to RE121 with 478 psi/in. The mean of k-values for the R-RE and R-LE are calculated in the same way as that for RE and LE based only on the edge k-values. Although, the mean and standard deviation of the k-values at the edges for both cases are not the same, mean of 85 psi/in and standard deviation of 50 psi/in for RE121 and mean of 64 psi/in and standard deviation of 30 psi/in for case R-RE121, the mid-slab longitudinal edge was still the critical location and their peak tensile stress magnitudes were similar as seen in Figure 44.

The randomly assigned k-values at 121 discrete locations for the left edge loading path had a smaller range of values with the mean k-value for R-LE121 of 81 psi/in, which

was higher than that of LE121 having 67 psi/in as its mean with both cases having a standard deviation of 17 psi/in. The increase in critical tensile stress of almost 5% for the randomly assigned LE case can be attributed to the effect of single axle being more sensitive to local stiffness changes in the soil. The frequency distribution of k-values shown in Figure 42 reports that R-LE121 has higher cluster of k-values near the mean relative to R-RE121. The magnitude of tensile stresses between R-LE 121 and R-RE121 are approximately the same at the mid-slab due to similar k-values as seen in Figure 42.

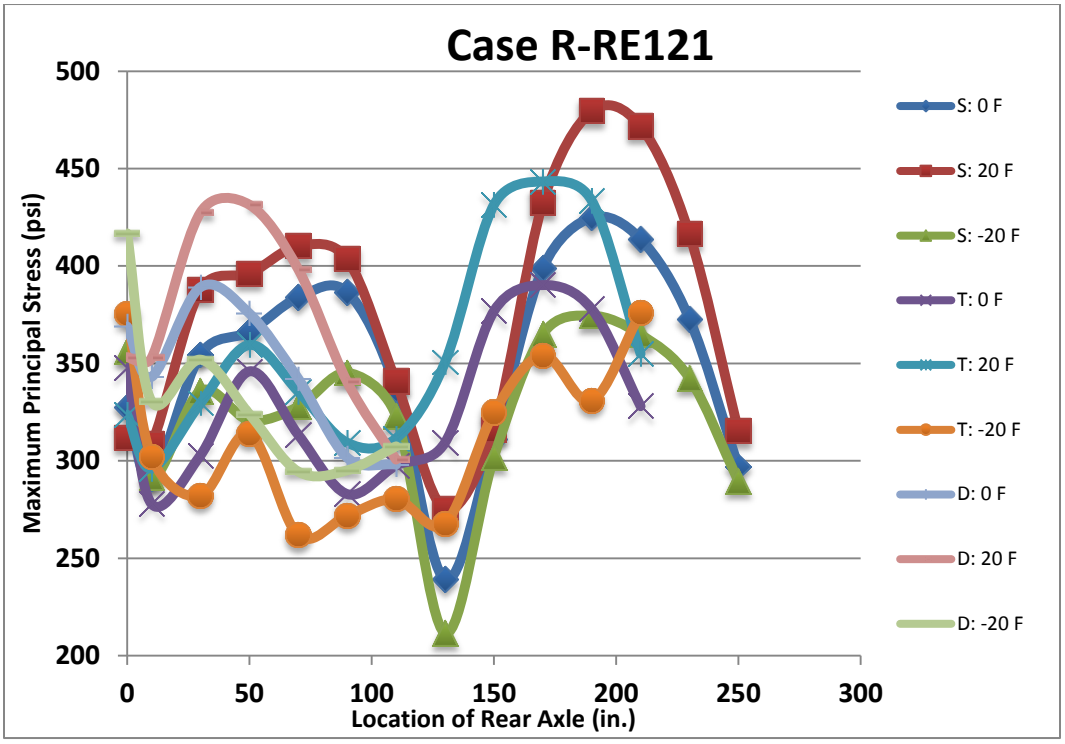

Figure 40: Maximum principal (tensile) stress for Case R-RE121 versus axle position

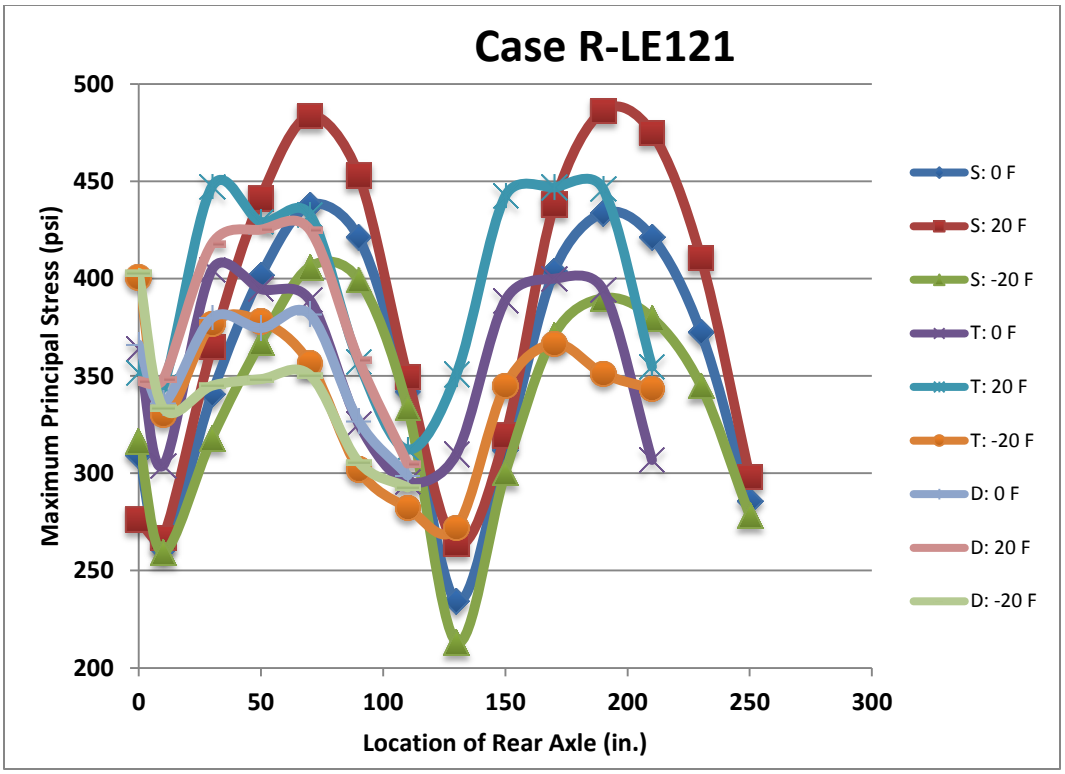

Figure 41: Maximum principal (tensile) stress for Case R-LE121 versus axle position

For the critical 36 k-value random assignment sub-case (Case R-RE, option IV), the results are presented in Figure 43. The tensile stresses are much higher between locations 30 in. and 70 in., which correspond to large variations in adjacent k-values along the edge loading path as seen in Figure 39, i.e., 1 to 67 and 12 to 81 psi/in. All three axle types with daytime curling produced high tensile stresses for this non-uniform support condition. The critical stresses in this area were 50% greater than the adjacent slab which has the same geometry but different randomly assigned k-values. The 1 psi/in support area could represent loosely graded base material, saturated soil, or loss of support/contact with the slab. Clearly, these tensile stress magnitudes are high enough to create premature cracking distress in the concrete pavement. From Figure 44 it can be seen that there is 32% percent increase in the average peak tensile stress between the non-uniform case R-RE36 and R-RE121 uniform support case which was partially due to increase in the pre-defined stiffness area from 0.7x0.7 m^2 to 1.16x1.16 m^2. The increase in average peak tensile stress was also 37% when going from the uniform support assumption to the random assignment with 36 k-values. The difference between the

overall peak tensile stress for cases RE121 (478 psi) and R-RE36 (608 psi) was 27%. Therefore, the combination of soft localized support at the mid-slab edge of case R-RE36 of a certain size was critical to magnitude of the tensile stress change. The critical tensile stress for RE of 608 psi occurs at (0, 83) on the bottom of the slab.

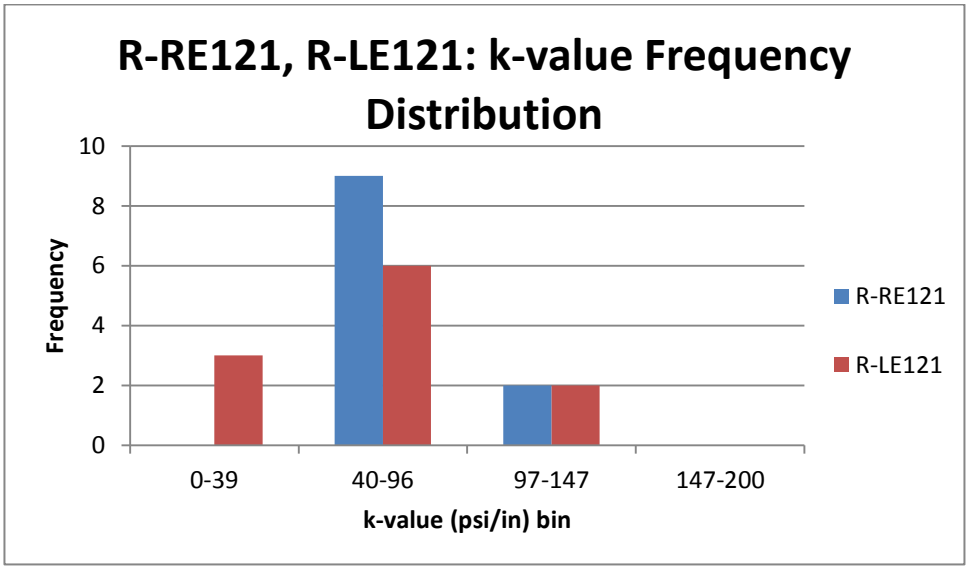

Figure 42: k-value distributions for case R-LE121 and R-RE121 for MI I-94 roadway

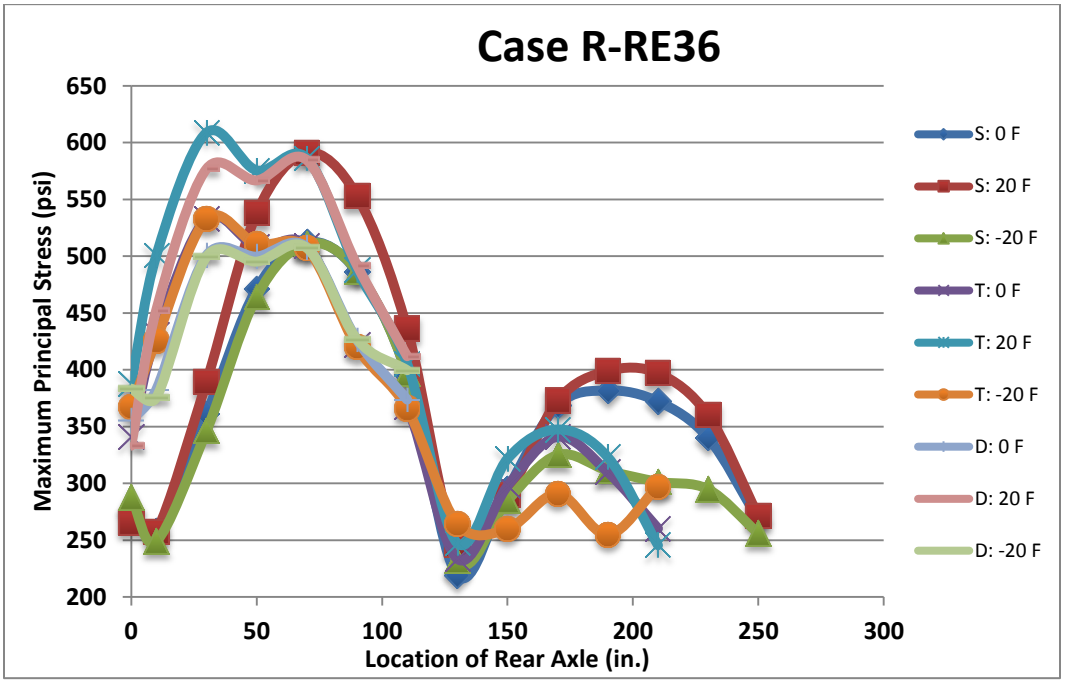

Figure 43: Maximum principal (tensile) stress for Case R-RE36 (Option IV) versus axle position

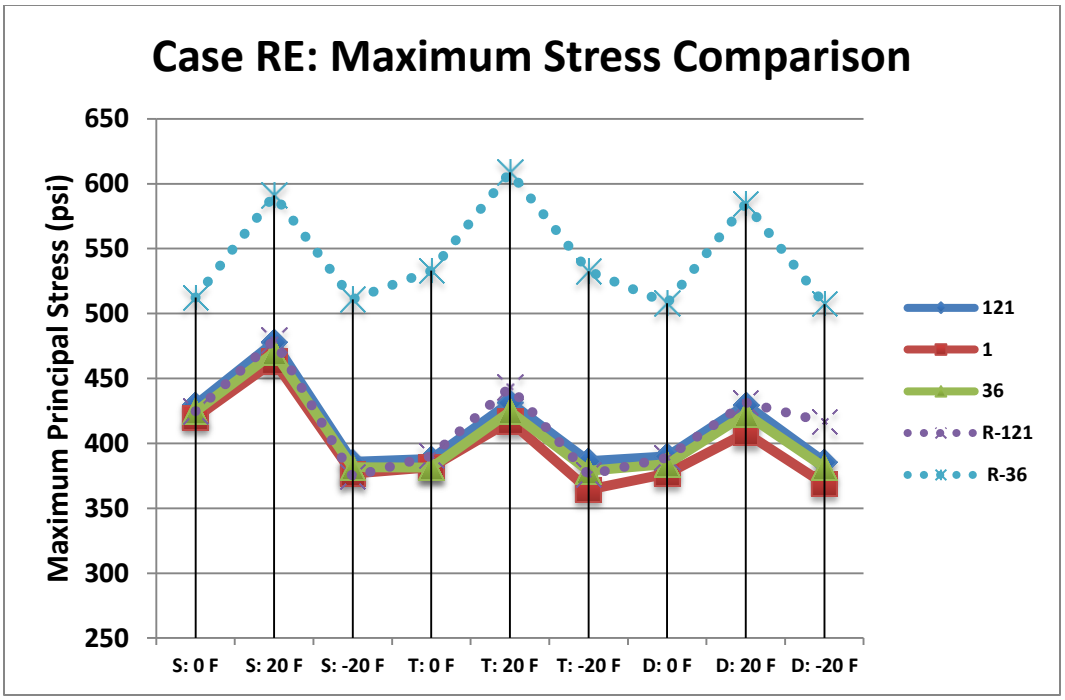

Figure 44: Comparison of the peak tensile stresses for Case RE for each input factor level and the 5 non-uniform support distributions

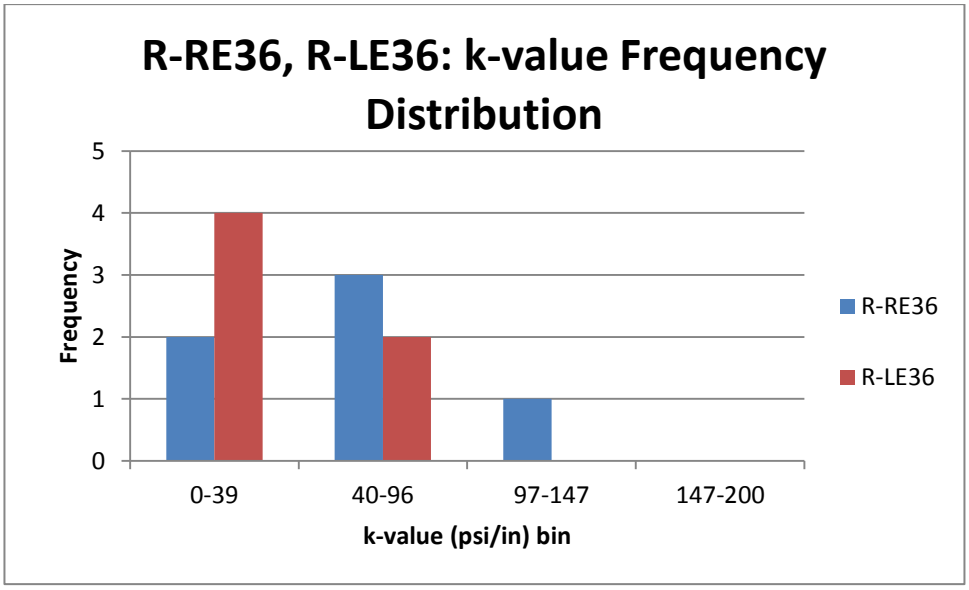

Figure 45: k-values for case R-LE36 and R-RE36 of MI I-94 roadway

Figure 46 shows the results of the maximum tensile stresses recorded at the each longitudinal position along the left edge (Case R-LE36). There is a clear difference with Case R-RE36 in Figure 43, which is linked to the local support conditions under each

axle position. The critical stresses near the mid-slab edge of the two slabs corresponded to the higher variations in adjacent k-value areas as seen in Figure 38d. The peak tensile stress was 8% lower than Case R-RE36 as the variations in non-uniformity in stiffness were not as extreme at the mid-slab edge as seen in Figure 39. This is substantiated by Case R-RE36 having a mean of 53 psi/in. and high standard deviation 40.9 psi/in and range of 1 to 111 psi/in along its loading path, whereas Case R-LE36 had a lower mean of 37 psi/in but a lower standard deviation of 20.1 psi/in and range of 7 to 69 psi/in along the left edge loading path. Figure 45 also shows this point by plotting the frequency distribution of support stiffness between R-RE and R-LE.

There was an increase of 20% in the average peak tensile stress from case R-LE121 with a grid size of 0.7x 0.7 m^2 to case R-LE36 with a grid size of 1.16x1.16 m^2 in Figure 47. The peak tensile stresses also occurred at the bottom the slab during daytime curling. For the left and right edges, single and tandem axles produced similar magnitudes for maximum tensile stresses, i.e., within 1%.

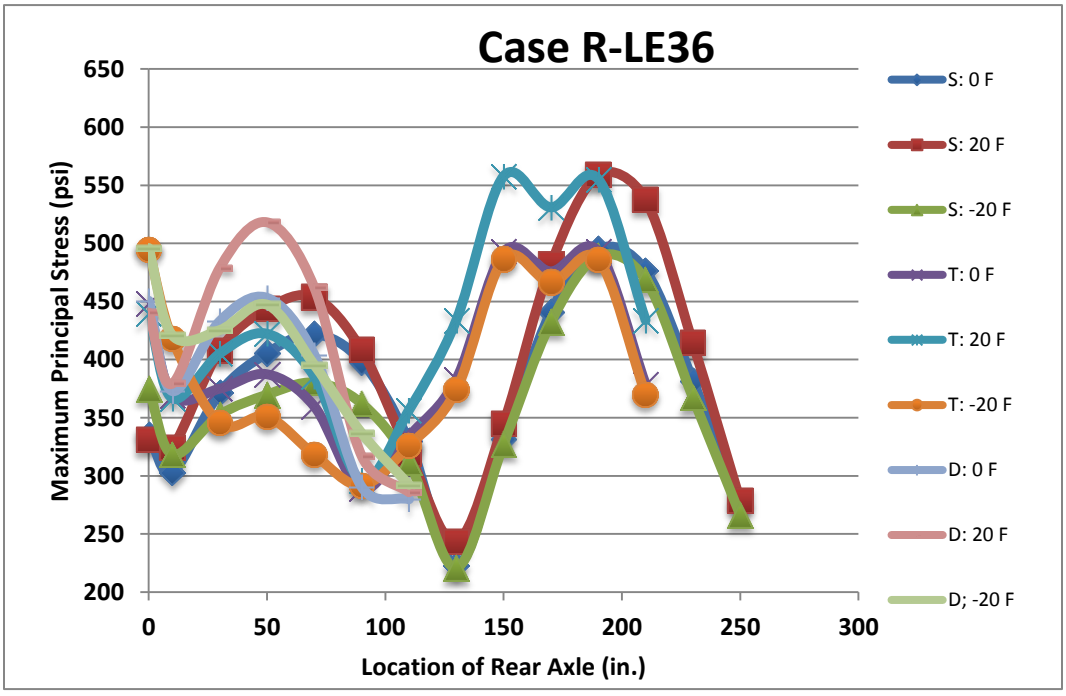

Figure 46: Maximum principal (tensile) stress for Case R-LE36 (Option IV) versus axle position

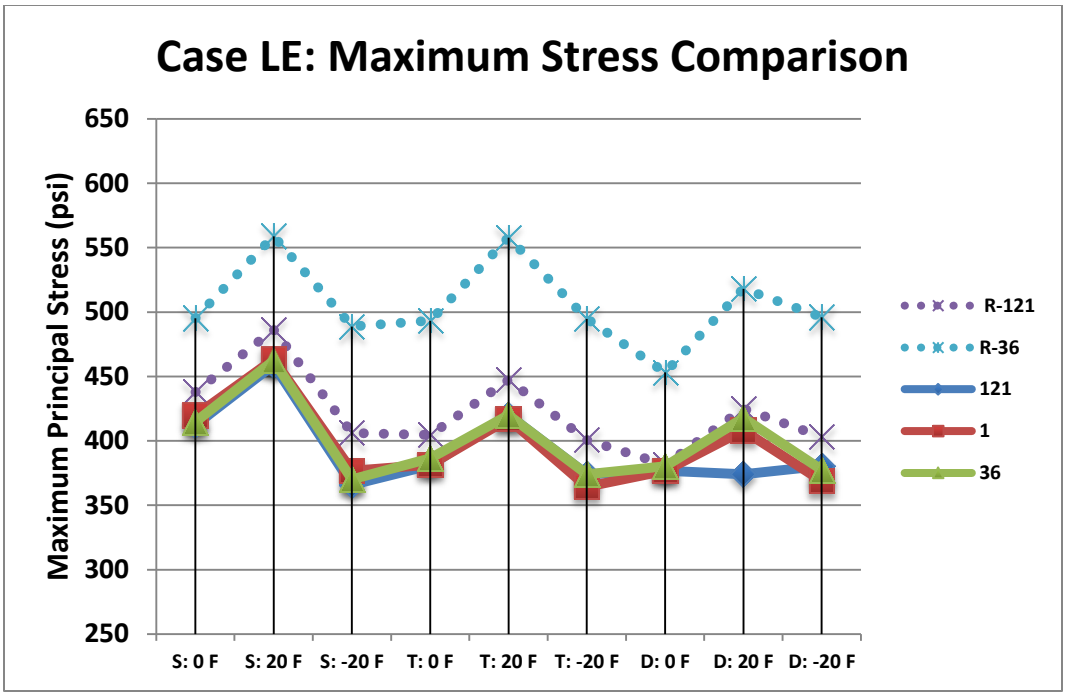

Figure 47: Comparison of the peak tensile stresses for Case LE for each input factor level and the 5 non-uniform support distributions

3.3.2 Stress Analysis of Randomly Assigned Support Stiffness for Middle of Lane (R-M) Cases

Figure 48 shows the maximum tensile stresses recorded for case R-M121 at the each longitudinal position. Random assignment of the 121 k-values increased the average peak tensile stress by 4% compared to M121. Since the middle of the lane with 36 k-values were not the critical cases, the maximum tensile stresses at each longitudinal position for case R-M36 were presented only in the appendix. As expected, the tensile stresses away from the transverse edge load positions for case R-M are much lower than the edge load paths. The size of the non-uniform stiffness areas for this loading path was not as critical as the edge loading paths. The middle of the lane k-values (R-M) was calculated similarly to case M where all the k-values areas under the wheel are taken into consideration as shown in Figure 50, which reports the majority of the k-values (i.e. 69%) in the 40-96 psi/in bin. The R-M121 case k-values had a standard deviation of 26.8 psi/in and mean of 62 psi/in which is essentially similar to the uniform k-value of 63 psi/in. Hence, from Figure 50 it can be interpreted that majority of the k-values were within one standard deviation. Overall Case R-M121 produced the highest tensile stresses for the

middle loading path but the change was only a 3% increase in the overall peak tensile stress moving from case M1 to R-M121. The maximum tensile stress occurred at the bottom of the slab during daytime curling. The tandem and the steer drive axles were critical for this case with similar magnitude of tensile stresses. All critical stresses are at the transverse edge which can be expected to be significantly reduced in the presence of a dowelled contraction joint.

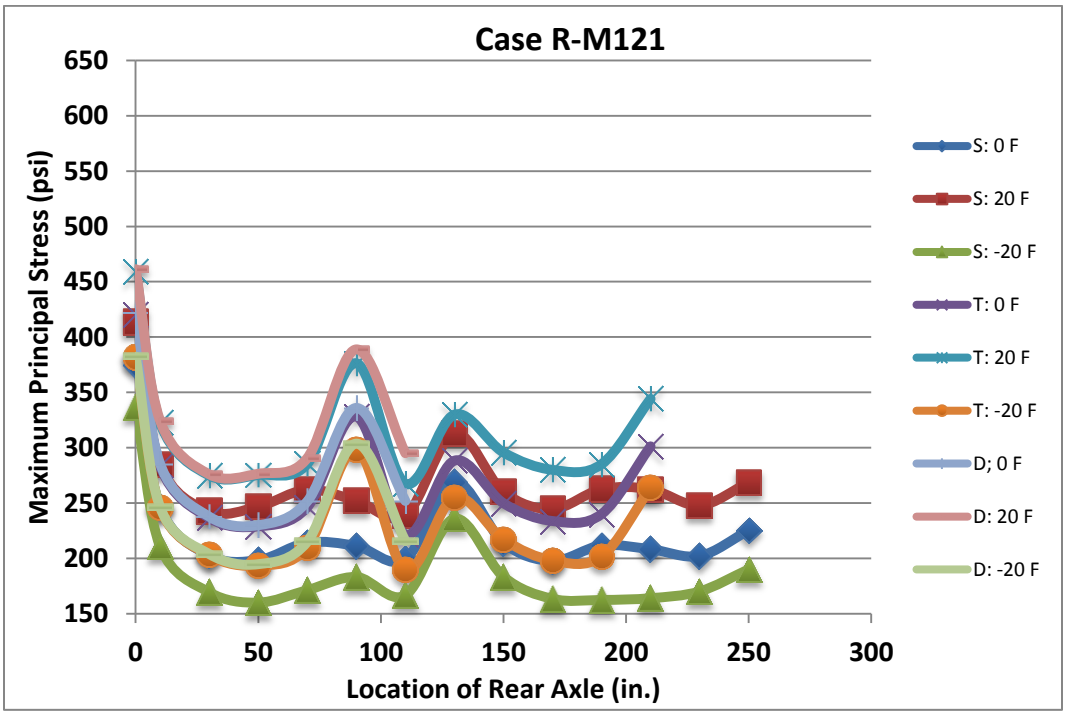

Figure 48: Maximum principal (tensile) stress for Case R-M121 versus axle position

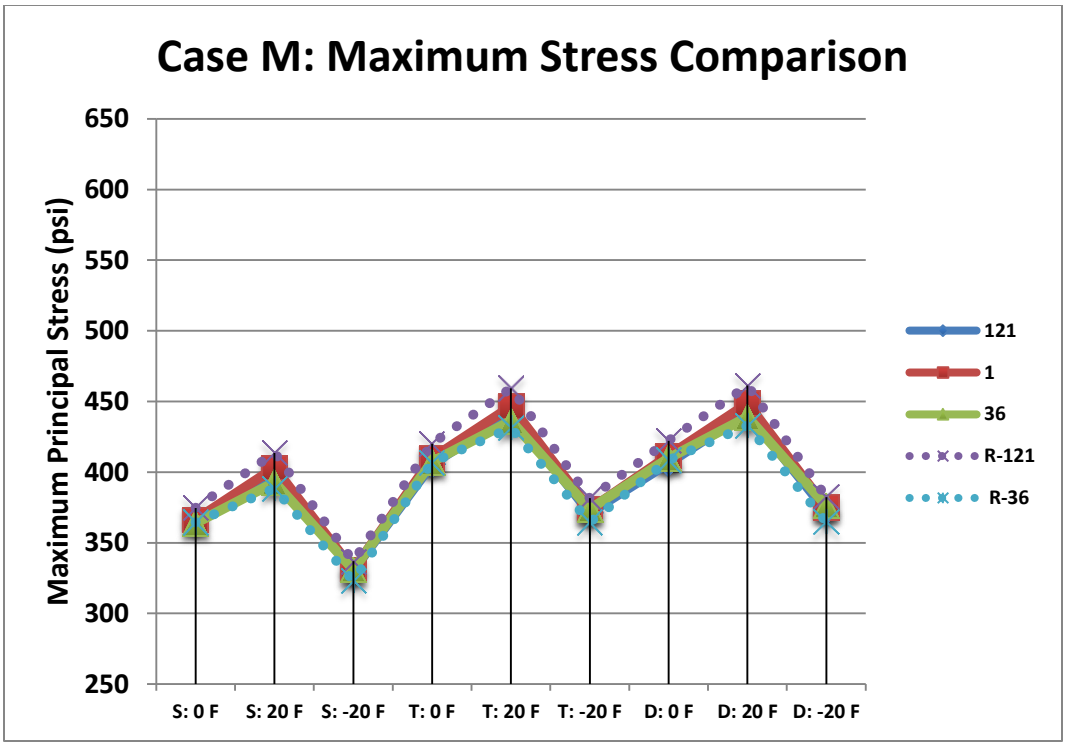

Figure 49: Comparison of the peak tensile stresses for Case M for each input factor level and the 5 non-uniform support distributions

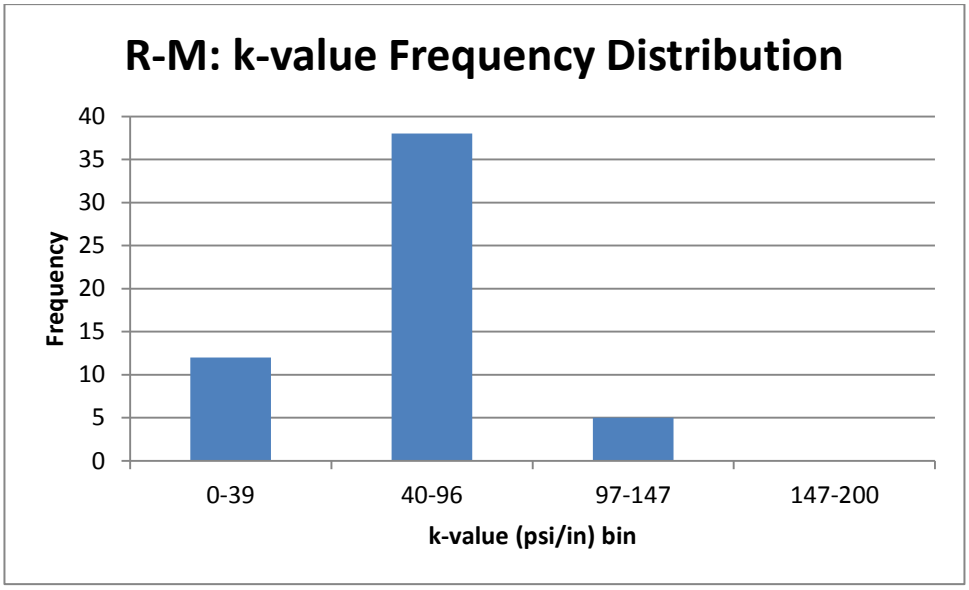

Figure 50: k-values for case R-M121 from MI I-94 roadway

3.3.3 Stress Analysis of Randomly Assigned Support Stiffness for Right Wheelpath (R-RW) and Left Wheelpath (R-LW) Cases

Figure 51 and Figure 52 represent loading path cases RW and LW, respectively along the right and left wheel path. As expected, the magnitude of tensile stresses recorded at the each longitudinal position for case R-RW36 and R-LW36 are lower than the free edge cases (R-RE36 and R-LE36). The maximum tensile stresses along the right and left wheel path occur on different slabs. However, the three axle types produced similar maximum stresses, i.e., within 5 to 7%, for both wheel paths as seen in Figure 53 and Figure 54. The peak tensile stress occurred at the bottom of the slab during daytime curling for the right wheel path. However, for the left wheel path the maximum stress occurs at the top of the slab during nighttime curling but at the initial loading position (transverse free edge condition). The maximum tensile stresses at each longitudinal position for cases R-RW121 and R-LW121 are included in the appendix. As seen in Figure 53 and Figure 54, the random assignment of 36 k-values significantly increased the maximum tensile stresses relative to the randomly assigned 121 k-values, i.e., 14% increase in the average peak tensile stress for both R-RW and R-LW cases.

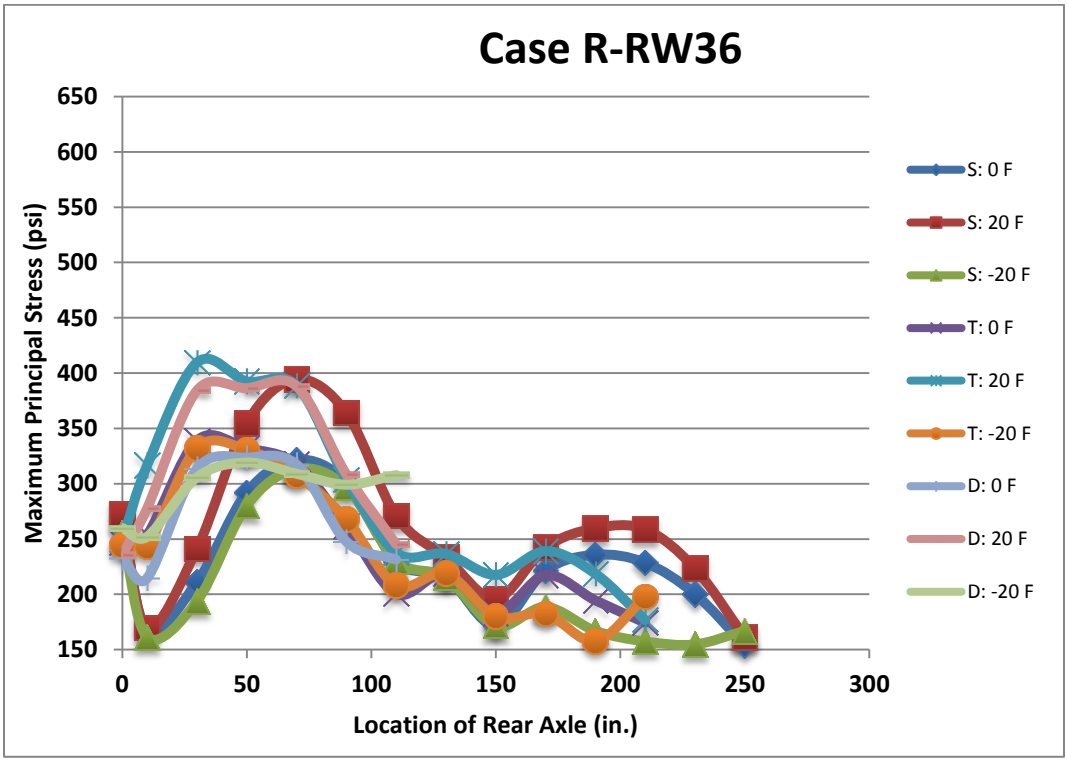

Figure 51: Maximum principal (tensile) stress for Case R-RW36 versus axle position

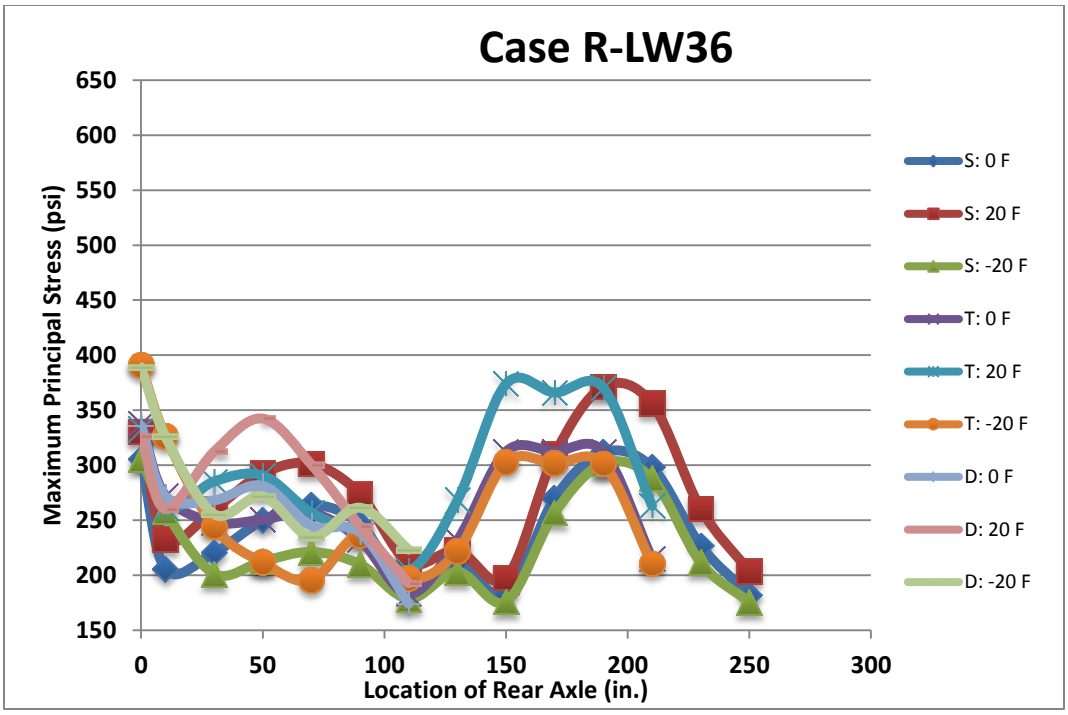

Figure 52: Maximum principal (tensile) stress for Case R-LW36 versus axle position

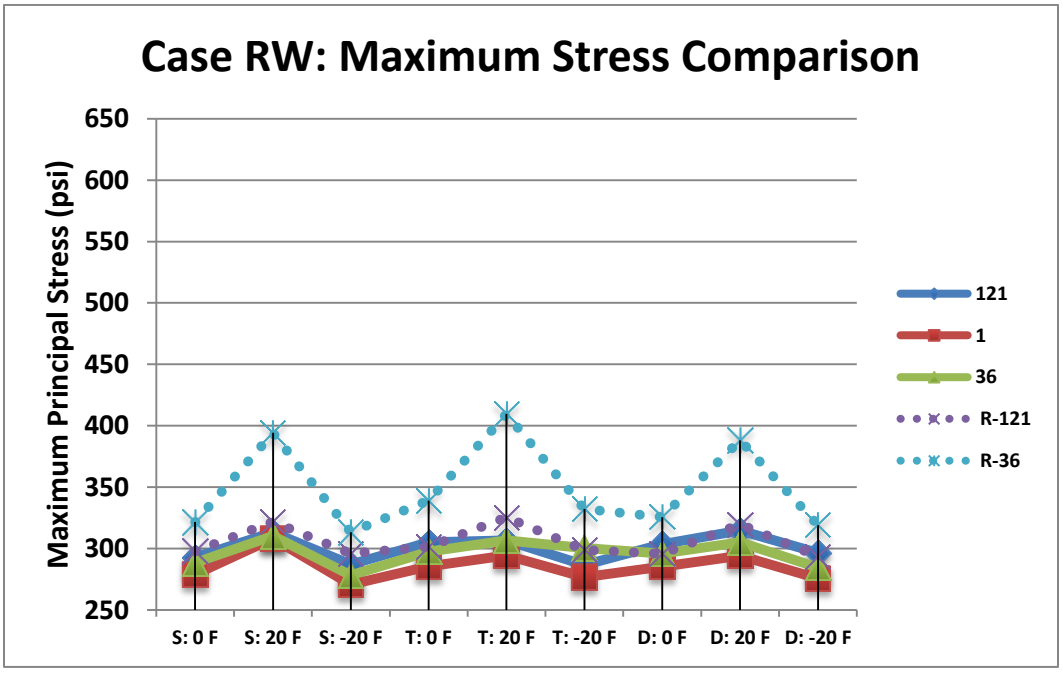

Figure 53: Comparison of the peak tensile stresses for Case RW for each input factor level and the 5 non-uniform support distributions

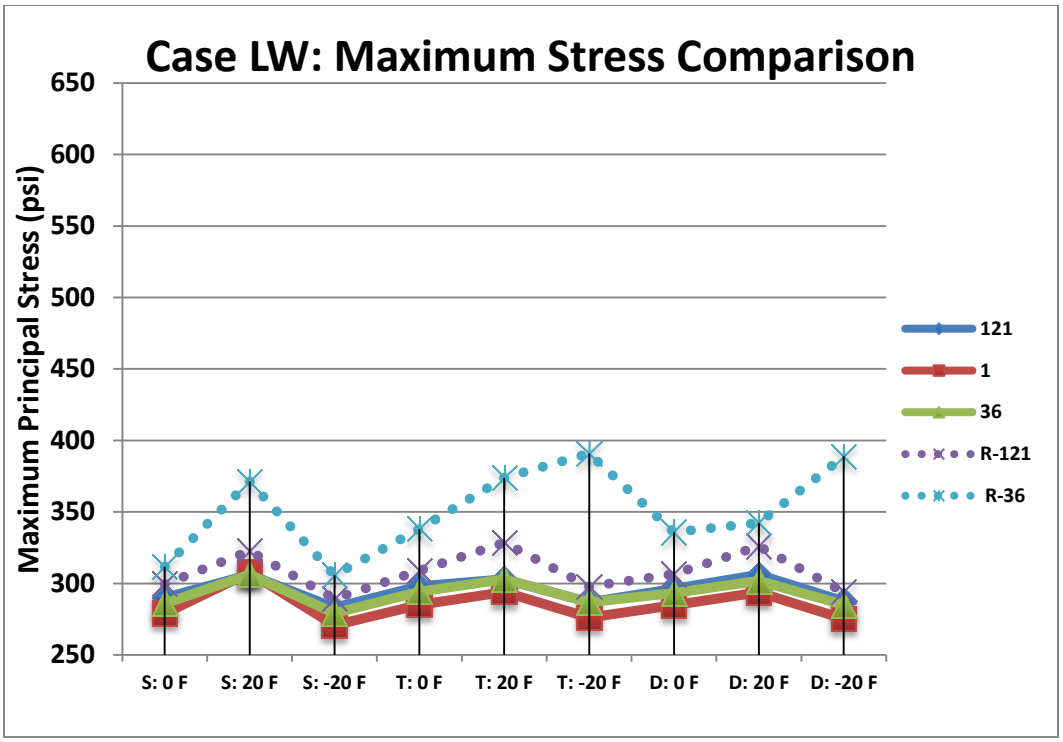

Figure 54: Comparison of the peak tensile stresses for Case LW for each input factor level and the 5 non-uniform support distributions

Clearly random assignment of the expected distribution of k-values produced greater tensile stresses in the slab, as seen in Figure 55, compared to the deterministic analysis which assigned k-value based on the spatially collected field data. With random assignment of the support stiffness, the individual size of uniform areas of stiffness affected the peak tensile stress in the concrete slab. As seen in Figure 55, larger areas of uniform stiffness (1.16 x 1.16 m^2), i.e., 36 k-values, generated substantially higher tensile stresses as compared to smaller areas (0.7 x 0.7 m^2), i.e., 121 k-values, or even a uniform area (single k-value) support condition. The defined area size of uniform k-value was especially sensitive for the longitudinal edge loading paths with the right edge producing the greatest tensile stress for the randomly assigned 36 k-value option IV. Comparing Table 9, case R-RE36 had a 37% increase in the average peak tensile stress compared to the loading on a uniform support and 31% increase in the overall peak tensile. Although there was a 33% increase in overall peak tensile stress between R-RW36 compared to uniform support, the magnitude of tensile stresses 409 psi (R-RE36) and 308 psi (RE1)

were not critical. For the middle of the lane loading path, the area size of pre-defined subgrade stiffness was not a factor in the peak tensile stresses.

Daytime curling conditions combined with axle loading produced the greatest tensile stresses in the slab except for case R-LW36, which occurred at the first loading position. As shown in Table 10, the peak tensile stresses were at the bottom of the slab for all the cases except for R-LW36. As in the deterministic analysis of the measured field data, the longitudinal edges produced the most critical loading locations. With respect to the axle configurations, there was not one axle that always produced the highest tensile stress which was significantly greater than the other two axles. The frequency distribution for case R-121 and R-36, shown in Figure 56 resembles a normal distribution for both the cases. The important thing to note in Figure 56 is that R-36 has 7% more k-values in the bin range of 0-40 psi/in with some values as low as 1 psi/in as reported earlier suggesting the presence of more softer areas than R-121. R-121 had a mean of 65 psi/in, standard deviation 27.4 psi/in with a coefficient of variation of 42% and case R-36 has a mean of 61 psi/in, standard deviation of 29.3 psi/in and coefficient of variation of 48%. The combination of lower k-value magnitudes along the free edges coupled with the larger area size with 36 independent k-values led to case R-36RE producing the most critical tensile stress (608 psi).

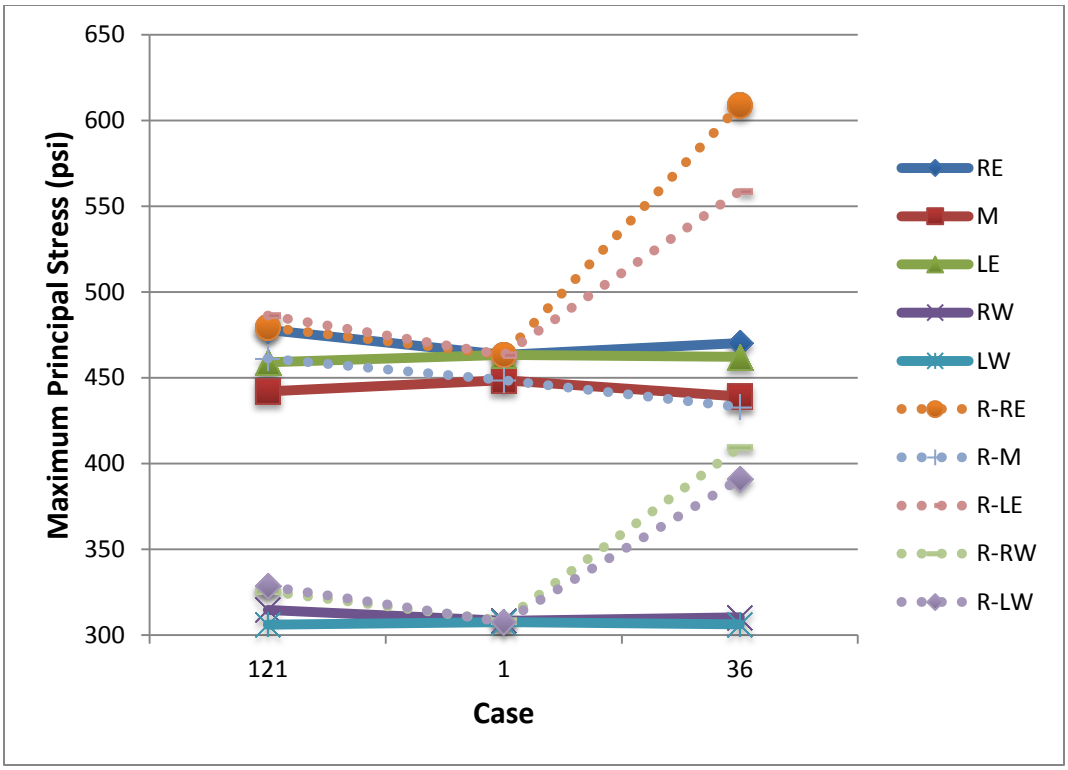

Figure 55: Comparison of overall peak tensile stress for each load location with different non-uniform subgrade support conditions for roadway MI I-94

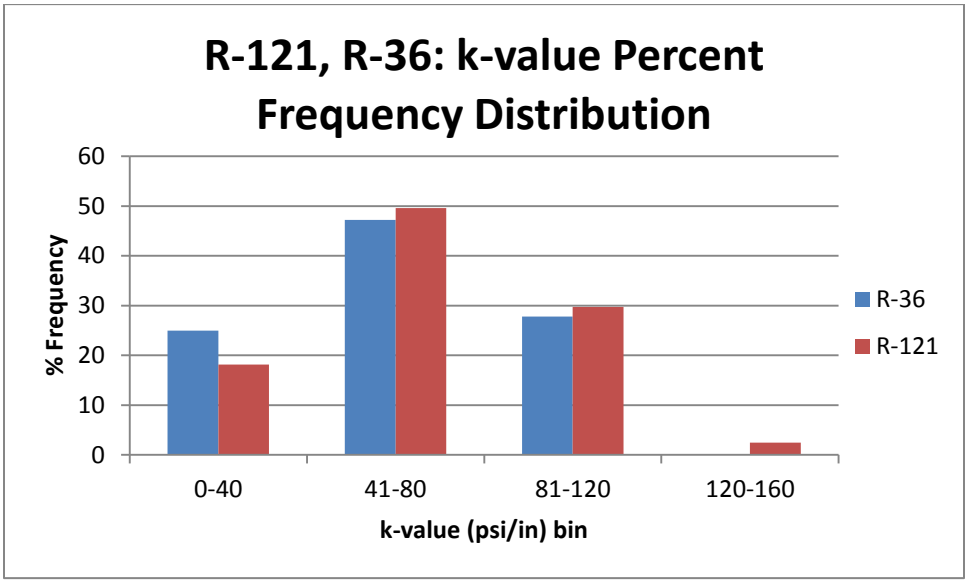

Figure 56: Percent frequency distribution of k-values for case R-121

Table 9: Summary of the percent change in overall and average peak tensile stress from random assignment of 36 k-value areas relative to uniform subgrade for each loading path

Loading Path	Change in Overall Peak Tensile Stress	Change in Average Peak Tensile Stress
Case RE (Right Lane Edge)	+31%	+37
Case M (Middle of Lane)	-3%	-2
Case LE (Left Lane Edge)	+21%	+28
Case RW (Right Lane Wheelpath)	+33%	+22
Case LW (Left Lane Wheelpath)	+27%	+23

Table 10: Location and magnitude of critical tensile stress for each factor level analyzed on MI I-94 randomly generated support stiffness

Case	Single Axle			Tandem Axle			Steer Drive Axle		
	0 F	20 F	- 20 F	0 F	20 F	- 20 F	0 F	20 F	- 20 F
R-RE121	425 (0,195,b)	479 (0,195,b)	374 (0,195,b)	390 (0,223,b)	443 (0,223,t)	376 (49,275,t)	389 (0,179,b)	431 (0,199,b)	416 (0,79,t)
R-RE36	512 (0,75,b)	591 (0,75,b)	510 (0,75,b)	532 (0,83,b)	608 (0,83,b)	532 (0,83,b)	507 (0,75,b)	584 (0,75,b)	507 (0,75b)
R-LE121	437 (275,75,b)	486 (275,195,b)	406 (275,75,b)	404 (275,83,b)	447 (275, 83,b)	400 (227,0,t)	381 (275,75,b)	425 (275,199,b)	403 (227,0,t)
R-LE36	495 (275,195,b)	558 (275,195,b)	488 (275,195,b)	493 (275,195,b)	557 (275,203,b)	494 (219,0t)	453 (275,199,b)	518 (275,199,b)	496 (219,0,t)
R-M121	374 (185,0,b)	413 (185,0,b)	336 (185, 0,b)	420 (185, 0,b)	459 (185,0,b)	381 (185, 0,b)	422 (185,0,b)	461 (185, 0,b)	382 (185,0,b)
R M36	364 (89,0,b)	388 (89,0,b)	323 (89,0,b)	406 (89,0,b)	431 (89,0,b)	364 (89,0,b)	408 (89,0,b)	432 (89,0,b)	364 (89,0,b)
R-RW121	297 (22,0,b)	321 (22,0,b)	295 (22,0,b)	301 (22,0,b)	325 (22,0,b)	298 (22,0,b)b	295 (22,0,b)	319 (22,0,b)	293 (0,83.7t)
R-RW36	321 (20,75,b)	394 (20,75,b)	313 (20,75,b)	339 (20,81,b)	409 (20,81,b)	332 (20,81,b)	323 (20, 55,b)	388 (20,75,b)	319 (20,101,b)
R-LW121	299 (157,0,b)	322 (255,75,b)	289 (157,0,b)	308 (157,0,b)	328 (157,0,b)	297 (157,0,b)	306 (157,0,b)	326 (157,0,b)	294 (157,0,b)
R-LW36	311 (255,195,b)	371 (255,195,b)	305 (211,0,b)	337 (211,0,t)	373 (255,203,b)	391 (209,0,t)	335 (211,0,t)	342 (255,199,b)	388 (209,0,t)
RE1/LE1	419 (0,195,b)	463 (0,175,b)	376.7 (0,195,b)	381 (0,175,b)	417 (0,55,b)	364.3 (42,0,t)	376.7 (0,179,b)	408.0 (0,179,b)	368.7 (44,0,t)
M1	366 (89,0,b)	403 (89,0,b)	330 (89,0,b)	409 (89,0,b)	446 (89,0,b)	373 (89,0,b)	411 (89,0,b)	448 (89,0,b)	374 (89,0,b)
RW1/LW1	279 (117,0,b)	308 (20,75,b)	270 (117,0,b)	285 (117,0,b)	294 (117,0,b)	276 (117,0,b)	285 (117,0,b)	294 (117,0,b)	275 (117,0,b)

b: Bottom; t: Top

3.4 MI I-94: Beta Distribution Assignment of Support Condition

The results of the analysis of the non-uniform subgrade support with random assignment of k-values showed that extremely weak areas, e.g., k-values = 1 psi/in, are linked to large tensile stress changes in the slab. Based on the normal distribution assumption and field data, the likelihood of such a low k-value is in the 1 percentile range. In order to limit the probability of unrealistic k-values, e.g., less than 0 psi/in, a beta distribution function was to provide a lower limit boundary. The probability density function of the beta distribution is described by the following equation (41):

$$f(x) = \frac{1}{B(\alpha,\beta)} \frac{(x-a)^{\alpha-1}(b-x)^{\beta-1}}{(b-a)^{\alpha+\beta-1}} \quad 3.1$$

where α and β are shape parameters and B(α,β) is the beta function with domain [0,1] and *a*, *b* are continuous boundary parameters (*a*<*b*). The lower limit k-value was set at *a= 20* psi/in, which was within two standard deviations of the mean of the field data set and the upper limit was *b*= 202 psi/in (highest k-value obtained from field data). By knowing the mean (μ) and variance (σ^2) of the deterministic field data, the shape factors can be determined (α= 1.9 and β=6) by solving the equations 3.2 and 3.3 below (41). Figure 57 shows the beta distribution selected for the field correlated k-values.

$$\mu = \frac{\alpha}{\alpha+\beta} \quad 3.2$$

$$\sigma^2 = \frac{\alpha\beta}{(\alpha+\beta)^2+(\alpha+\beta+1)} \quad 3.3$$

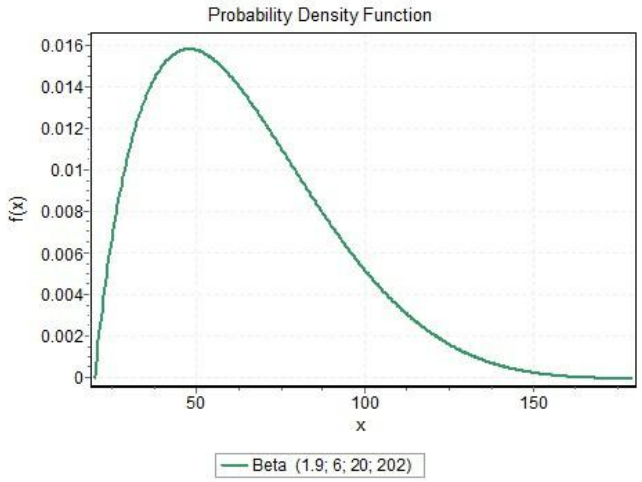

Figure 57: Beta distribution of field correlated k-values

The conclusions from the previous two sets of analysis showed that the right and left edge loading paths were critical and thus the wheel path and middle of lane cases were not analyzed with the beta distribution k-value assignment. The analysis did include the three different axle configuration and temperature differentials. A random number generator was used to assign k-values to 36 discretized areas of 1.16x1.16 m^2, as shown in Figure 58, using the above defined beta distribution. Five different distributions of k-value were generated and only the distribution deemed to give the higher tensile stresses was kept for further analysis. For nomenclature, a prefix of "B" is added to the sub-cases to distinguish from the original deterministic and random assignment of k-value despite the beta distribution assignment also being "random."

Case B-RE36 would be movement of the vehicle along the right lane edge in Figure 59 that shows the results of the tensile stresses recorded at the each longitudinal position for case B-RE36 with the magnitude of stresses being similar to the original field data case RE36 as seen in Figure 60. This is due to the change in adjacent stiffness areas were not as drastic (i.e. around a factor of two) as compared with the random assignment with the normal distribution shown in Figure 39. The mean k-value of B-RE36 was 85 psi/in with a standard deviation of 33.9 psi/in, which was similar to RE121's mean of 86 psi/in and standard deviation of 50 psi/in. The relatively similar peak tensile stress behavior suggested that a small change between adjacent k-value areas, e.g., factor of 2 in Figure 58, causes small stress variations but fails to produce the same tensile stress

increase of 31% as in case R-RE36. For the random assignment with the beta distribution, the peak tensile stress was at the bottom of the slab during daytime curling. Single axle caused the highest stress for this case with the tandem and steer drive axle behaving similar in magnitude, i.e., 10% less than the single axle.

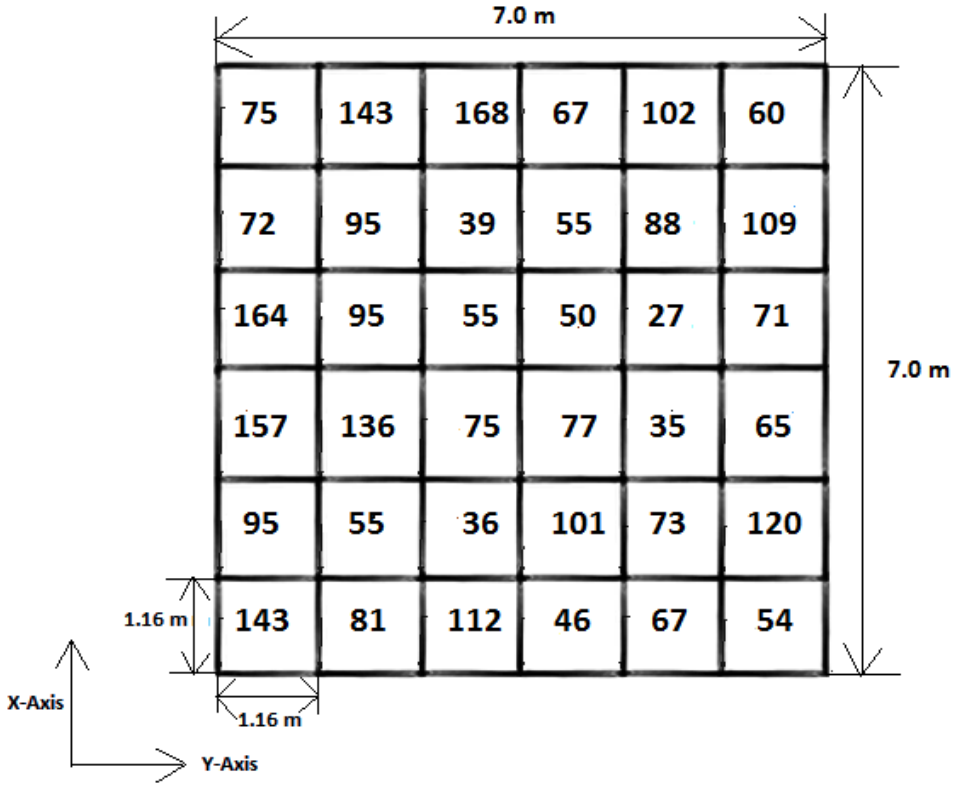

Figure 58: Case B-36 with 36 discretized k-value areas

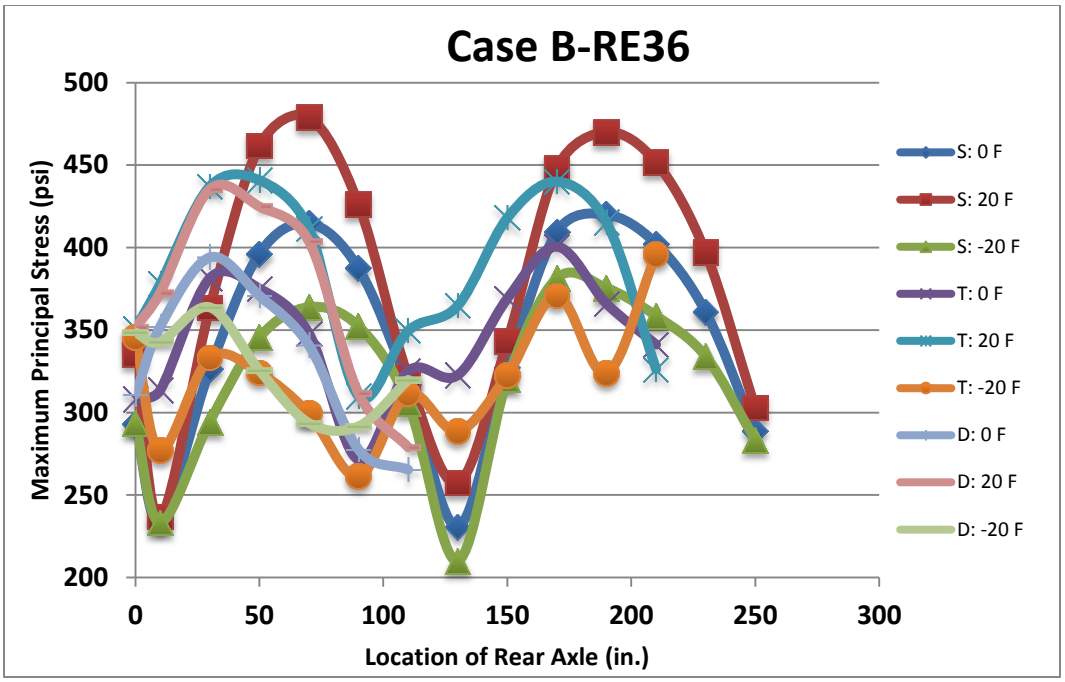

Figure 59: Maximum principal (tensile) stress for Case B-RE121 versus axle position

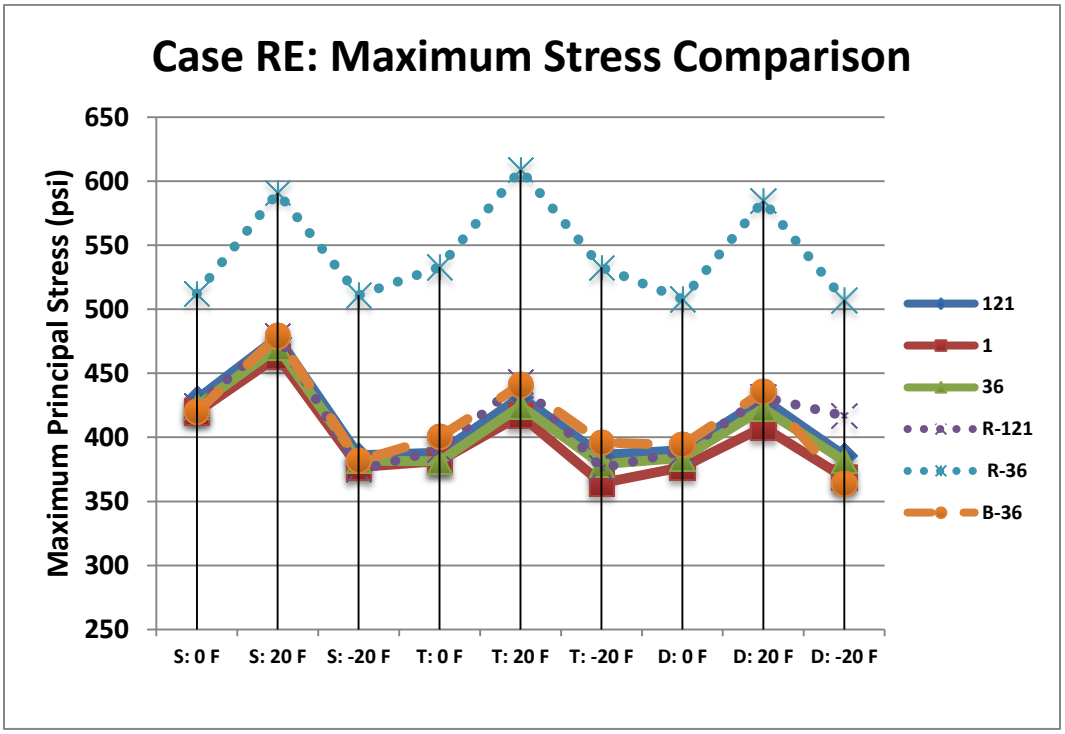

Figure 60: Comparison of the peak tensile stresses for Case RE for each input factor level and the 6 levels of non-uniform support

Case B-LE36 represents the longitudinal movement of the vehicle along the left edge of the slab. Figure 61 shows the results of the maximum tensile stresses recorded at each longitudinal position were slightly lower in magnitude than case B-RE36. The peak tensile stresses of B-RE36 were 8% higher than B-LE36 as seen in Table 11. Figure 63 shows that the k-value for both the edges do not show a uniquely different pattern and confirm why the tensile stresses for the two loading paths were similar. Case B-LE had a slightly higher mean of 103 psi/in than B-RE with 84 psi/in. The effect of a higher standard deviation of 40.3 psi/in for B-LE was negated by its larger mean. The magnitudes of the peak tensile stresses were similar to corresponding field data case LE-36 as seen in Figure 62. The behavior of the all the axle configurations was similar with single axle causing slightly higher peak tensile stress. The critical tensile stress occurs at the bottom of the slab during day time curling. Although there were adjacent areas with relatively high variation in k-value, i.e., 168 to 39 psi/in, the tensile stress changes were not as great as with very low support stiffness at the critical load location with adjacent stiffer support, e.g. see Figure 39 and Figure 43.

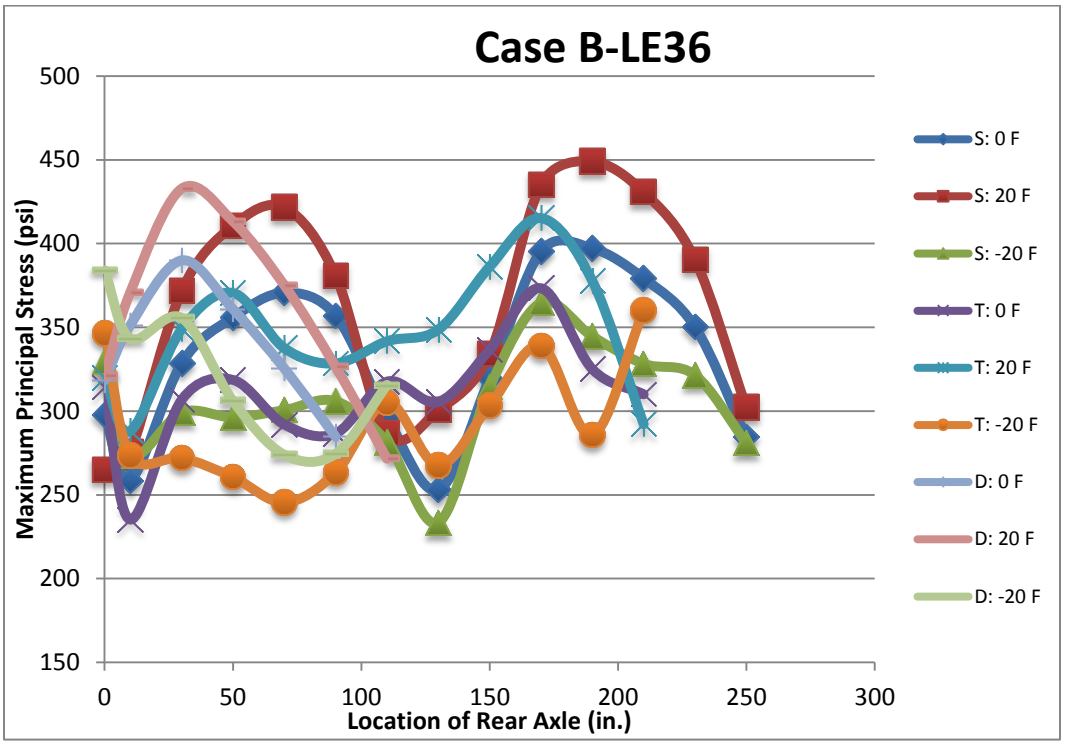

Figure 61: Maximum principal (tensile) stress for Case B-LE121 versus axle position

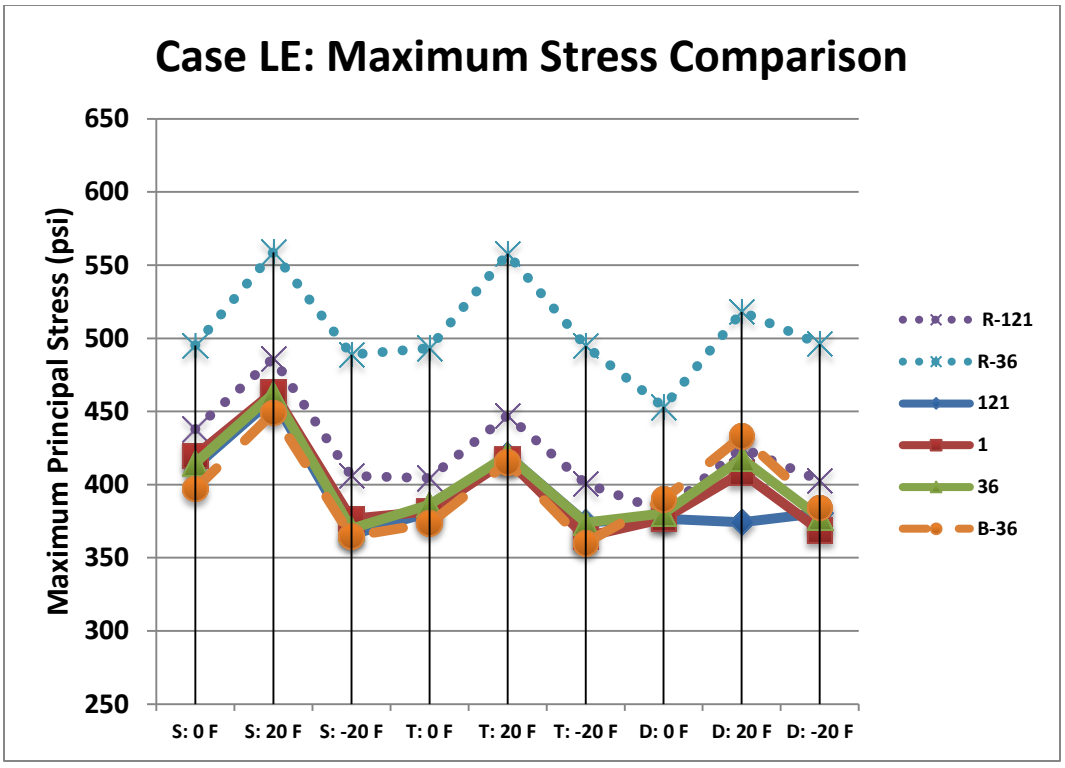

Figure 62: Comparison of the peak tensile stresses for Case LE for each input factor level and the 6 levels of non-uniform support

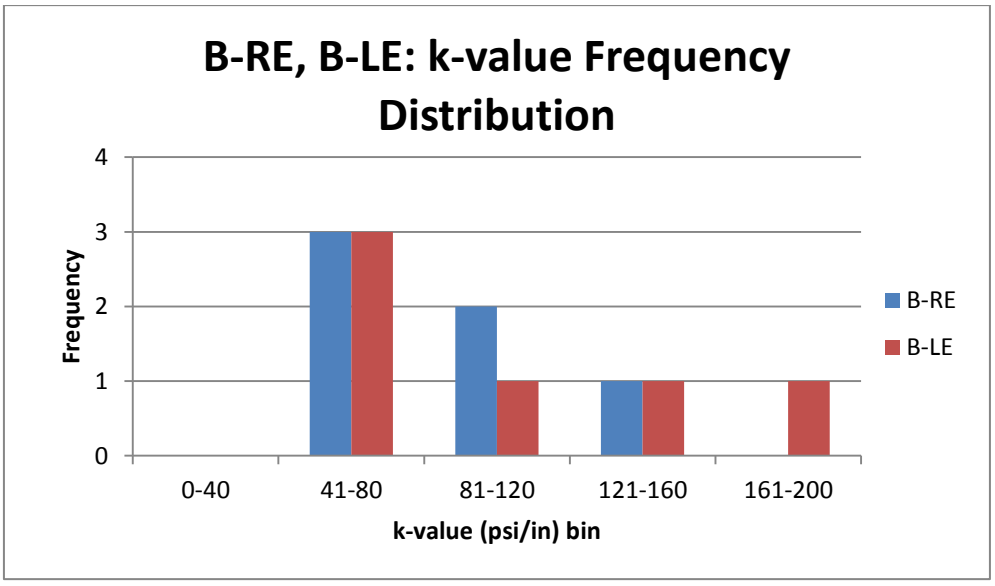

Figure 63: k-values for case B-RE and B-LE for MI I-94 roadway

Table 11: Location of peak tensile stresses for randomly assigned k-value with beta distribution for MI I-94

Case	Single Axle			Tandem Axle			Steer Drive Axle		
	0 F	20 F	- 20 F	0 F	20 F	- 20 F	0 F	20 F	- 20 F
B-RE36	420 (0,195,b)	479 (0,75,b)	381 (0,175,b)	400 (0,175,b)	440 (0,55,b)	395 (51,275,t)	394 (0,179,b)	435 (0,180,b)	363 (0,179,t)
B-LE36	397 (275,195,b)	448 (275,195,b)	364 (275,75,b)	373 (275,175,b)	415 (275,175b)	360 (223,275,t)	389 (275,179,b)	432 275,79,b)	384 (275,79,t)

b=Bottom of slab; t=Top of slab

The result of carrying out a beta distribution assignment proved having extremely soft spots, e.g., k-value of 1 psi/in as in case R-RE36, were detrimental to the concrete slab in the presence of an adjacent higher k-value area. Increasing the k-value along the edge lowered the magnitude of peak tensile stresses even with adjacent non-uniform stiffness. Due to the low probability of occurrence of low k-values the beta distribution showed that minimum stiffness values for the support conditions can avoid future high tensile stress concentrations.

3.5 MI I-96: Field Data of Support Condition

3.5.1 MI I-96 Project Background

The field analysis was extended to another site in Michigan, along the I-96 roadway. In-situ testing was carried out in a similar manner to the test sections of MI-I96. The subgrade was is an A-4 ML, a medium plasticity silt according to the AASHTO soil classification. The pavement structure to be constructed was 11.5 in. PCC, 5 in. cement-stabilized open-graded drainage course, and 11 in. sand subbase on top of the subgrade. The subbase was a poorly-graded sand, which resulted in it having lower CBR values than the subgrade. The in-situ testing consisted of intensive testing on a spatial test bed comprising of 8 x 8 m^2 plot as shown in Figure 64. The test locations are represented in the form of nodes spaced at approximately 1m from each other in both the longitudinal and transverse direction. DCP tests were carried out on top of the sand subbase layer

underlain by subgrade. CBR values were obtained at each nodal location based on the dynamic penetration index as seen in equation 2.1. DCP test were carried out at all nodal location except for the ones marked with black dots in Figure 64. The moisture content of each test location was known based on nuclear moisture density gauge (NG). A linear relationship was developed between moisture content and CBR at all the nodal locations except for the eight unknown CBR nodes. Based on this linear relationship, the CBR at the locations without DCP tests were estimated. The limitation of such a procedure is noted but due to lack of specific field data for k-value such assumptions were made. Based on these nodal CBR values, k-values were correlated based on the empirical equation 2.8. As no PLTs were carried on this roadway section, an empirical correlation for CBR to k-values specific to this test section could not be made. Hence, based on geographical proximity and to provide a base of comparison between the two roadway sections, i.e., MI I-94 versus MI I-96, equation 2.8 was used for deriving the support conditions. There were 81 CBR values which were correlated to k-values (see appendix). As the conclusions from the MI I-94 analysis suggested that an area of approximately 1m was critical for stress development and based on the spacing of the in situ testing locations being 1m apart on a slab geometry of 8x8 m^2, the discretized support case was developed. The 81 k-values with its assigned areas of 1x1 m^2 were called case 81 as shown in Figure 65.

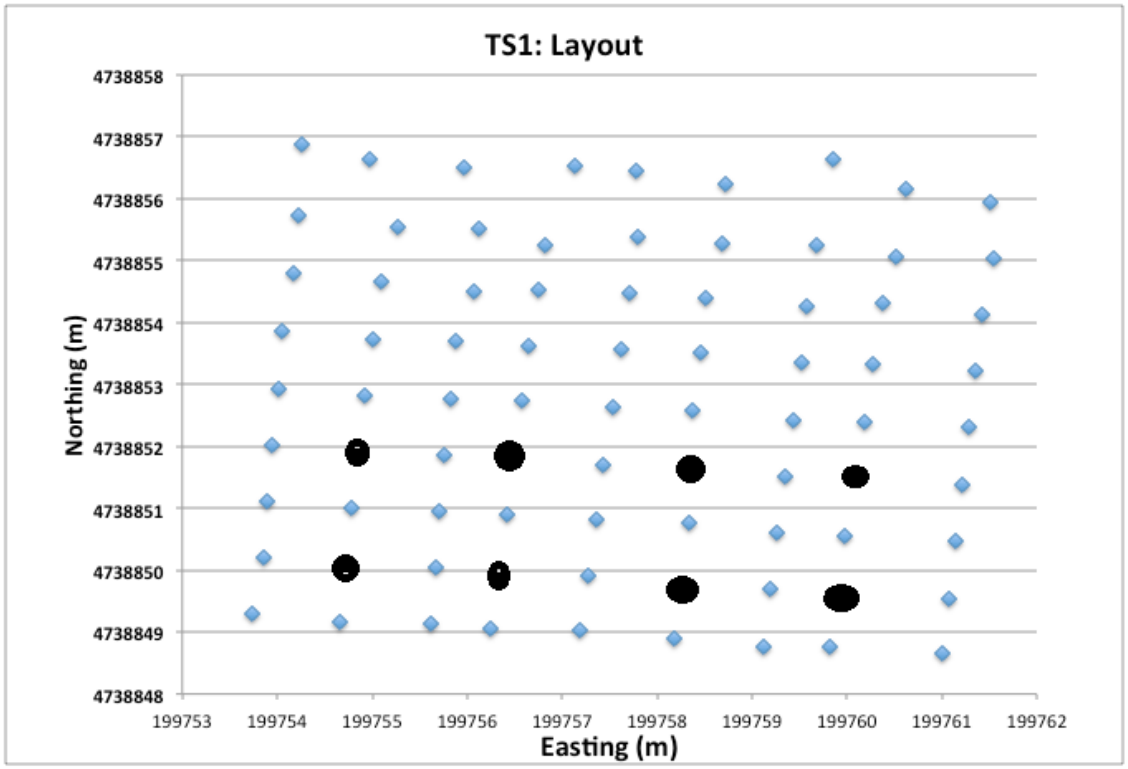

Figure 64: Coordinates of DCP tests for test section 1 (TS1) on MI I-96

The frequency distribution of the field correlated k-values, seen in Figure 66, shows that MI I-96 is a distinctly stiffer subgrade as compared to MI I-94. Figure 66 shows the subgrade stiffness distribution for case 81 was skewed left of the mean but still very good k-values for pavement construction. The range of the k-values for MI I-96 is 235-713 psi/in, a mean of 397 psi/in and a standard of variation of 95.1 psi/in. The coefficient of variation of k-values in the dataset is 24%. Hence, this roadway section is a good case to compare with MI-I94 which was a significantly softer subgrade support. The directions of x and the y axes have been reversed form the conventional Cartesian coordinate system to conform to the coordinate system in ISLAB2000. The second support condition analyzed was the uniform case A1, which was based on averaging the 81 k-values (397psi/in) as seen in Figure 67. The prefix "A" is used to avoid ambiguity with the uniform support condition of MI I-94.

The input parameters for the stress analysis are the same as used for MI I-94 shown in Table 2. Three axle configurations (single, tandem and steer drive) are used for loading of the slab subject to three linear temperature differentials: 0°F, 20°F and -20°F,

as was used for analyzing MI I-94. However, based on the conclusions of MI I-94 analysis wheelpath loading cases were not considered since they never produced the peak tensile stress for a set of inputs.

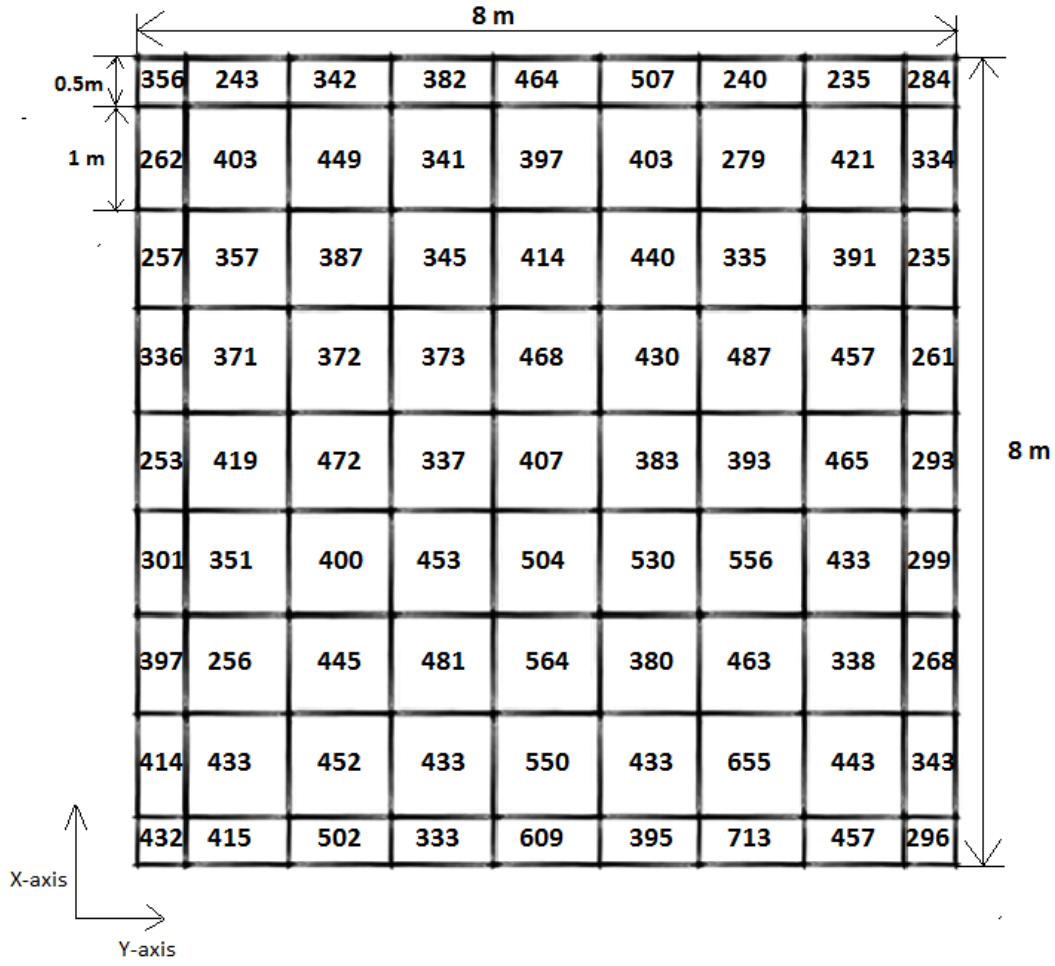

Figure 65: Case 81 with 81 discretized k-value areas assigned to test section 1 of MI I-96 roadway

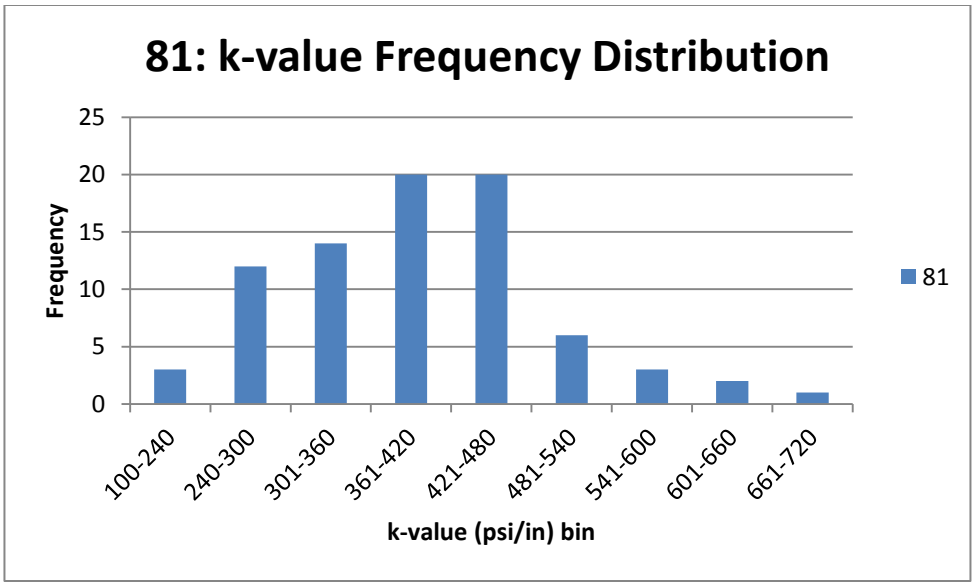

Figure 66: Frequency distribution of k-values for case 81

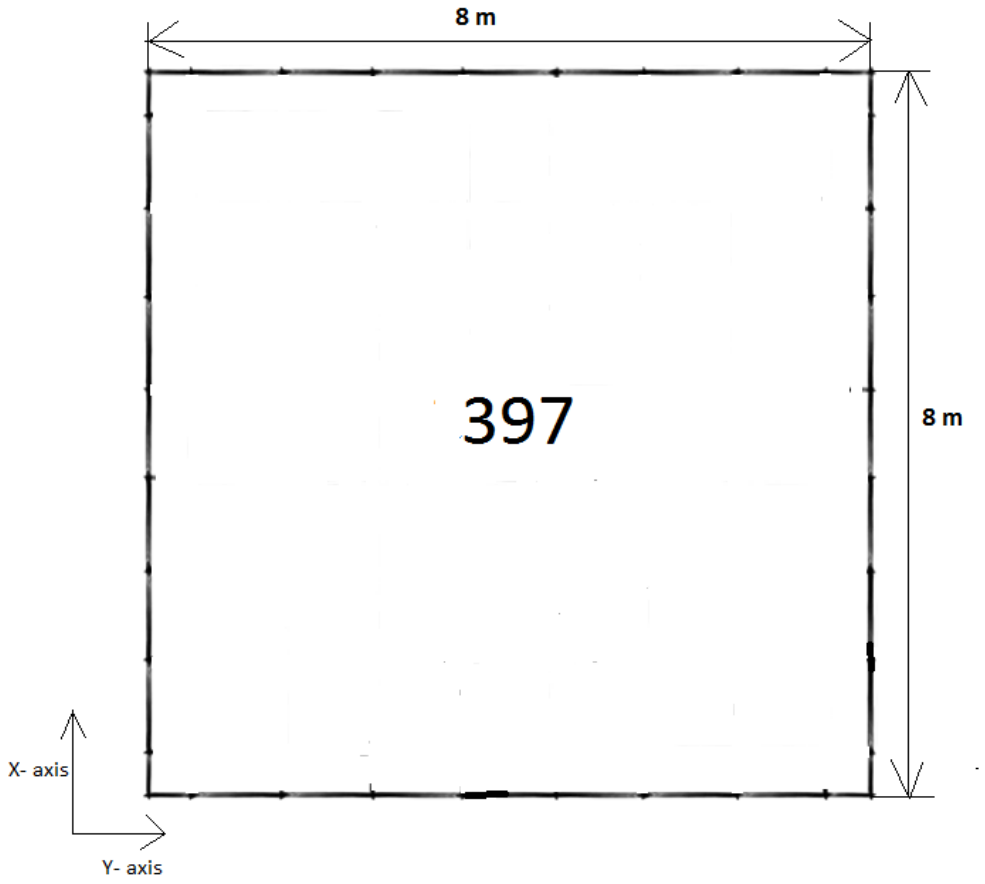

Figure 67: Case A1 with single, uniform k-value area assigned to TS1 on MI I-96 roadway

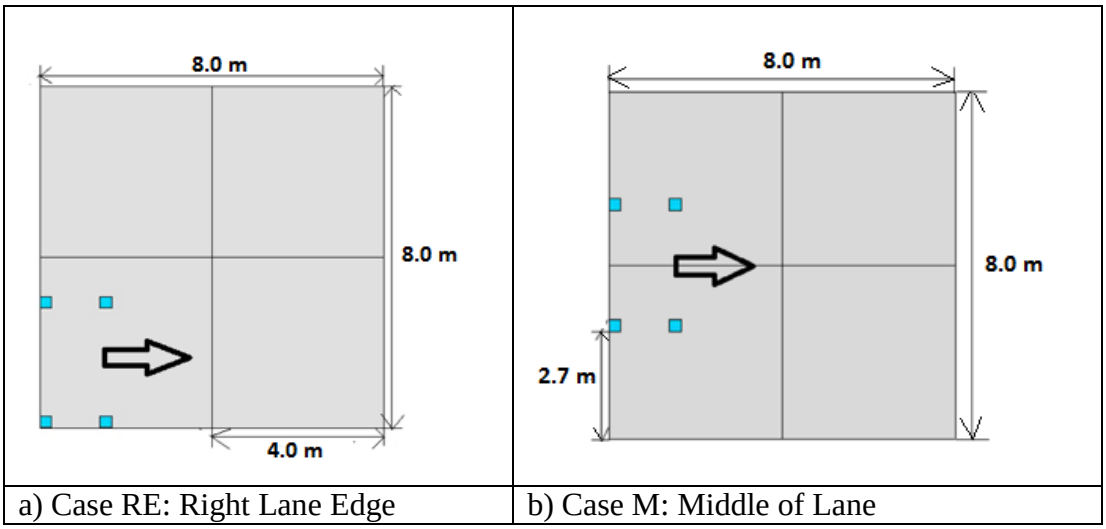

a) Case RE: Right Lane Edge

b) Case M: Middle of Lane

c) Case LE: Left Lane Edge

Figure 68: Axle loading location and paths for analysis of MI I-96 field data

Figure 68 shows the three loading paths for the three axles used to longitudinally traverse the slab. The slab geometry was slightly modified from MI I-94. The support measurements were over an 8x8 m^2 (~ 26x26 ft^2) area and the four slab assembly 4x4 m^2 (~ 13x13 ft^2) was used to assess the effects of the non-uniformity. This slab geometry was adopted for analysis purpose primarily to encompass the entire field data measurements. The distinction between left lane and right lane is made with respect to the longitudinal direction. The three axle types are the same as in Figure 11. The axles start at the transverse free edge with the first movement at 10 in. (0.25 m) followed by subsequent loading locations at 20 in. intervals with respect to the rear axle. Based on the

dimensions of the slab and axles, the single axle needs 17, the tandem requires 14 and steer drive 9 loading locations to simulate movement of the axle across the 8 m section as seen in Figure 68. The nomenclature designating the axle types and temperature differential (see Table 3) remains the same as the MI I-94 field analysis.

3.5.2 Slab Tensile Stress Results for Deterministically Assigned Field Data Measurements

3.5.2.1 Stress Analysis of Right Edge (RE) Case for MI I-96 Roadway

Case RE81 represents the longitudinal movement of the vehicle along the right lane edge of the slab. Figure 70 shows the results of the peak tensile stresses recorded at each axle position. The overall peak tensile stress was near the midslab location for both slabs with slightly varying magnitudes (approximately 5%) on account of different local stiffness. Two important distinctions for MI I-96 is that it is a stiffer subgrade support and the individual slabs are 0.5 longer and wider relative to the MI I-94 analysis.

The percent change in k-value is not as great for the MI I-96. The MI I-96 has a k- value range of approximately 500 psi/in, which is 2.5 times the maximum k-value for MI I-94 section. The peak tensile stress at the mid-slab location on the first slab is primarily due to the presence of a lower stiffness area next to an adjacent higher stiffness area (502 psi/in and 333 psi/in) as seen in Figure 69 which controls for all three axle types with daytime curling conditions. Although the single axle produced the peak critical stress, the peak tensile stress for the tandem and steer drive during daytime curling were within 5% of each other. Even with a large range in k-value (case A81), the peak tensile stresses are very similar in magnitude to the uniform subgrade support case A1 as seen in Figure 71. The overall peak stress change from uniform to Case A81 decreased 1% while the average peak stress increased by 1%. The maximum tensile stresses at each longitudinal position for case REA1 is in the appendix.

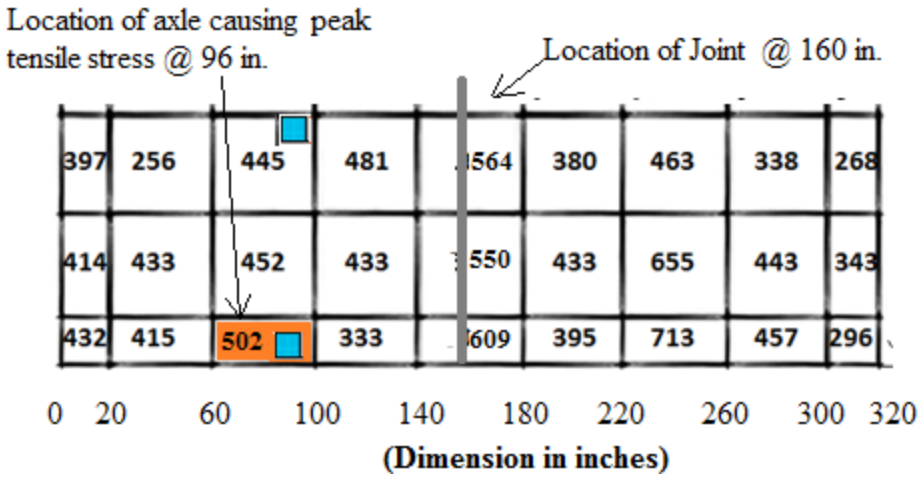

Figure 69: Local variation in k-values along right hand edge of the slab for case RE81

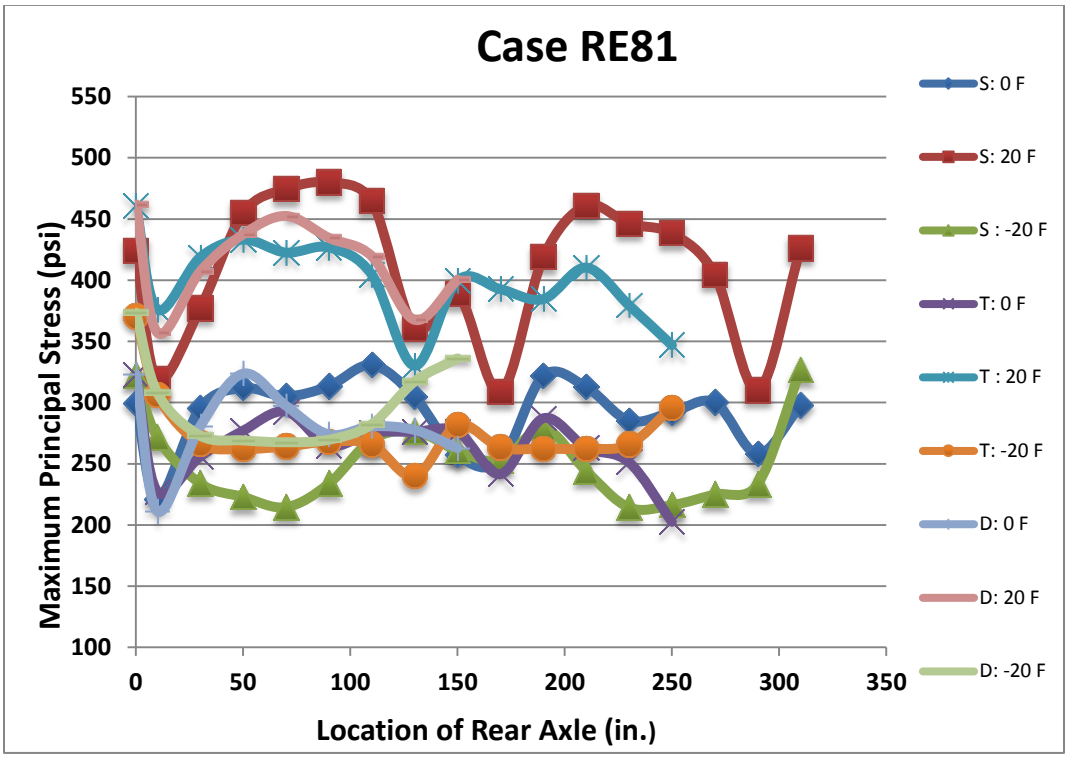

Figure 70: Maximum principal (tensile) stress for Case RE81 versus axle position

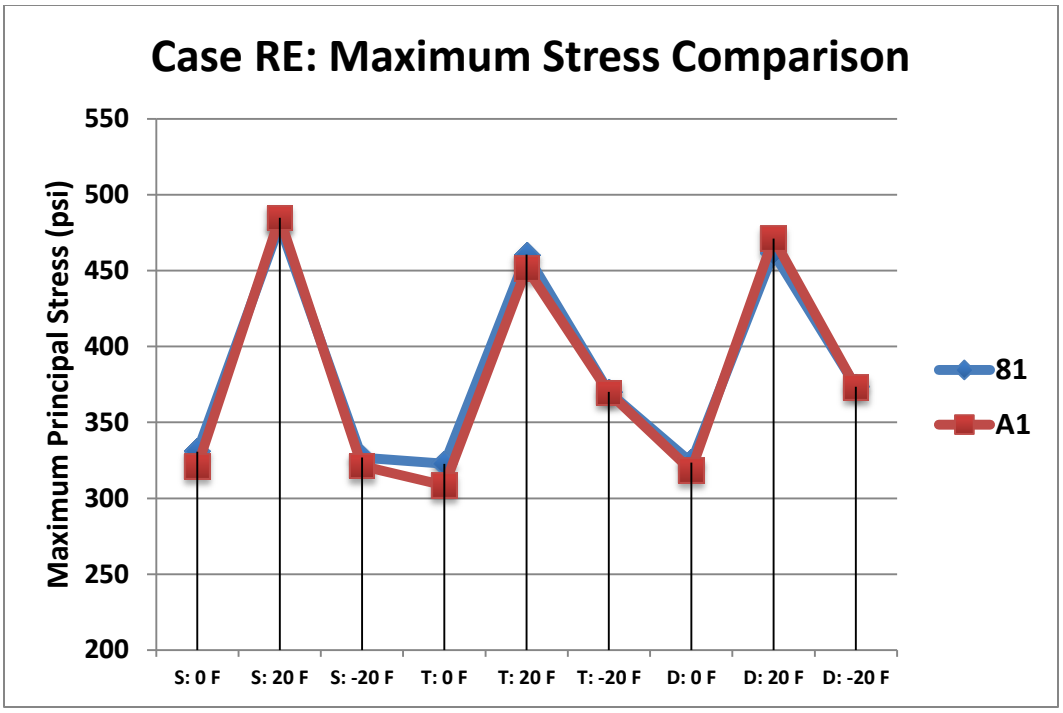

Figure 71: Comparison of the peak tensile stresses for Case RE of MI-I-96 roadway for each input factor level and the 2 levels of non-uniform support

Overall, the peak tensile stresses were highest for daytime curling conditions for all axle types and both support conditions. However, one noticeable feature of the MI I-96 higher k-values was the difference in peak tensile stresses for daytime curling and none or nighttime curling were higher than I-94. The average peak tensile stress increase between the no temperature differential and positive temperature differential case was 43% and there was a 32% increase in average peak tensile stress between the negative temperature differential and positive temperature differential cases seen in Figure 71. For input combinations, the peak tensile stress always occurred at the bottom of the slab.

3.5.2.2 Stress Analysis of Left Edge (LE) Case for MI I-96 Roadway Section

Case LE81 represents the movement of the vehicle along the longitudinal left lane edge of the slab and the peak tensile stresses are shown in Figure 73. The peak tensile stresses occurred near the midslab position but not as the position of RE81 as seen in Figure 72 due to the different localize support stiffness. The overall peak tensile stress of LE81 was approximately 6% higher than RE81 mostly because the frequency of k-values on LE are higher for the lowest stiffness bin of 250-350 psi/in shown in Figure 75. The

mean of the k-value along the left edge is 339 psi/in with a standard deviation of 93.6 psi/in compared to the higher mean of 461 psi/in with standard deviation of 123.8 psi/in at the right edge. The overall peak stress change from uniform to non-uniform (LE81) increased 6% with an average increase in peak tensile stress of 4%. A 52% increase in average peak tensile stress between the no temperature differential and positive temperature differential case and a 36% increase in average peak tensile stress between negative temperature differential and positive temperature differential cases is observed as seen in Figure 74. Table 12 shows that nighttime curling along both the edges caused critical tensile stresses at the top of slab for both the support conditions (uniform and non-uniform) while no and positive temperature differentials produced peak tensile stresses at the bottom of the slab.

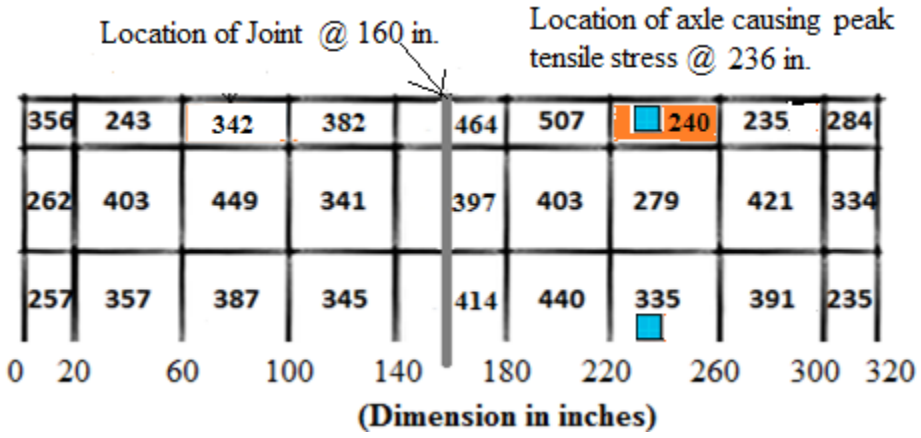

Figure 72: Local variation in k-values along left hand edge of the slab for case RE81

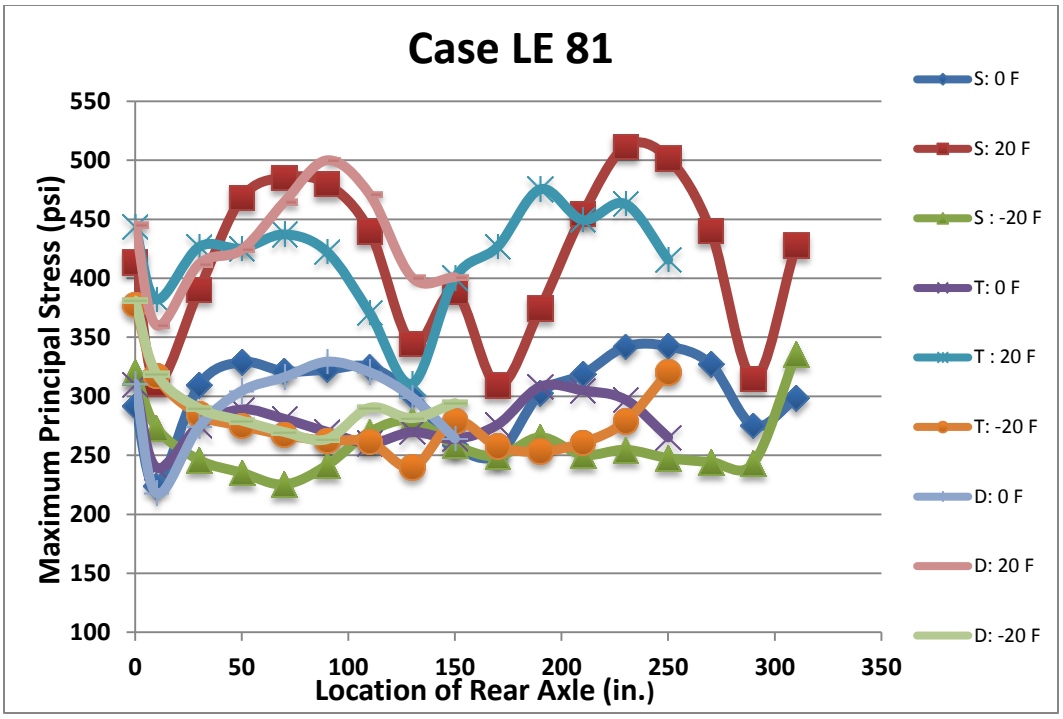

Figure 73: Maximum principal (tensile) stress for Case LE81 versus axle position

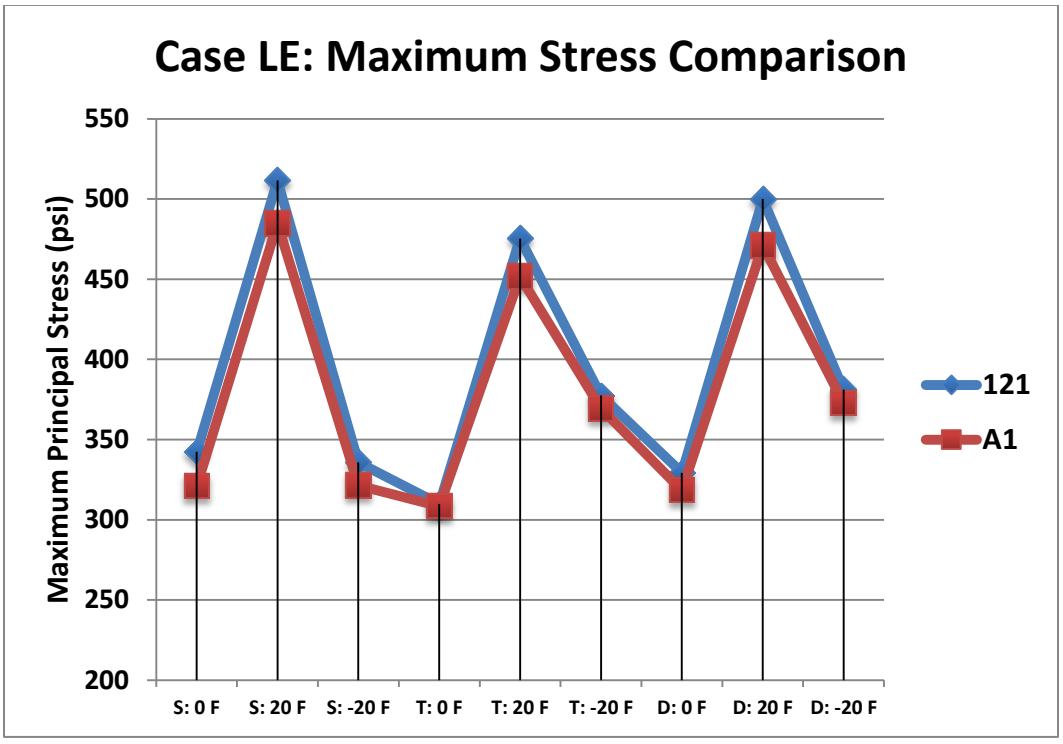

Figure 74: Comparison of the peak tensile stresses for Case LE of MI-I-96 roadway for each input factor level and the 2 levels of non-uniform support

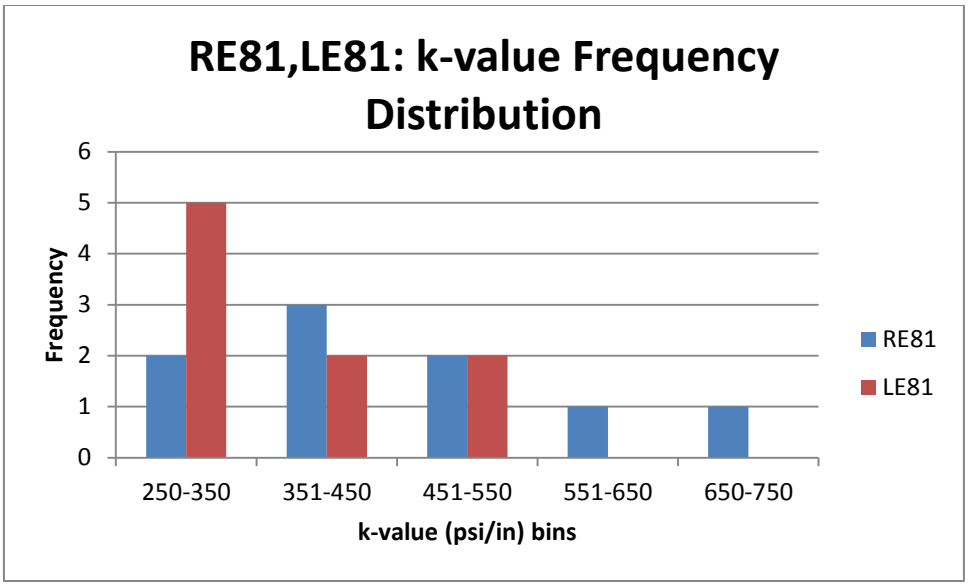

Figure 75: k-values for case RE81 and LE81 on MI I-96 roadway

3.5.2.3 Stress Analysis of Middle of Lane (M) Case for MI I-96 Roadway Section

As expected, M81 results for the maximum tensile stresses were lower in magnitude than LE81 as seen in Figure 76. The maximum tensile stresses occurred at the free transverse edges also which would be reduced with addition of adjacent slabs with load transfer. With higher k-values a difference of 100-150 psi/in does not constitute the same definition of non-uniformity as seen in support condition of MI I-94. The frequency distribution of k-values in Figure 79 suggests the presence of relatively uniform subgrade support in the middle of the slab with a mean of 382 psi/in and standard deviation of 116.4 psi/in. The maximum tensile stresses at each longitudinal position for cases MA1 is presented in the appendix. No significant difference between the overall peak tensile stresses of uniform and non-uniform cases was observed as seen in Figure 77 due to interior loading position of the axle and relatively lower non-uniformity. The overall peak tensile stress had a 2% increase from uniform to non-uniform (M81), while there was an increase in the average peak tensile stress of 4%. With the higher k-values, there was a 34% increase in the average peak tensile stress between no temperature differential and positive temperature differential case and 78% increase in average peak tensile stress between no temperature differential and positive temperature differential case as observed in Figure 78. The three axle types behaved in a similar pattern in terms of

magnitude of tensile stresses and location of critical stresses. As seen in Table 12, most of the critical tensile stress cases occurred at the free transverse edge.

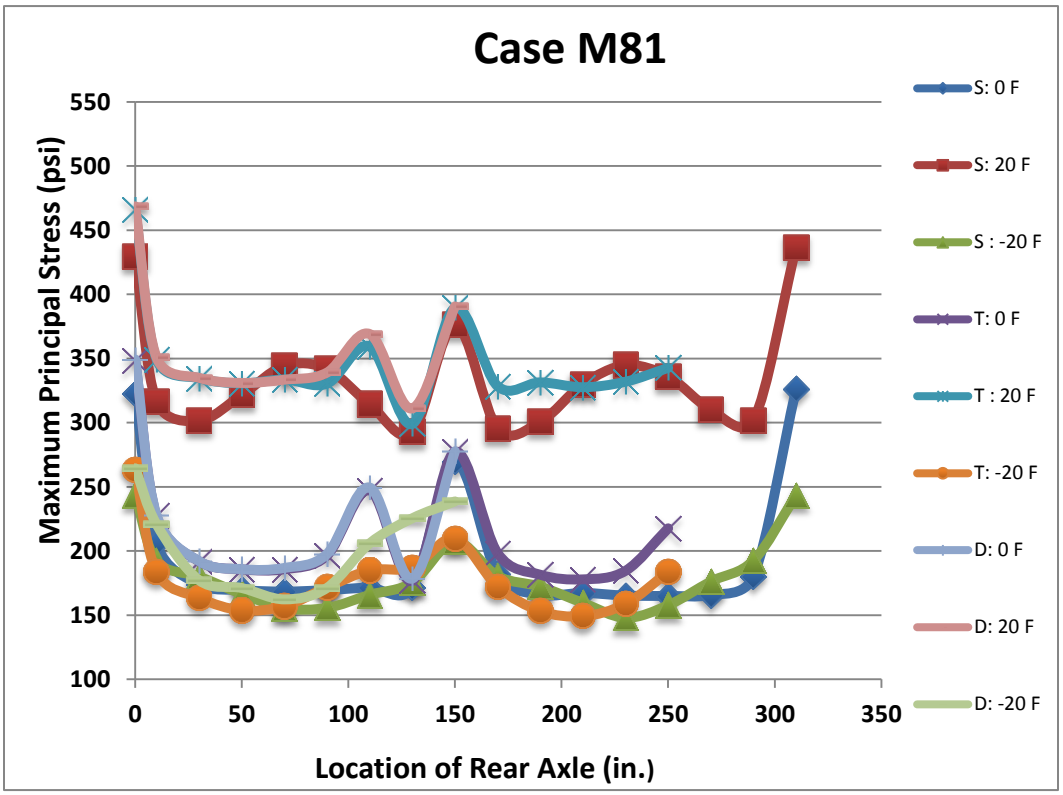

Figure 76: Maximum principal (tensile) stress for Case M81 versus axle position

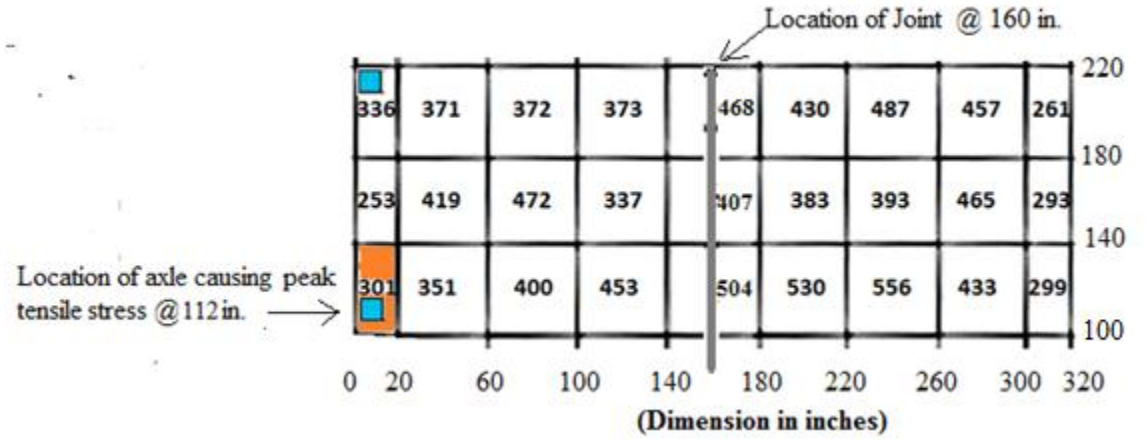

Figure 77: Local variation in k-values along middle of the slab for case M81

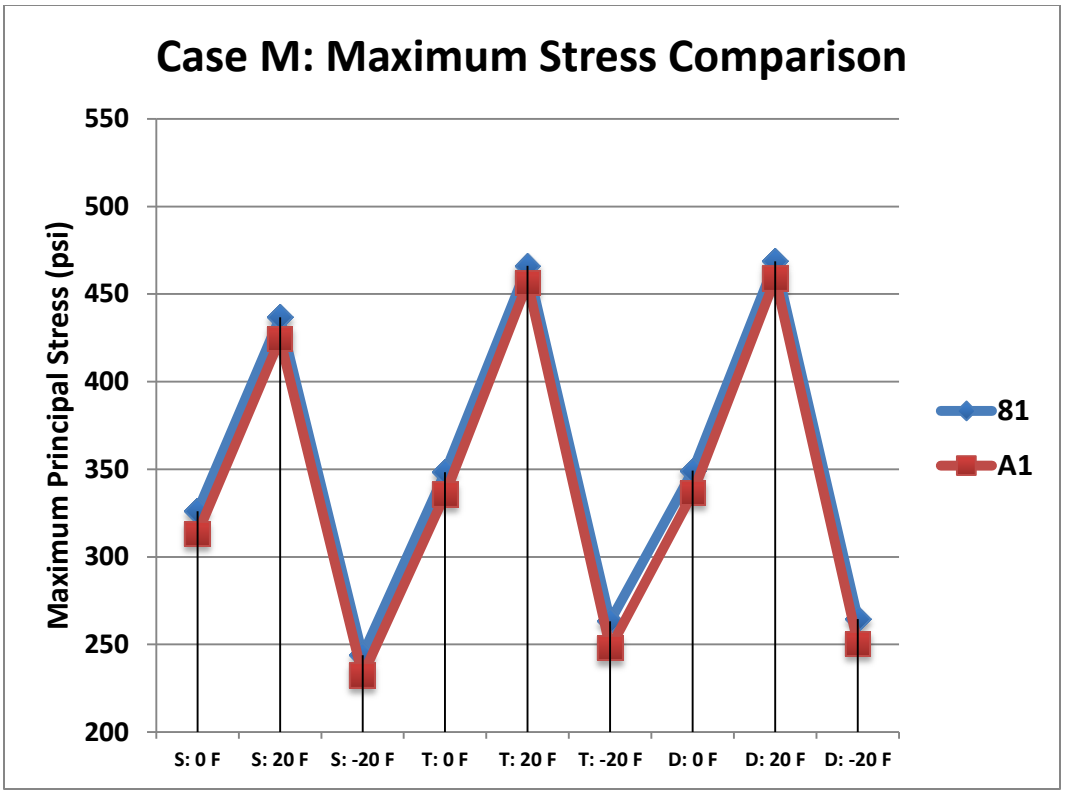

Figure 78: Comparison of the peak tensile stresses for Case M of MI-I-96 roadway for each input factor level and the 2 levels of non-uniform support

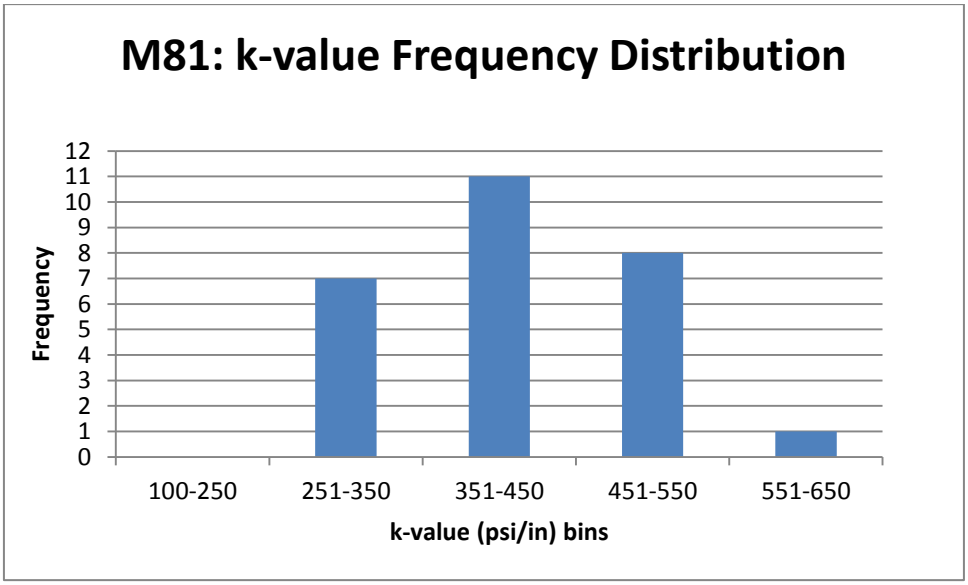

Figure 79: k-values for case M81 on MI I-96 roadway

Table 12: Location and magnitude of peak tensile stresses for non-uniform support condition on MI-I96 roadway

Case	Single Axle			Tandem Axle			Steer Drive Axle		
	0 F	20 F	- 20 F	0 F	20 F	- 20 F	0 F	20 F	- 20 F
RE81	330 (0,116.b)	479 (0,96,b)	326 (44,320,t)	322 (102,0,b)	460 (102,0,b)	370 (44,0,t)	323 (102,0,b)	461 (102,0,b)	373 (44,0,t)
REA1	321 (102,0,b)	484 (102,0,b)	321 (46,0,t)	308 (102,0,b)	451 (102,0,b)	369 (46,0,t)	318 (0,200,b)	471 (0,240,b)	372 (44,0,t)
LE81	342 (320,236,b)	511 (320,236,b)	335 (276,320,t)	309 (218,0,b)	475 (320,244,b)	377 (274,0,t)	329 (320,240,b)	499 (320,240,b)	381 (274,0,t)
LEA1	321 (320,114,b)	484 (320,76,b)	321 (274,0,t)	308 (218,0,b)	451 (218,0,b)	369 (274,0,t)	318 (320,200,b)	471 (320,220,b)	372 (276,0,t)
M81	326 (208,320,b)	436 (208,320,b)	243 (112,0,b)	348 (112,0,b)	466 (112,0,b)	263 (112,0,b)	349 (112,0,b)	468 (112,0,b)	264 (112,0,b)
MA1	313 (208,0,b)	424 (208,0,b)	232 (112,0,b)	335 (208,0,b)	456 (112,0,b)	247 (112,0,b)	336 (208,0,b)	458 (112,0,b)	250 (112,0,b)

b= Bottom of slab; t: Top of slab

3.5.3 Analysis of Slab Tensile Stresses with Random Assignment of Subgrade Support

A random number generator using the mean and the standard deviation of the field data for MI I-96 (case 81) was carried out to analyze if a random assignment of the k-value following the measured field data distribution (normality assumed) would produce significantly greater tensile stresses than just the uniform support assumption. This analysis was similar to MI I-94 except for the k-values were much greater for MI I-96. Figure 80 shows the spatial plot developed through random generation of k-values in an unbiased manner. The frequency distribution of case R-81 is shown in Figure 81 having more k-values in the lowest stiffness bin of 100-240 psi/in compared to case 81. R-81 has a mean of 390, standard deviation of 112.6, coefficient of variation of 29% and range of 132-647 psi/in. The analysis matrix for different axle types and temperature differentials remained the same as previous sections with the loading path at the right lane edge, left lane edge, and middle of the slab only.

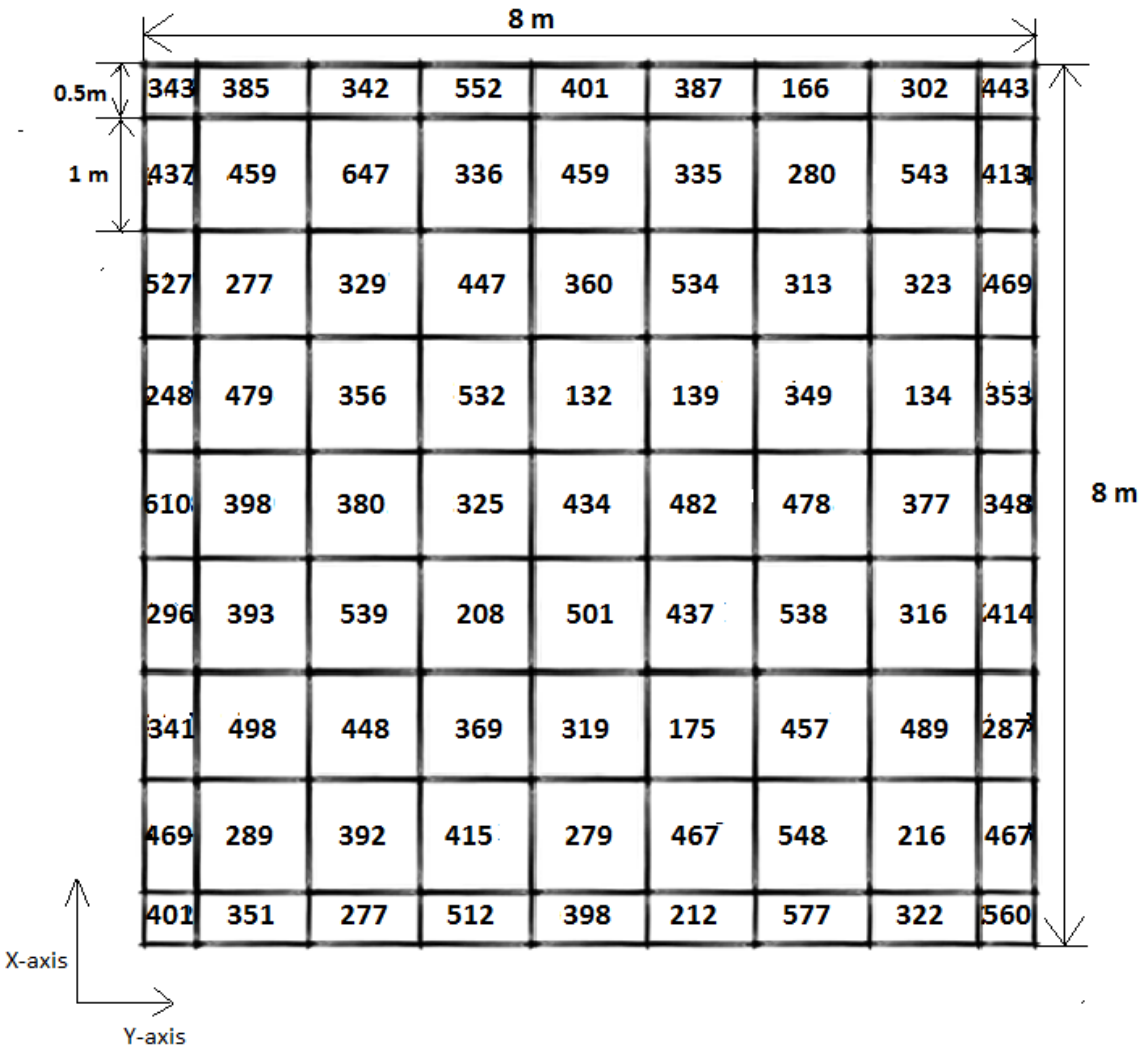

Figure 80: Case R-81 with 81 discretized k-value areas randomly assigned from MI I-96 project

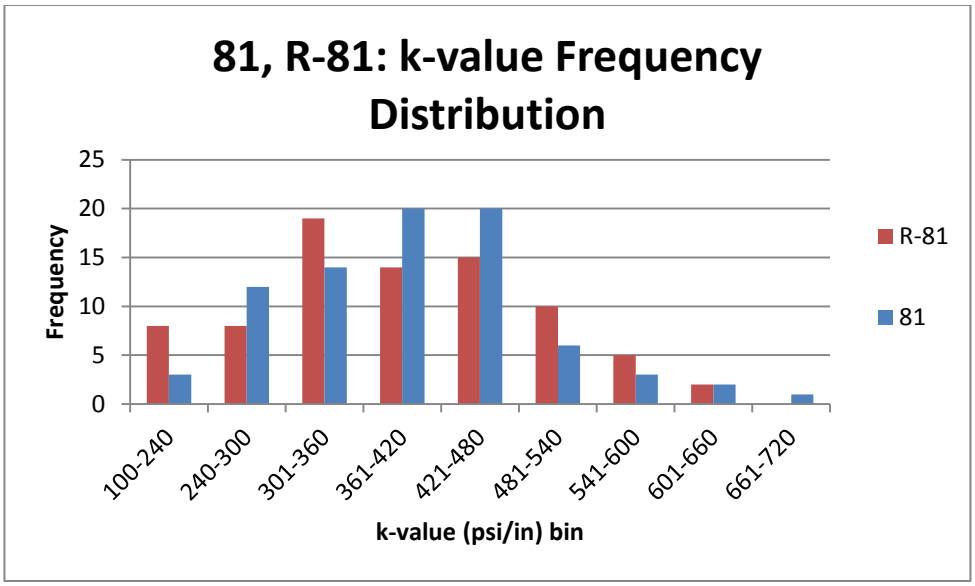

Figure 81: Frequency distribution of k-values for case R-81

3.5.3.1 Stress Analysis of Randomly Assigned Support Condition for Right Edge (R-RE) and Left Edge (R-LE) Cases on MI I-96 Roadway Section

The results of Case R-RE81 in Figure 82 show the maximum tensile stresses recorded at each longitudinal position. Case R-RE81 had slightly higher overall peak tensile stress (approximately 8%) compared to RE-81. In Figure 83, a similar pattern with previous runs was observed with respect to the magnitudes of the critical stresses caused by each axle type, i.e., the single axle with daytime curling was the critical set of input factors. From Figure 83, random assignment of the k-values did not have a significant impact in terms of increase in tensile stress between case R-81 and case A1 (uniform) for a particular combination of axle type and temperature differential. The peak tensile stresses occurred at the midslab position of the first slab as seen in Figure 84 at location of lower k-value (277 psi/in) adjacent to a higher stiffness area of 512 psi/in, albeit only a factor of 2. The overall and average peak stress change from uniform to non-uniform (R-RE81) increased 5%, which was much less than the increases found with the MI I-94 analysis with random assignment with lower support stiffness.

The difference between the critical daytime curling stresses compared to the nighttime curling and loading case was again significant. A 47% increase in average peak tensile stress between the no temperature differential and positive temperature differential

case and a 37% increase in average peak tensile stress between negative temperature differential and positive temperature differential cases was observed in Figure 83. The critical tensile stresses were located at the bottom of the slab as listed in Table 13.

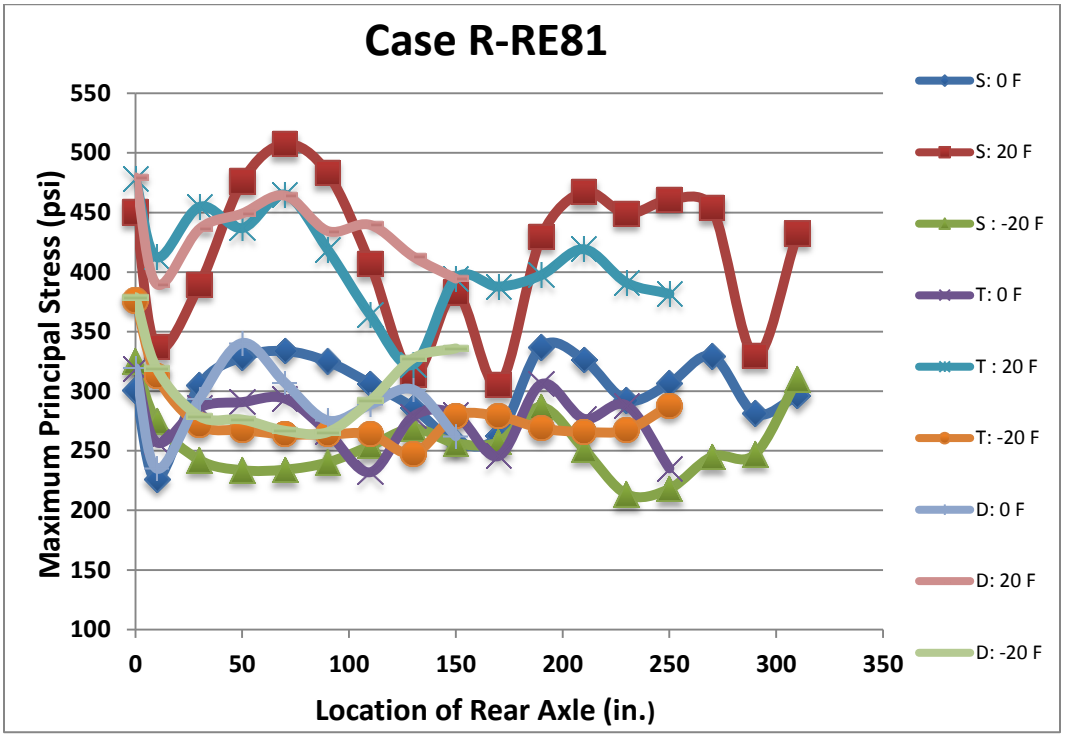

Figure 82: Maximum principal (tensile) stress for Case R-RE81 versus axle position

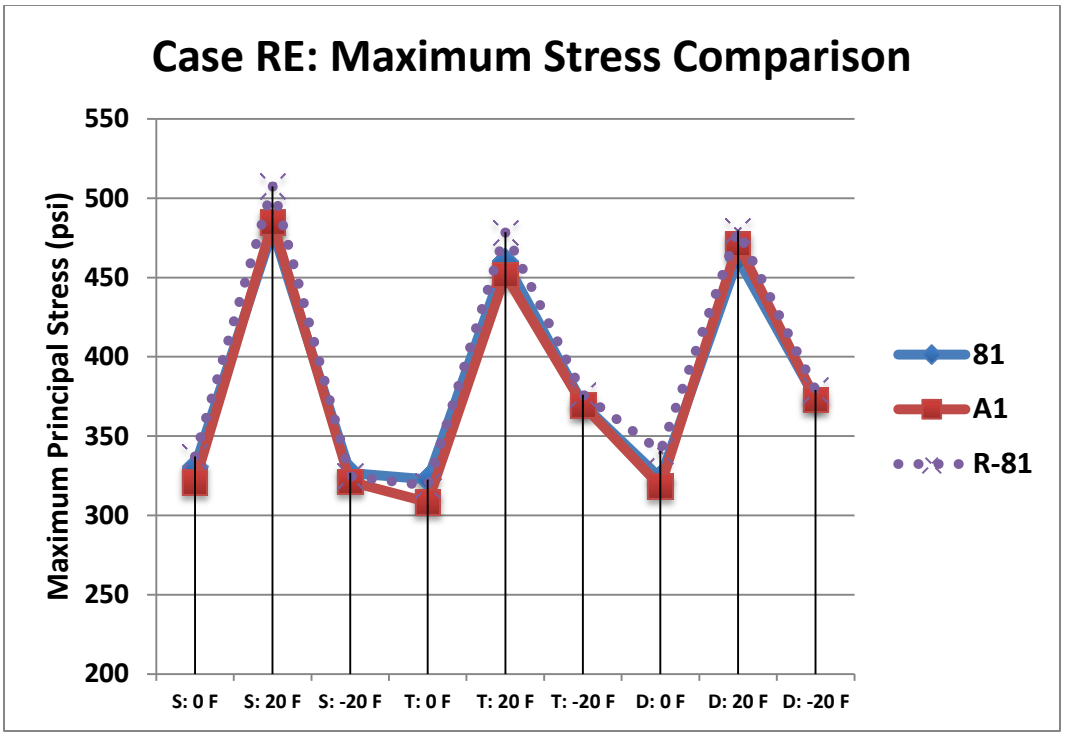

Figure 83: Comparison of the peak tensile stresses for Case RE of MI-I-96 roadway for each input factor level and the 3 levels of non-uniform support

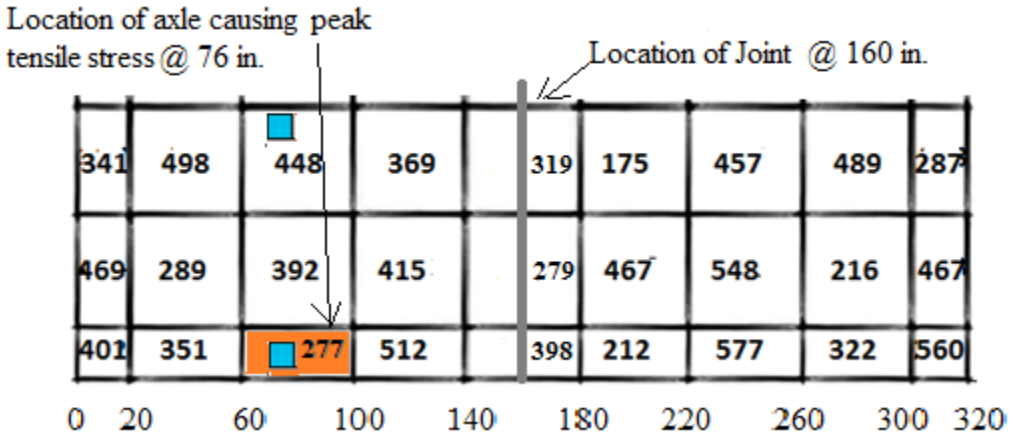

Figure 84: Local variation in k-values along right hand edge of the slab for case R-RE81

The maximum tensile stresses for the left edge loading path (case R-LE81) in Figure 86 showed greater overall peak tensile stress than case R-RE81. In fact, the overall and average peak tensile stress changes from R-RE81 to R-LE81 were 7% and 3%. The reason for this behavior was the lowest k-value of R-LE81 was 166 psi/in, which

occurred near the midslab load location as seen in Figure 85. Figure 88 does not support the difference in peak tensile stresses since the frequency distribution between R-LE and R-RE were approximately the same despite R-LE81 having a slightly lower mean of 369 psi/in, compared to 401 psi/in for R-RE81. However, the k-value near the critical load location for R-RE81 was 277 psi/in, which supports the conclusion that the non-uniformity spatial position and magnitude are important factors in generating high tensile stresses in the slab.

The overall peak stress change from uniform (A1 to non-uniform (R-LE81) increased 11% with an increase in the average peak tensile stress of 8%. A 53% increase in average peak tensile stress between the no temperature differential and positive temperature differential case and a 43% increase in average peak tensile stress between negative temperature differential and positive temperature differential cases was observed as seen in Figure 87. The overall peak tensile stress was produced by the single axle and was located at the bottom of the slab.

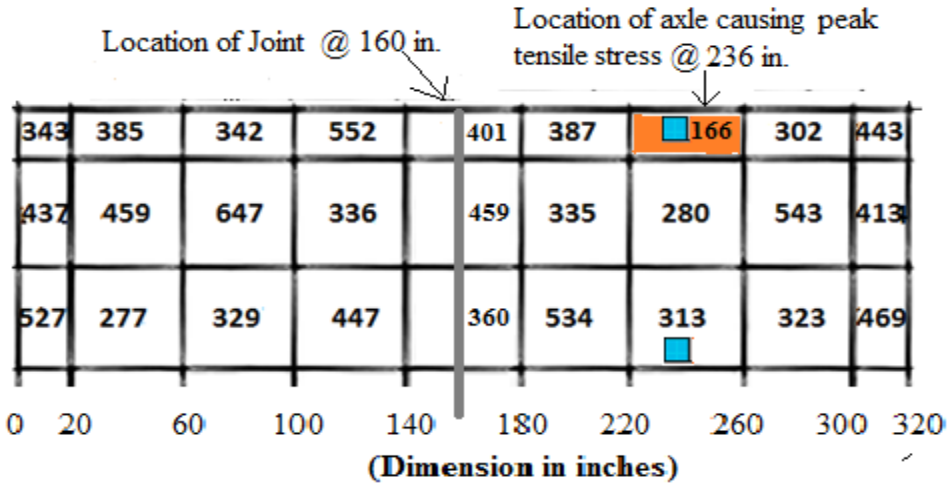

Figure 85: Local variation in k-values along left hand edge of the slab for case R-LE81

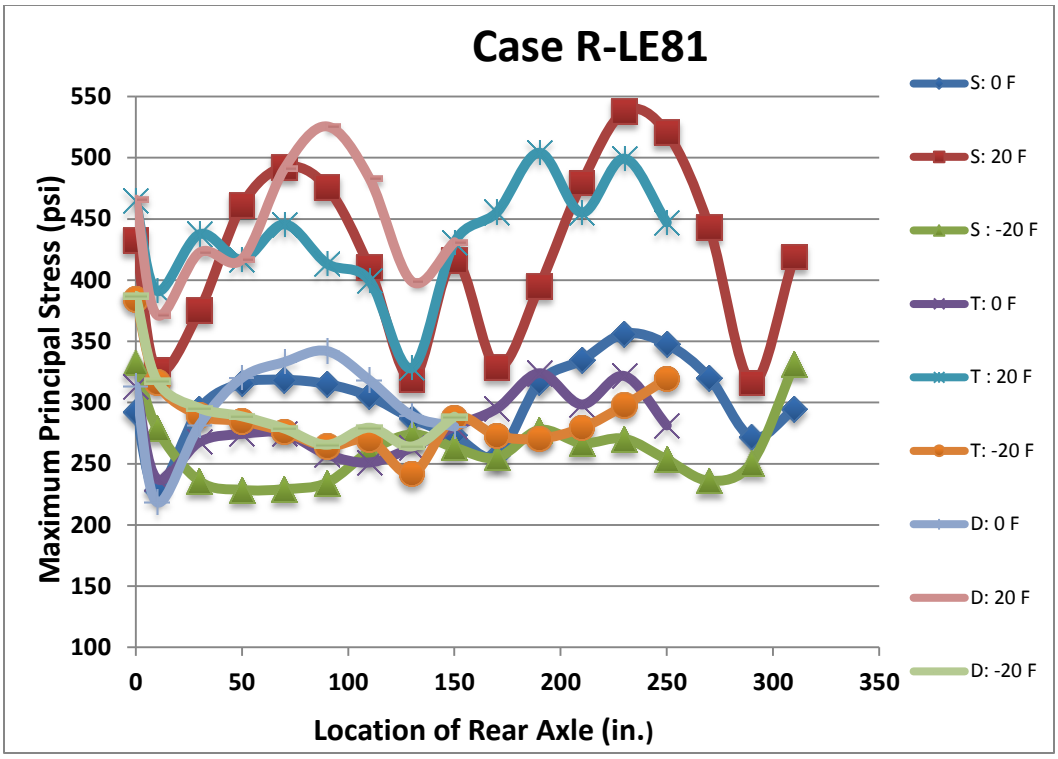

Figure 86: Maximum principal (tensile) stress for Case R-LE81 versus axle position

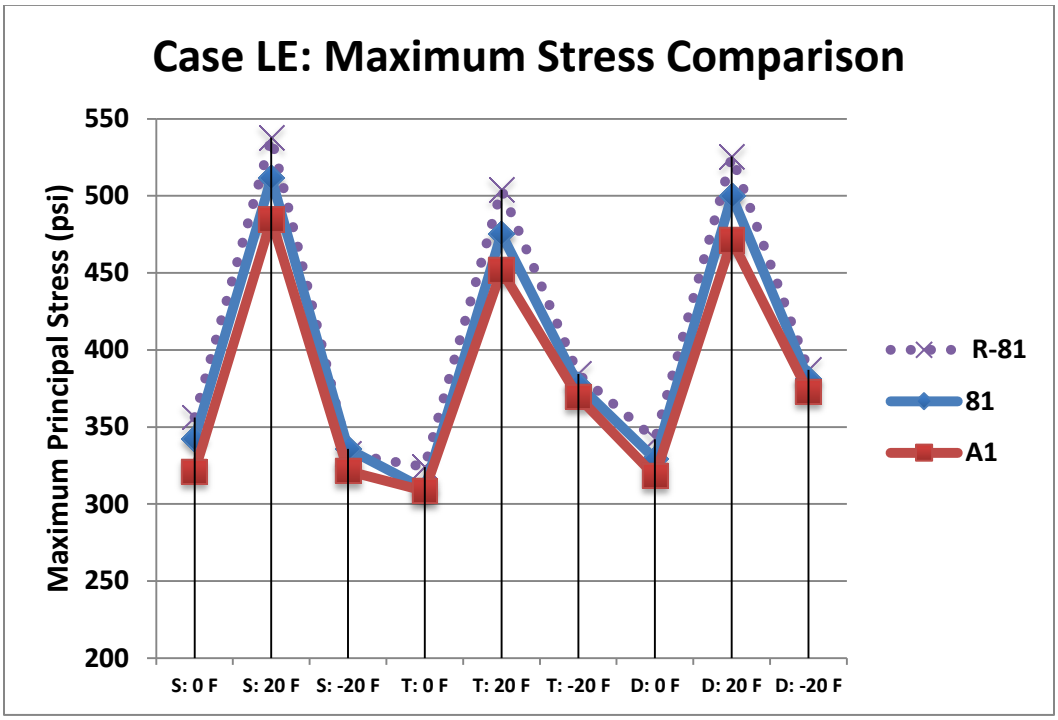

Figure 87: Comparison of the peak tensile stresses for Case LE of MI-I-96 roadway for each input factor level and the 3 levels of non-uniform support

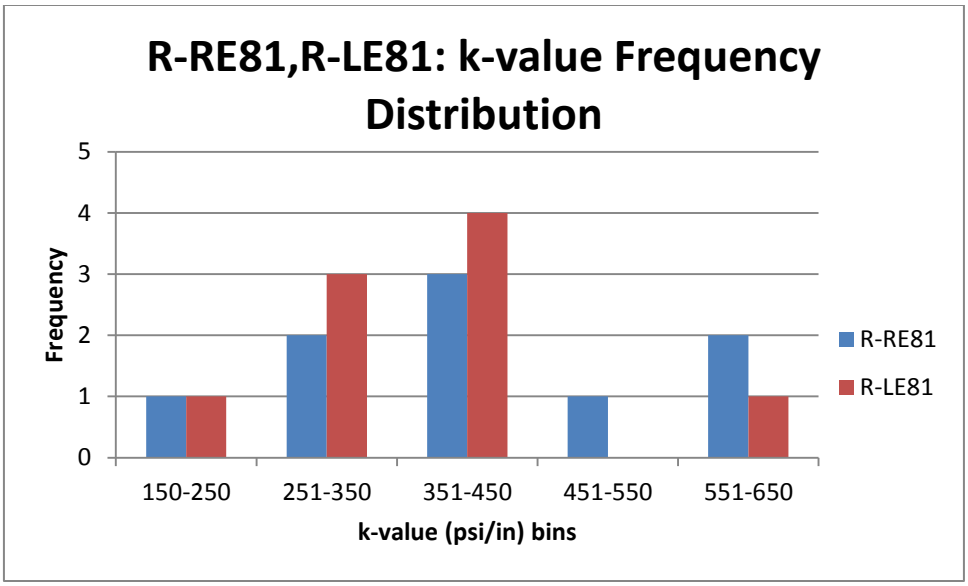

Figure 88: k-values for case R-RE81 and R-LE81 on MI I-96 roadway

3.5.3.2 Stress Analysis of Randomly Assigned Support Condition for Middle of Lane (R-M) Case on MI I-96 Roadway Section

Figure 91 shows the results of the maximum tensile stresses recorded at the each longitudinal position of the axle for case R-M81. The maximum tensile stress for the middle of the slab loading path occurred at the bottom of the slab at the transverse edge. Peaks in the tensile stresses are observed due to a significant drop in support stiffness from 532 to 132 psi/in at 110 in. from the initial loading location. The frequency distribution of R-M81, Figure 90, shows that the k-values for the lowest stiffness bin of 100-250 psi/in were higher than M81 which did not have a single k-value in this bin. A 5% increase in overall peak tensile stress was realized from case M-81 to R-M81 due to presence of softer stiffness areas especially at the transverse edge and joint position as seen in Figure 89. The overall peak stress change from uniform to non-uniform (R-M81) increased 8% with an average increase in peak tensile stress of 6%. In Figure 92, a 39% increase in average peak stress between the no temperature differential and positive temperature differential case and an 88% increase in average peak stress between negative temperature differential and positive temperature differential cases was observed.

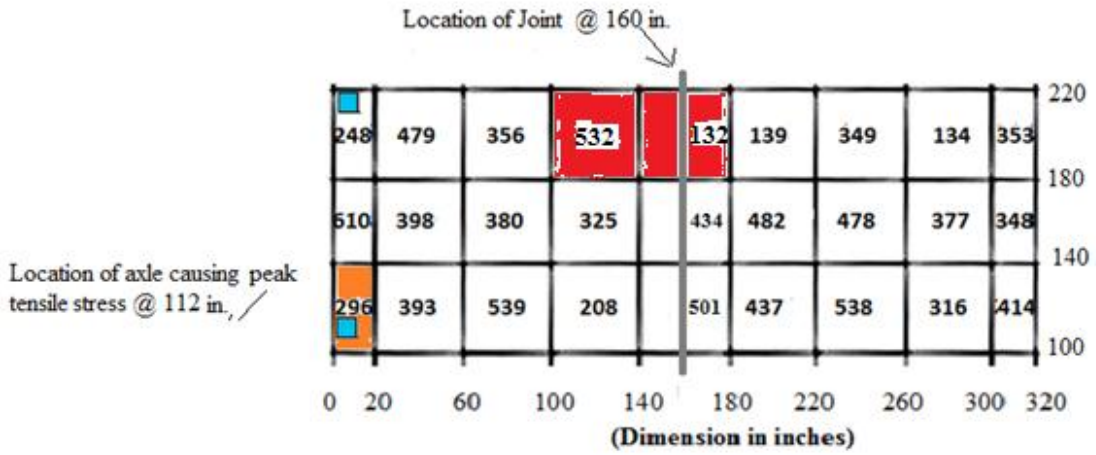

Figure 89: Local variation in k-values along middle of slab for case R-M81

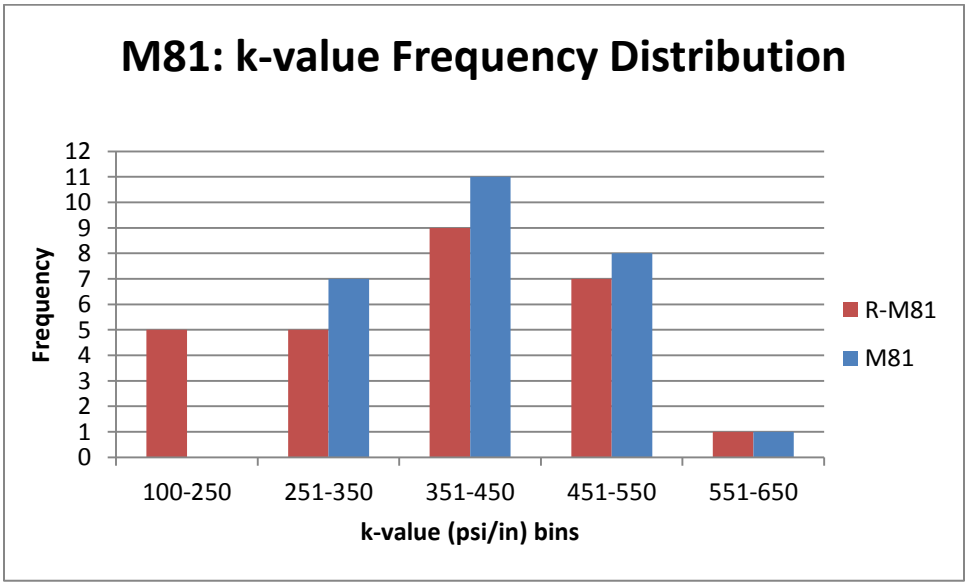

Figure 90: k-values for case R-M81 on MI I-96 roadway

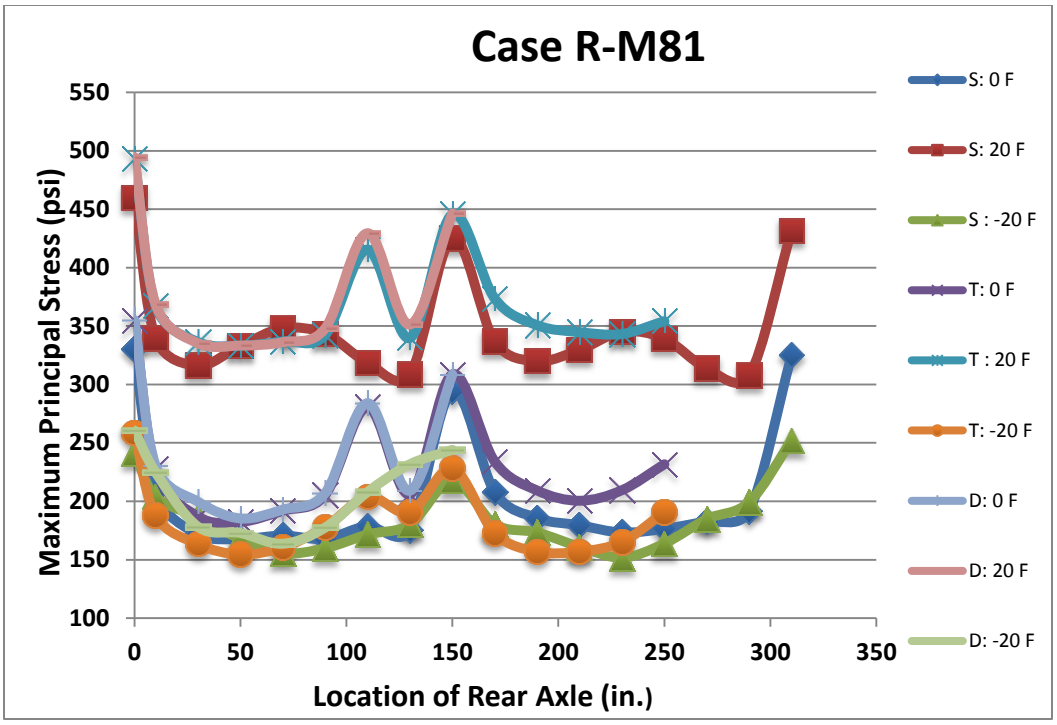

Figure 91: Maximum principal (tensile) stress for Case R-M81 versus axle position

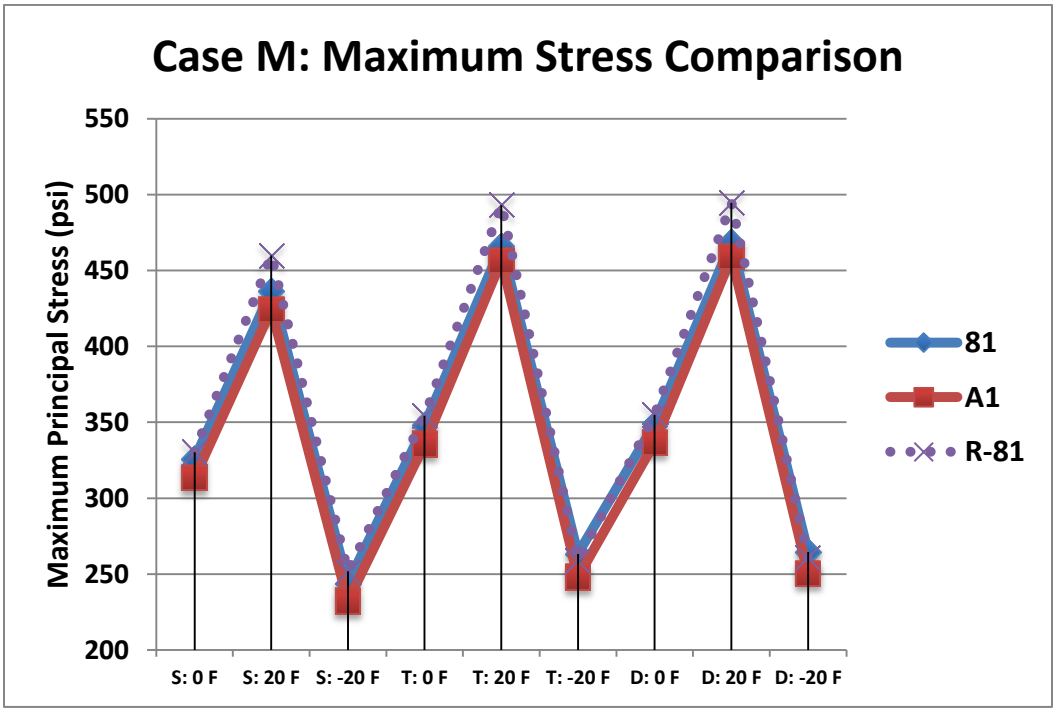

Figure 92: Comparison of the peak tensile stresses for Case M of MI-I-96 roadway for each input factor level and the 3 levels of non-uniform support

Table 13: Location and magnitude of peak tensile stresses for randomly assigned k-value support condition for MI I-96 roadway

Case	Single Axle			Tandem Axle			Steer Drive Axle		
	0 F	20 F	- 20 F	0 F	20 F	- 20 F	0 F	20 F	- 20 F
R-RE81	337 (0,196,b)	507 (0,76,b)	324 (46,0,t)	318 (102,0,b)	478 (102,0,b)	376 (46,0,t)	340 (0,200,b)	479 (102,0,b)	378 (46,0,t)
R-LE81	356 (320,236,b)	537 (320,236,b)	332 (276,0,t)	323 (320,244,b)	504 (320,244,b)	384 (276,0,t)	342 (320,240,b)	525 (320,240,b)	387 (276,0,t)
RE/LE A1	321 (102,0,b)	484 (102,0,b)	321 (46,0,t)	308 (102,0,b)	451 (102,0,b)	369 (46,0,t)	318 (0,200,b)	471 (0,240,b)	372 (44,0,t)
R-M81	330 (112,0,b)	459 (112,0,b)	251 (208,320,b)	354 (112,0,b)	493 (112,0,b)	258 (208, 0,b)	355 (112,0,b)	494 (112,0,b)	260 (112,0,b)
MA1	313 (208,0,b)	424 (208,0,b)	232 (112,0,b)	335 (208,0,b)	456 (112,0,b)	247 (112,0,b)	336 (208,0,b)	458 (112,0,b)	250 (112,0,b)

b= Bottom of slab; t: Top of slab

Table 13 shows the location and magnitude of the peak tensile stresses for the different sets of inputs analyzed. Nighttime curling along the longitudinal free edges caused maximum tensile stresses at the top of the slab whereas for the rest of the subcases the maximum tensile stresses were at the bottom of the slab. As shown in Figure 93, confirms an increase in 11% between the overall peak tensile stress of non-uniform case R-LE81 and uniform support condition.

Comparing the overall peak tensile stresses between the critical cases of MI I-94 and MI I-96 (deterministic and randomly assigned data set) there was a 13% increase from case R-LE81 to R-RE36. Also, the average peak tensile stress increased by 36% between these critical cases

Table 14: Summary of the percent change in overall and average peak tensile stress from uniform support relative to deterministically assigned field non-uniform support (81 k-values)

Loading Path	Change in Overall Peak Tensile Stress	Change in Average Peak Tensile Stress
Case RE (Right Lane Edge)	-1	+1
Case LE (Left Lane Edge)	+6	+4
Case M (Middle of Lane)	+2	+4

Table 15: Summary of the percent change in overall and average peak tensile stress from uniform subgrade relative to random assignment of 81 k-value areas each loading path

Loading Path	Change in Overall Peak Tensile Stress	Change in Average Peak Tensile Stress
Case RE (Right Lane Edge)	+5	+5%
Case LE (Left Lane Edge)	+11	+8%
Case M (Middle of Lane)	+8	+6%

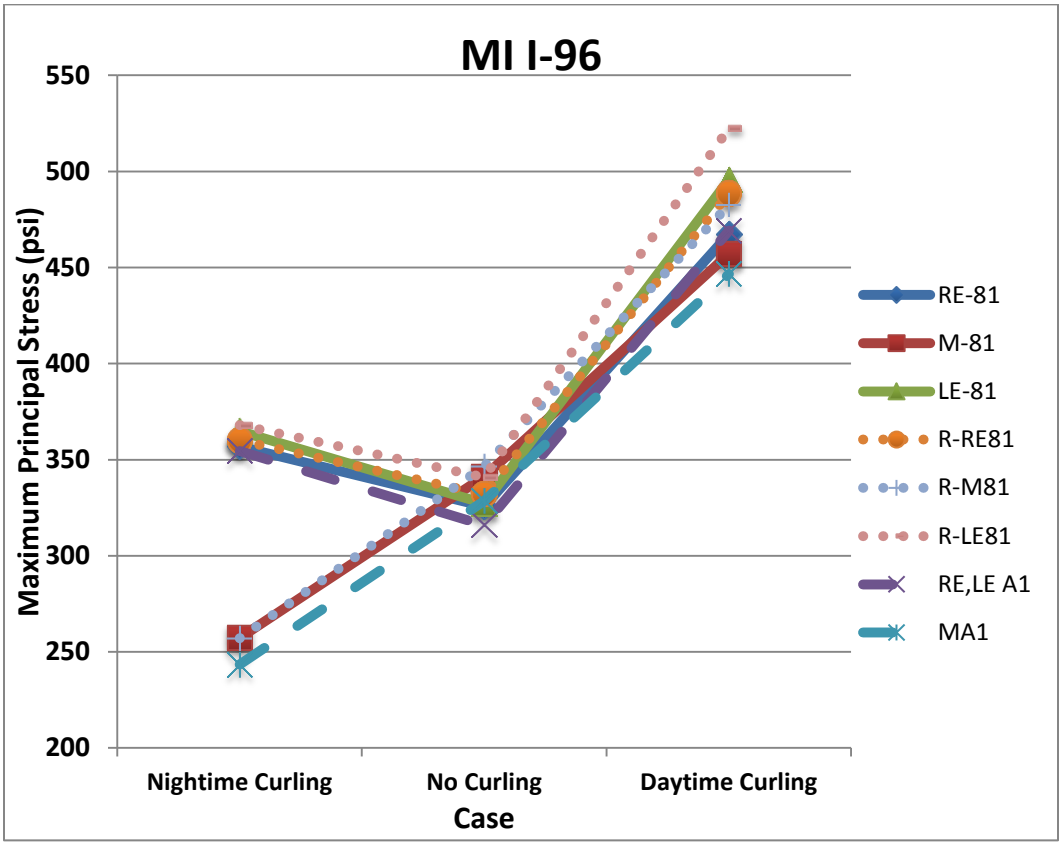

Figure 93: Comparison of effect of temperature differential on the non-uniform subgrade support cases of MI I-96 roadway

Table 16: Percentage difference between the average peak tensile stresses of the temperature differential cases for a given loading path and subgrade type combination

Case	No temperature to Positive Temperature Differential (%)	Negative temperature to Positive Temperature Differential (%)
RE81	+43	+32
R-RE81	+47	+37
M81	+34	+78
R-M81	+39	+88
LE81	+52	+36
R-LE81	+53	+43

Based on the stress analysis carried for the MI I-96 roadway for the measure spatial stiffness, the overall and average peak tensile stresses were not as sensitive to difference between adjacent k-values as MI I-94 due to the relatively stiff subgrade support magnitude as seen in Table 14 and Table 15. The deterministically assigned support values only increased the overall and average peak tensile stress by 6% and 4%, respectively, when moving from uniform and non-uniform support condition. Random assignment of the k-values on the field spatial plot lead to 11% increase in overall peak tensile stress between a uniform support and a non-uniform support condition and a 8% increase in average peak tensile stress. The stiffer support was more sensitive to changes in temperature curling conditions, as expected. The overall peak tensile stresses produced by the three axle types along the different loading locations on account of a non-uniform stiff subgrade support were still relatively high between 450-525 psi/in during the daytime curling for the slab, loading, and material inputs assumed. Furthermore, daytime curling compared to the other temperature differential condition in Figure 93 and Table 16 produced significant increases in peak tensile stresses for all input cases.

Chapter 4: Conclusions and Recommendations

Concrete pavement design has historically used the dense liquid foundation model to characterize the subgrade support under the rigid pavement systems. The assumption of a single, homogenous k-value for the foundation layer has been the acceptable pattern despite the known spatial variation of the soil stiffness. Pavement and geotechnical engineers have known for a time that the soil support condition varies with the project length and soil depth due to variability in the soil physical and geological properties, environmental factors, and construction process. With the development of intelligent compaction equipment, there is a need to better quantify the effect of soil non-uniformity on the concrete slab responses and performance and re-evaluate the single k-value assumption. The main objective of this study was to determine the change in slab critical tensile stresses given a set of input parameters and non-uniform support condition relative to a uniform support assumption.

In-situ testing was carried out on two roadway segments, MI I-94 and MI I-96, in order to gather field data on the spatial variation in soil stiffness. Dynamic Cone Penetrometer (DCP) tests were conducted on top of the subbase material for both sections that were used to correlate to California Bearing Ratio (CBR) values. Plate load tests (PLT) conducted on one test section (MI I-94) were correlated to the CBR data to develop an empirical relationship that was used to correlate CBR to k-value on both test sections intensive data collection sites. These measured stiffness variations over a small area were defined as support non-uniformities in this study. Pavement stress analysis was completed using a 2-D finite element software, which utilized the spatially-derived k-values as an input support parameter. These k-values were either deterministically or randomly assigned to a pre-defined support area size. Multiple non-uniform support cases were developed to theoretically analyze based on defining the size of each individual area of uniform k-value, e.g., case 121 would represent a 121 individual k-value areas of 0.7 by 0.7 m^2. A total of 4 non-uniform support conditions were analyzed for each set of inputs: single k-value, 36 k-values of 1.16x1.16 m^2, 81 k-values of 1x1 m^2, and 121 k-values of 0.7x0.7 m^2. These non-uniformities support conditions were analyzed for three different axle configurations (single, tandem, and steer-drive axle), three temperature

differential (+20°F, 0°F, -20°F), and loading paths (left/right edge, middle of the lane, and left/right wheelpath). All analysis was completed on a four slab assembly with a single slab thickness. The axles were traversed across the slabs in the various loading paths to determine the peak tensile stress for a given set of inputs.

The results of the finite element analysis on the MI I-94 test for the two sets of deterministically assigned non-uniform support conditions (121 and 36 k-values, and single mean k-value) showed that there was little difference between the non-uniform support with 121 k-values and using the mean k-value of 63 psi/in to characterize the support. Even though the measured k-value range was 31 to 202 psi/in or a factor of almost 7 difference for case 121, the overall peak tensile stresses were only 3.2% different than the uniform case with the average peak tensile stress increasing only 3.6% for each set of inputs. For the highest case (Case 121), the peak tensile stress occurred for the single axle along the right edge loading path.

In order to further determine the critical size of the non-uniform support area, a random assignment of the k-value using a normal distribution with the mean and standard deviation of the field data for two cases, 121 and 36 k-values, was completed. For MI I-94 the mean k-value was 63 psi/in (standard deviation = 25.6 psi/in) and for the randomly generated k-values less than zero, a value of 1 psi/in was assigned. When the same analysis was run with the 2D finite element program, the non-uniform support condition with randomly assigned k-values into 36 pre-defined areas (case R-36) produced a range of 22% to 37% increase in average peak tensile stress for the edges and wheelpath cases. More importantly, an increase in 31% in overall peak tensile stress was determined when going from a non-uniform subgrade support condition (case R-RE36) to an uniform subgrade support condition with edge loading and random assignment of k-values. For this critical case, the overall peak tensile stress in the slab was 608 psi and was produced by a single axle and daytime curling conditions at the bottom of the midslab edge. This level of tensile stress increase over a uniform support case (478 psi) can easily lead to premature cracking since many agencies use a design flexural strength of the concrete of 650 psi.

The size of the non-uniformity also affected the tensile stress increase over uniform support. With random assignment for the MI I-94 project, moving from a 0.7x0.7 m^2 to 1.16 x 1.16 m^2 increased the peak tensile stress by 27%. Another key finding from this analysis demonstrated that the non-uniformity was the most critical especially in the presence of very low support conditions (<20 psi/in) found beneath the location of expected maximum tensile stress. Interestingly, the middle of the lane loading path was not affected significantly impacted by large differences in spatial support distribution assuming there was adequate load transfer across the joints.

A random assignment using a beta distribution of the same field data was done in order to provide an upper and lower boundary on the values for expected field k-values, i.e., minimum and maximum k-values of 20 and 202 psi/in. By introducing a lower boundary for k-value, the tensile stresses were very similar for all predefined support area sizes and loading paths including the uniform k-value case. The primary reason for this finding with the beta distribution was a lack of very low stiffness areas, as seen in the random assignment through normal distribution cases, in the region of expected maximum tensile stress.

The MI I-96 section was analyzed in a similar manner to MI I-94. The axle configurations and the temperature differentials remained the same, however, the wheelpath loading cases were not run based on their lack of sensitivity to support changes found during the MI I-94 analysis. The subgrade support on MI I-96 was significantly stiffer (mean k-value = 397 psi/in) compared to the MI I-94 section (mean k-value = 63 psi/in). The greatest increase in peak tensile stress from uniform to non-uniform subgrade conditions was 6% (increase of 4% for average peak tensile stress) for the left edge loading path with 81 k-values (1x1 m^2 area) deterministically assigned and single axle configuration. The k-value ranged from 235-713 psi/in representing a difference of 478 psi/in but the ratio from minimum to maximum was around 3, which was less than MI I-94 field data k-values which had a factor of almost 7 difference.

Random assignment of the support stiffness using a normal distribution with the mean and standard deviation defined from the field data (81 k-values) did not provide the same critical results as obtained by loading paths along the edges for case R-36 of MI I-

94. The left loading path with 81 k-values randomly assigned in predefined spatial areas produced an 11% increase in overall peak tensile stress over uniform support with the average peak tensile stress increasing for this support case by 8%. This 11% is in comparison to a 31% increase in tensile stress for the MI I-94 field section with significantly lower k-values. The overall peak tensile stress for the MI I-96 section occurred at the bottom of the slab at the midslab edge region with the peak tensile stresses during daytime curling significantly higher than nighttime and no curling conditions.

In summary, non-uniformity in the subgrade stiffness did not produce significant increases in peak tensile stresses compared to uniform support when deterministically assigned but when the field data distribution was randomly assigned to predefined areas, the peak tensile stresses did increase significantly. For the softer soil section, MI I-94, the stress increases with subgrade non-uniformity was higher than the stiffer section, MI I-96. Furthermore, for the slab geometry, axle configurations, and temperature conditions, the size of the predefined area of uniform support which produced the largest tensile stress increases was approximately 1.3 m^2. Extremely soft areas with less than 20 psi/in affected the local slab stresses especially when they were located near areas of expected maximum tensile stress. In all cases analyzed, the free edge loading paths produced the most critical fatigue damage locations, which should be areas where the foundation stiffness and variability be monitored closely.

The comparison of the two roadway sections in terms of subgrade stiffness variability confirms that non-uniform subgrade support is a complex interaction between the k-value range, the magnitude of k-values, the distribution of the support stiffness relative to the critical loading location, and the size of the predefined area. The field data suggested the presence of changing soil stiffness changes even over a small area, e.g., 1.16x1.16 m^2, can produce significant tensile stresses. The findings from this research can be used to detect very low stiffness zones with IC near the edge loading path. The next step in this research must be to spatially map a concrete pavement foundation layer with the variability level presented in this study and then utilize accelerated load testing until failure in order to link slab failures with changes in the spatial foundation stiffness.

References

(1) Rufino, D., and J. R. Roesler. *Stress and Deflection Analysis of Concrete Pavement for Different Load Conditions and Subgrade Support Models*. Pavement Design II Class Notes, University of Illinois at Urbana-Champaign, Urbana, 2011.

(2) Westergaard, H. M. Stresses in Concrete Pavements Computed by Theoretical Analysis. *Proceedings of Highway Research Board*, Part I, 1926, pp. 90-112.

(3) Darter, M. I., K. T. Hall, and C-M. Kuo. *Support Under Concrete Pavements*. NCHRP Report No. 1-30, University of Illinois at Urbana-Champaign, Urbana, 1994.

(4) Levey, J. R. A Method for Determining the Effects of Random Variation in Material Properties on the Behavior of Layered Systems. *Doctorate Dissertation*. 1968

(5) Phoon, K-K., and F. H. Kulhawy. Characterization of Geotechnical Variability. *Canadian Geotechnical Journal*, Vol. 36, 1999, pp. 612-624.

(6) Hammitt, G. M. *Statistical Analysis of data from comparative Laboratory Test Program Sponsored by ACIL*. U.S. Army Engineer Waterways Experiment Station, Vicksburg, 1966.

(7) Johnston, M. M. Laboratory Comparison Tests Using Compacted Fine-Grained Soils. *Proceedings of the 7th International Conference on Soil Mechanics and Foundation Engineering*, Vol. 1, 1974, pp. 199-204.

(8) Singh, A., and K. L. Lee. Variability in Soil Parameters. *Proceedings of the 8th Annual Engineering Geology and Soils Engineering Symposium*, Idaho, pp. 159-185.

(9) White, D. J., T. Rupnow., and H. Ceylan. Influence of subgrade/subbase Non-uniformity on Pavement Performance. *Proceeding of Geo-Trans 2004-Geotechnical Engineering for Transportation Projects*, ASCE, 2004, pp. 1058-1065.

(10) Chu, T. Y., S. N. Chen, S. S. Guram, R. L. Stewart, and K. W. Humphries. Soil Moisture as a Factor in Subgrade Evaluation. *ASCE Transportation Engineering Journal*, Vol. 103, No. 1, 1977, pp. 87-102.

(11) Qian, J., Qiu, X, and Ling J. In-situ Testing and Evaluation of Moisture Content in Existing Subgrade. *Geotechnical Special Publication*, ASCE, No. 203, 2010, pp.- 379-384.

(12) Hudson, W. R., and H. Matlock. Analysis of Discontinuous Orthotropic Pavement Slabs Subjected to Combined Loading. *Highway Research Record*, No. 131, 1966, pp. 1-48.

(13) Leonards, G. A., and M .E. Harr. Analysis of Concrete Slab on Ground. *ASCE Journal of Soil Mechanics and Foundations Division*, Vol. 85, No. SM3, 1959, pp. 35-58.

(14) Richart, F.E., Jr., and P. Zia. Effect of Local Loss of Support on Foundation Design. . *ASCE Journal of Soil Mechanics and Foundations Division*, Vol. 88, No. SM1, 1962, pp. 1-27.

(15) Westergaard, H. M. Analysis of Stresses in Concrete Roads Caused by Variations of Temperature. *Public Roads*, Vol. 8, No. 3, 1927, pp. 54-60.

(16) Hveem, F. N., and B. Temper. Some Factors Influencing Shrinkage of Concrete Pavements. *Proceedings of American Concrete Institute*, Vol. 53, 1957, pp. 781-789.

(17) Huang, Y. H. Finite Element Analysis of Slabs on Elastic Solids. *ASCE Transportation Engineering Journal*, Vol. 100, No. 2, 1974, pp. 403-416.

(18) Tabatabai, A. M., and E. J. Barenberg. Finite-Element Analysis of Jointed or Cracked Concrete Pavements. *Transportation Research Record*, No. 671, 1978, pp. 11-19.

(19) Tayabji, S. P., and B. E. Colley. *Analysis of Jointed Concrete Pavements*. Federal Highway Administration, National Information Service, New York, 1981.

(20) Roesler, J. R., and L. Khazanovich. Finite-Element Analysis of Portland Cement Concrete Pavement with Cracks. *Transportation Research Record*, No. 1568, 1997, pp. 1-9.

(21) Shoukry, S. N., M. Fahmy, J. Prucz, and G. William. Validation of 3DFE Analysis of Rigid Pavement Dynamic Response to Moving Traffic and Nonlinear Temperature Gradient Effects. *ASCE International Journal of Geomechanics*, Vol. 7, No. 1, 2007, pp. 16-24.

(22) ISLAB 2000 (Version 1.1) [Software]. Applied Research Associates, Champaign, 1999.

(23) Wang, B., R. Popescu, and J. H. Prevost. Effect of Boundary Conditions and Partial Drainage on Cyclic Simple Shear Test Results- A Numerical Study. *International Journal for Numerical and Analytical Methods in Geomechanics*. Vol. 28, 2004, pp. 1057-1082.

(24) Kelley, E. J. The Effects of Soil Moisture on Pavement Systems. *Masters Dissertation*, Ohio University, 1999.

(25) Barenberg, E. J., P. F. Wilbur, and S. D. Tayabji. Mathematical Analysis of Pavements with Non-uniform Paving Materials. *Transportation Research Record*, No. 574, 1976, pp. 27-55.

(26) Gallivan, V. L., K. G. Chang, and R. D. Horan. Intelligent Compaction for Improving Roadway Construction. *Geotechnical Special Publication*, ASCE, No. 218, 2011, pp. 117-124.

(27) Vennapusa, P. K. R., D. J. White, and M. D. Morris. Geostatistical Analysis for Spatially Reference Roller-Compacted Compaction Measurements. *ASCE Journal of Geotechnical and Geoenvironmental Engineering*, Vol. 136, No. 6, 2010, pp. 813-822.

(28) Vennapusa, P. K. R. Determination of Optimum Base Characteristics for Pavements. *Masters Dissertation*, Iowa State University, 2004.

(29) Mooney, M. A., R. V. Rinehart, N. W. Facas, O. M. Musimbi, D. J. White, and P. K. R. Vennapusa. *Intelligent Soil Compaction Systems*. NCHRP Report-676, Transportation Research Board, Washington D.C., 2010.

(30) White, D. J., D. S. Harrington, H. Ceylan, and T. Rupnow. *Fly Ash Soil Stabilization for Non-Uniform Subgrade Soils Volume II: Influence of Subgrade Non-Uniformity on PCC Pavement Performance*. Iowa Highway Research Board Project TR-461, Iowa State University, Ames, 2005.

(31) Bowles, J. *Foundation Analysis and Design*. McGraw-Hill, New York, 1996.

(32) Brand, A. S. and J. R. Roesler. *Effect of Non-uniform Foundation Support on Concrete Slab Responses*. Proceedings of 10th International Conference on Concrete Pavements, Quebec City, 2012.

(33) ASTM D6951-03. *Standard Test Method for use of the Dynamic Cone Penetrometer in Shallow Pavement Applications*. American Standard for Testing Methods (ASTM), West Conshohocken, 2010.

(34) White, D. J., P. K. R. Vennapusa, H. H. Gieselman, A . J. Wolfe, S. Douglas, and J. Li. *Pavement Foundation Layer Reconstruction Project- Michigan I-94 Field Study*. Center for Earthworks Engineering Research Report: ER 11-03, 2011.

(35) Terzaghi, K., and R. B. Peck. *Soil Mechanics in Engineering Practice*, 2nd Ed., John Wiley & Sons, Inc., New York, 1967.

(36) Airport Pavement Design and Evaluation. *Advisory Circular No. 150/5320-6E*, FAA, US DOT, Washington D.C., 2009.

(37) AASHTO. *AASHTO Guide for Design of Pavement Structures*. Washington D.C., 1993.

(38) Lysmer, J., and J. M. Duncan. *Stresses and Deflections in Foundations and Pavements*. 4th Ed., University of California at Berkeley, Berkeley, 1969.

(39) Departments of the Army and the Air Force. *Rigid Airfield Pavements*. TM 5-888-9/AFM 88-6, Washington D.C., 1966.

(40) EasyFit(Version 5.5) [Software]. Mathwave Technologies, 2012.

(41) Evans, M., N. Hastings, and I. A. Stegun. *Statistical Distributions*, Wiley, New York, 2000, pp. 34-42.

Appendix A

Table A1: Field CBR to k-value for MI I-94 roadway (121 data points)

Field CBR	k-value eq. 2.8	Field CBR	k-value eq. 2.8	Field CBR	k-value eq. 2.8	Field CBR	k-value eq. 2.8
3.0	55	2.2	43	3.3	60	1.7	36
2.5	48	1.8	37	5.7	91	4.8	80
7.6	114	6.0	95	3.3	60	2.4	47
2.9	54	6.0	95	2.8	52	2.7	51
3.2	58	2.1	42	2.4	47	3.9	68
3.7	65	7.5	113	7.2	109	3.9	68
1.7	36	3.3	60	5.8	92	3.5	62
5.4	87	1.8	37	3.0	55	6.0	95
6.2	97	5.7	91	3.3	60	6.9	106
2.4	47	5.1	84	2.2	43	1.4	31
3.0	55	1.9	39	3.0	55	2.8	52
3.1	57	4.9	81	2.6	50	3.1	57
4.5	76	2.9	54	6.3	99	4.0	69
3.8	67	5.5	89	3.3	60	2.0	40
4.8	80	5.2	85	3.7	65	1.5	32
1.4	31	3.2	58	1.7	36	3.8	67
2.5	48	2.2	43	6.3	99	4.1	71
2.8	52	6.2	97	4.1	71	6.1	96
2.4	47	2.1	42	3.7	65	3.3	60
1.6	34	5.1	84	5.8	92		
2.2	43	4.8	80	2.7	51		
2.7	51	7.6	114	3.4	61		
10.6	148	1.7	36	3.1	57		
4.1	71	3.0	55	7.4	112		
3.7	65	4.2	72	4.6	77		
1.9	39	4.1	71	4.2	72		
2.9	54	2.5	48	1.4	31		
2.0	40	2.2	43	3.1	57		
3.3	60	3.0	55	3.3	60		
3.1	57	2.5	48	3.5	62		
2.3	45	4.8	80	4.4	75		
4.0	69	2.0	40	2.2	43		
2.4	47	5.4	87	1.7	36		
15.8	202	2.5	48	2.6	55		

Table A2: Field CBR to k-value for MI I-96 roadway

Field CBR	k-value eq. 2.8	Field CBR	k-value eq. 2.8	Field CBR	k-value eq. 2.8
33	356	35	371	42	433
20	243	30	336	44	452
31	342	21	253	42	433
36	382	40	419	40	414
46	464	47	472	42	432
52	507	30	337	40	415
20	240	39	407	51	502
19	235	36	383	30	333
25	284	37	393	65	609
30	334	46	465	37	395
41	421	25	293	80	713
24	279	26	299		
38	403	42	433		
38	397	58	556		
31	341	55	530		
44	449	51	504		
38	403	45	453		
22	262	38	400		
22	257	32	351		
33	357	26	301		
36	387	38	397		
31	345	21	256		
40	414	44	445		
43	440	48	481		
30	335	59	564		
37	391	36	380		
19	235	46	463		
22	261	31	338		
45	457	23	268		
49	487	31	343		
42	430	42	433		
47	468	72	655		
35	373	42	433		
35	372	57	550		

Appendix B

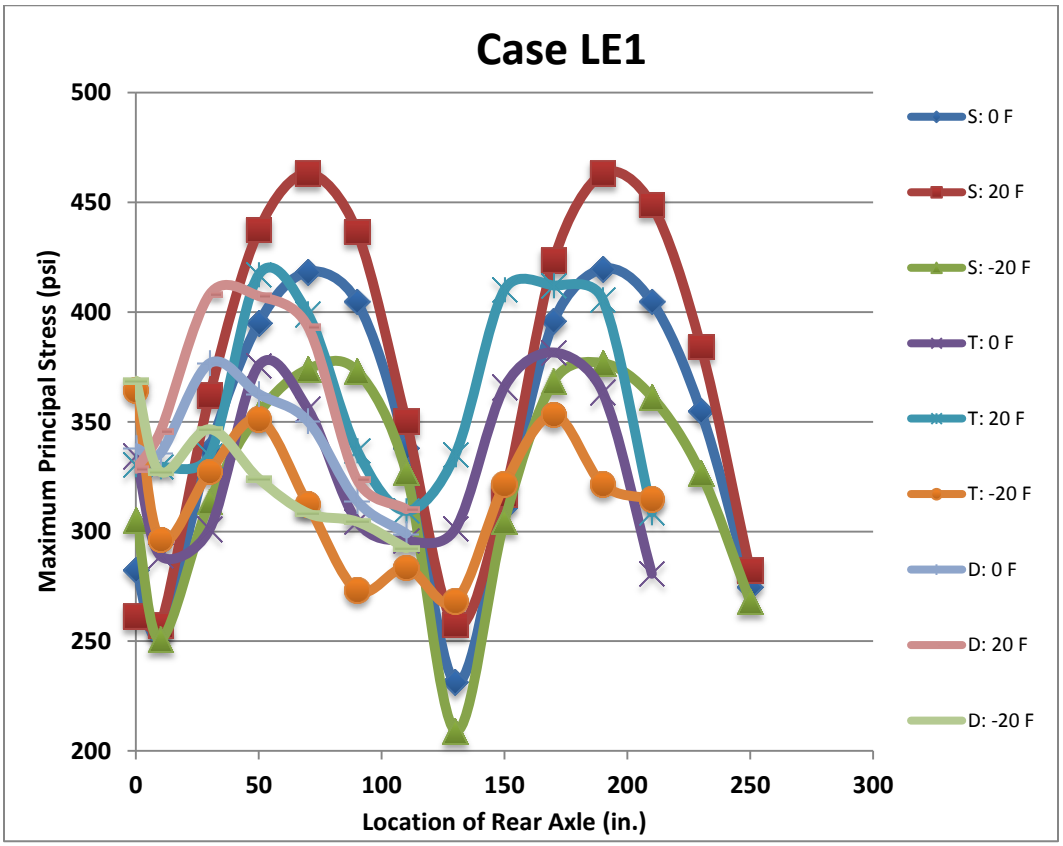

Figure B1: Maximum principal (tensile) stress for Case LE1 versus axle position

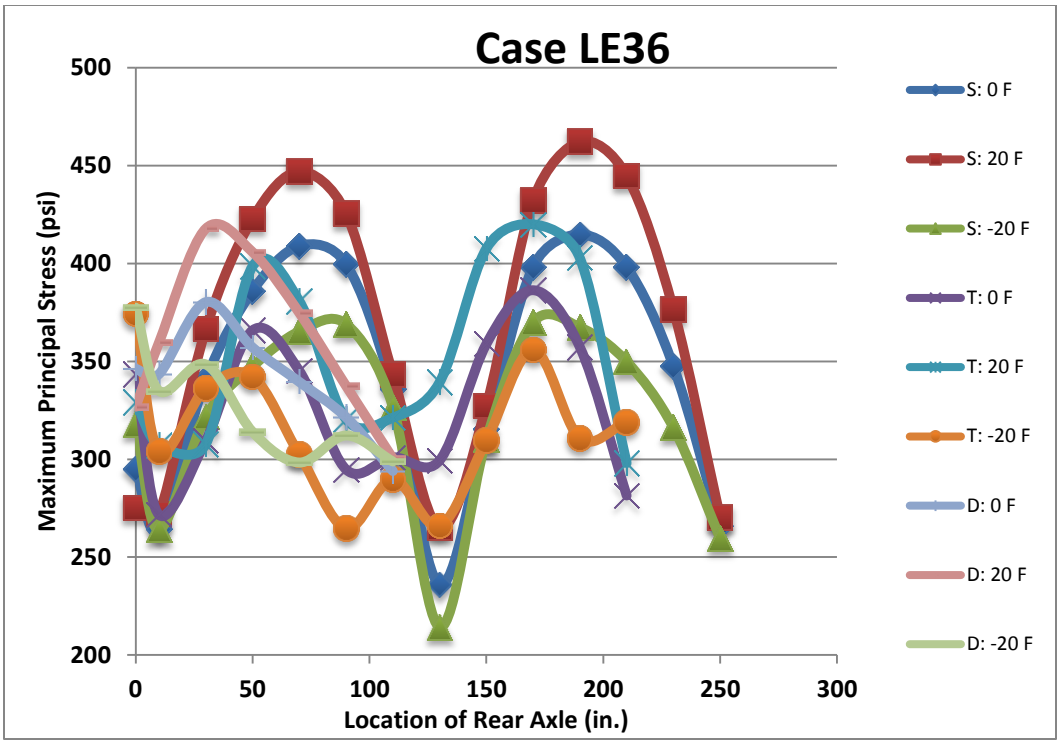

Figure B2: Maximum principal (tensile) stress for Case LE1 versus axle position

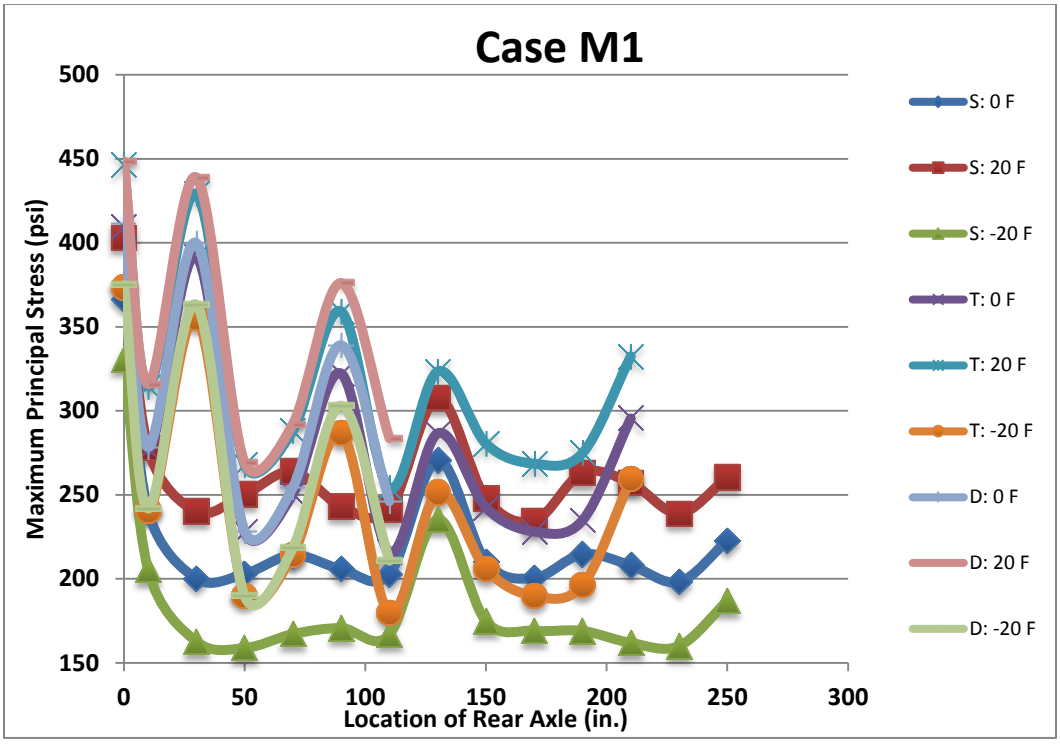

Figure B3: Maximum principal (tensile) stress for Case M1 versus axle position

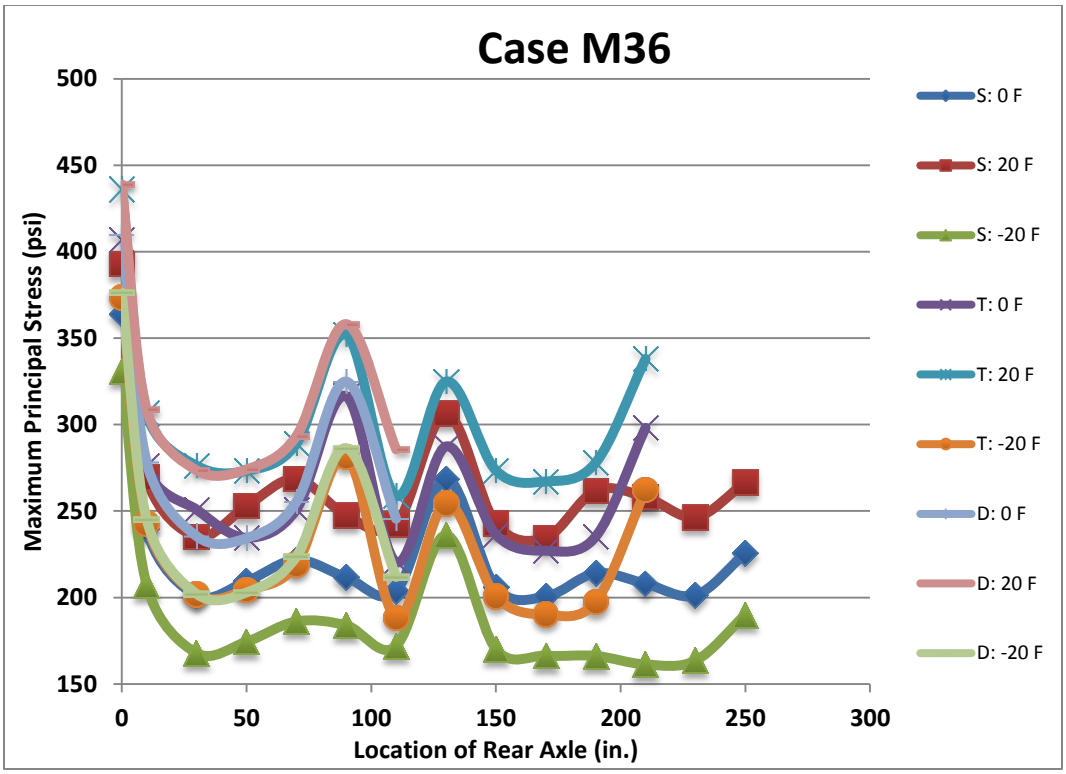

Figure B4: Maximum principal (tensile) stress for Case M36 versus axle position

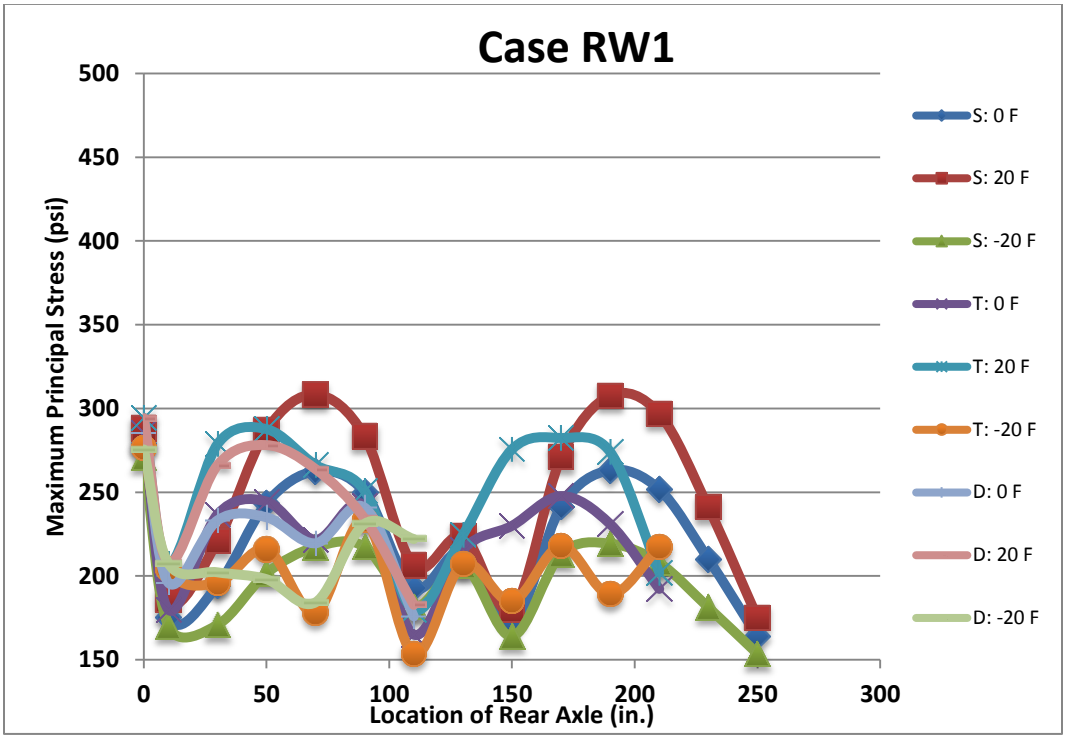

Figure B5: Maximum principal (tensile) stress for Case RW1 versus axle position

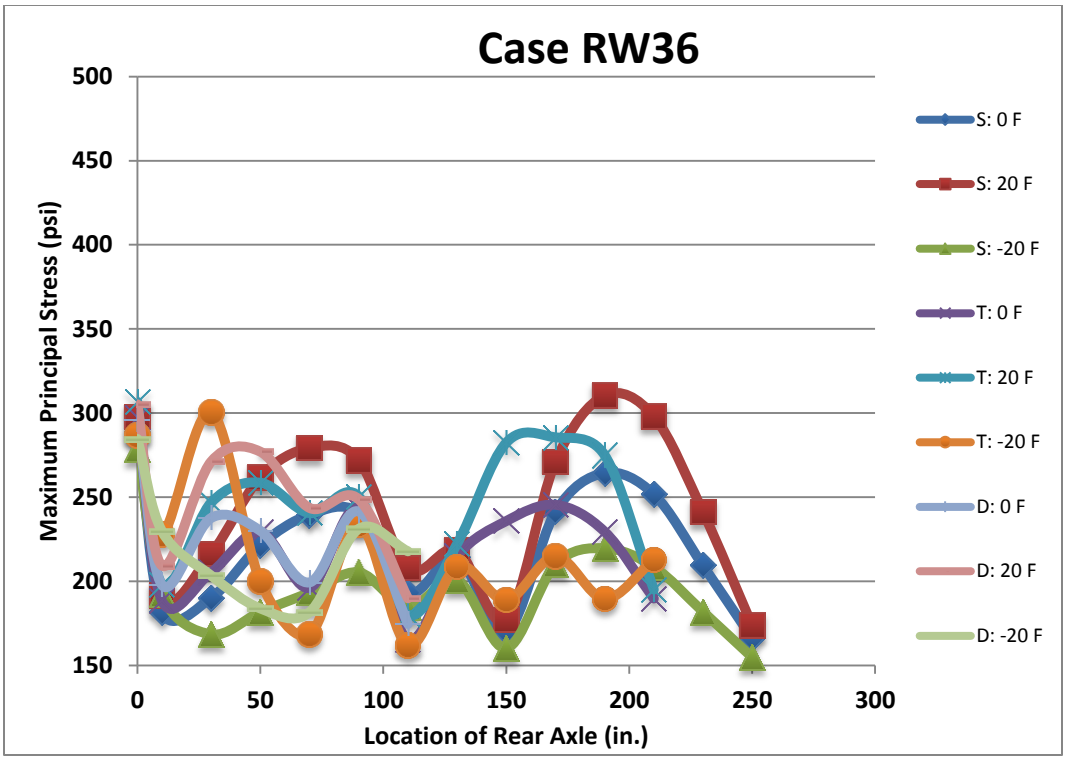

Figure B6: Maximum principal (tensile) stress for Case RW36 versus axle position

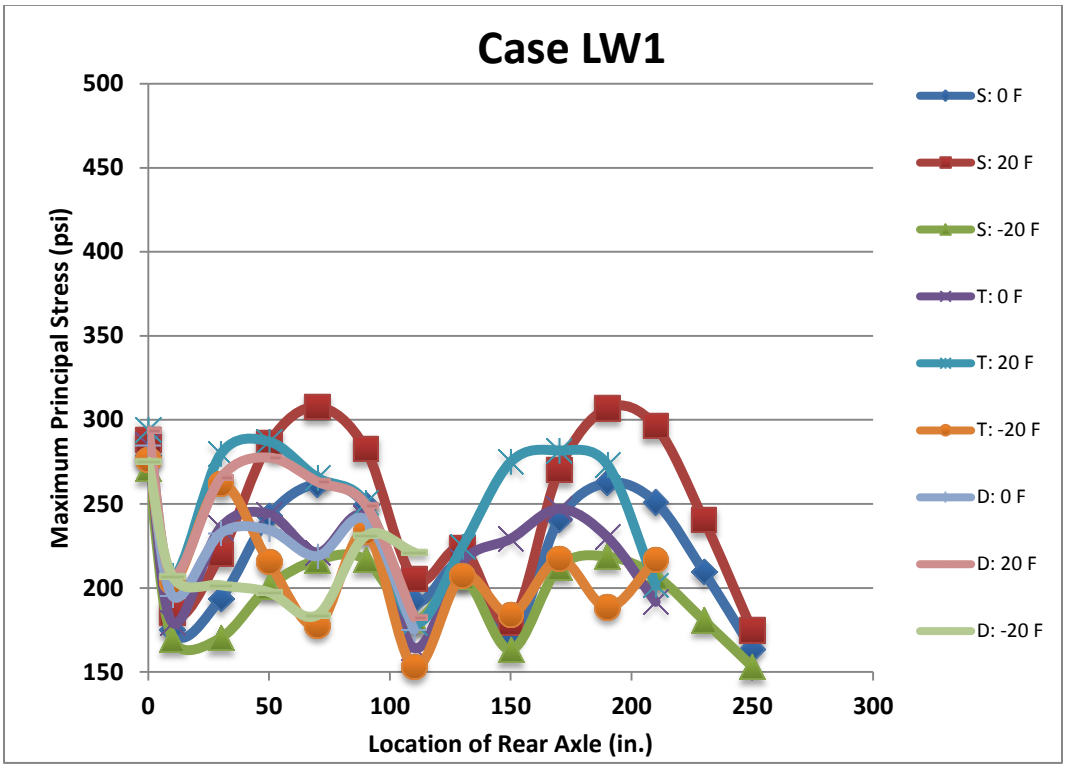

Figure B7: Maximum principal (tensile) stress for Case LW1 versus axle position

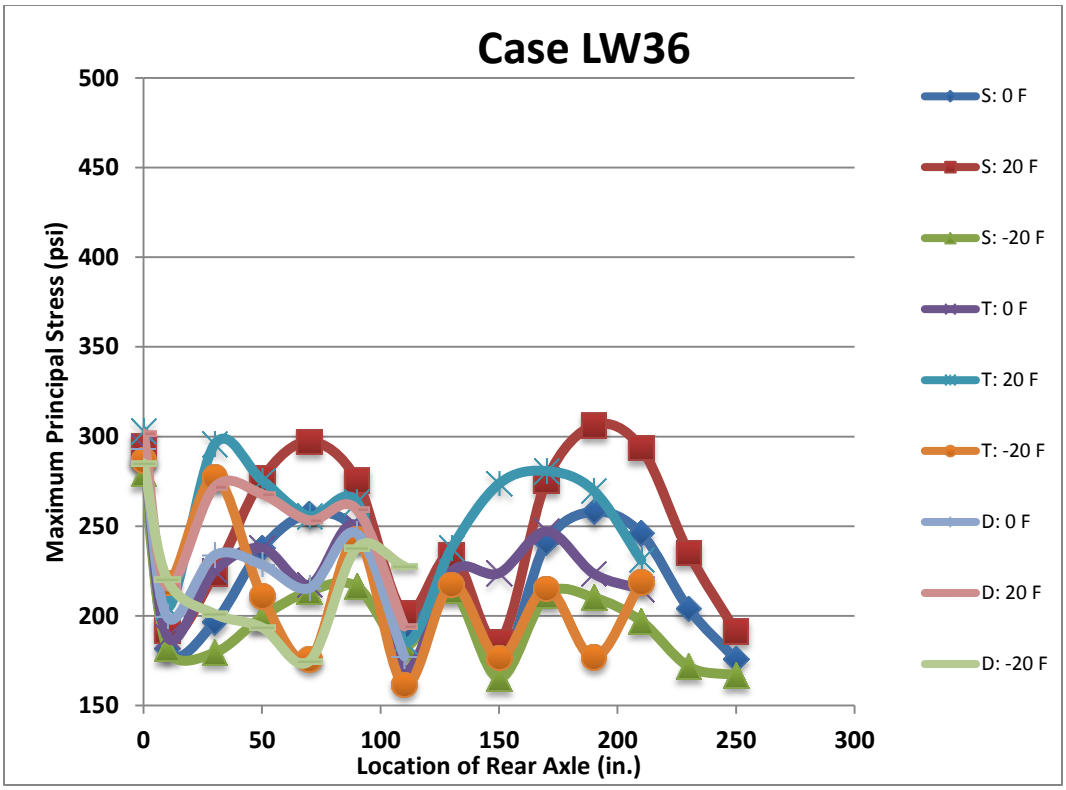

Figure B8: Maximum principal (tensile) stress for Case LW36 versus axle position

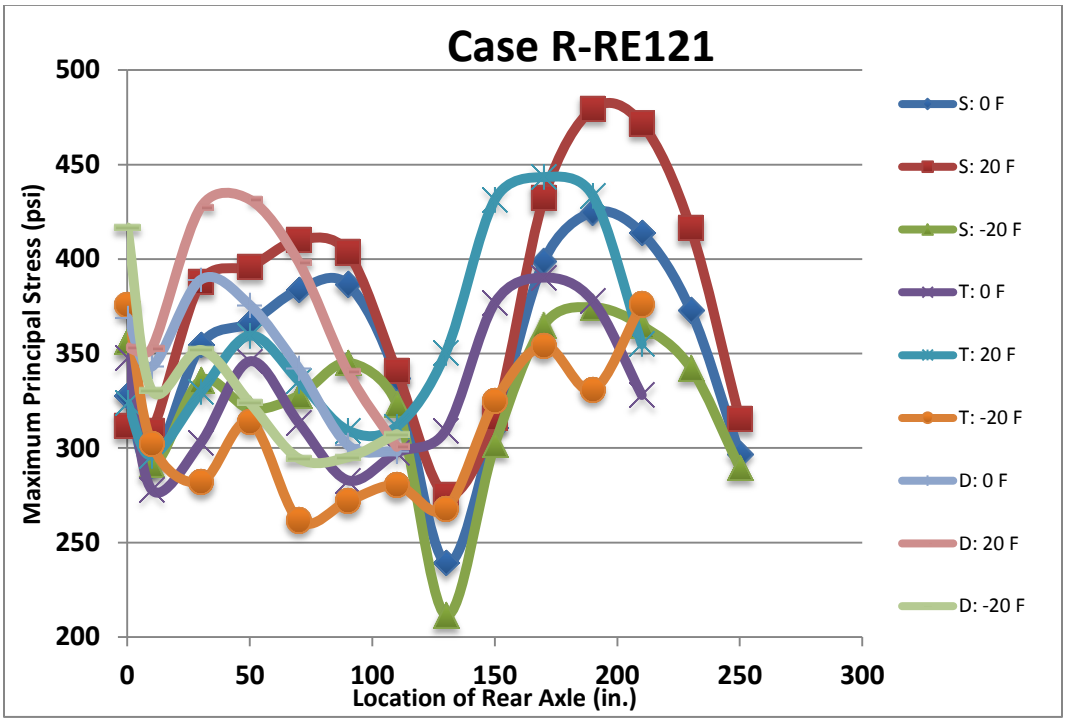

Figure B9: Maximum principal (tensile) stress for Case R-RE121 versus axle position

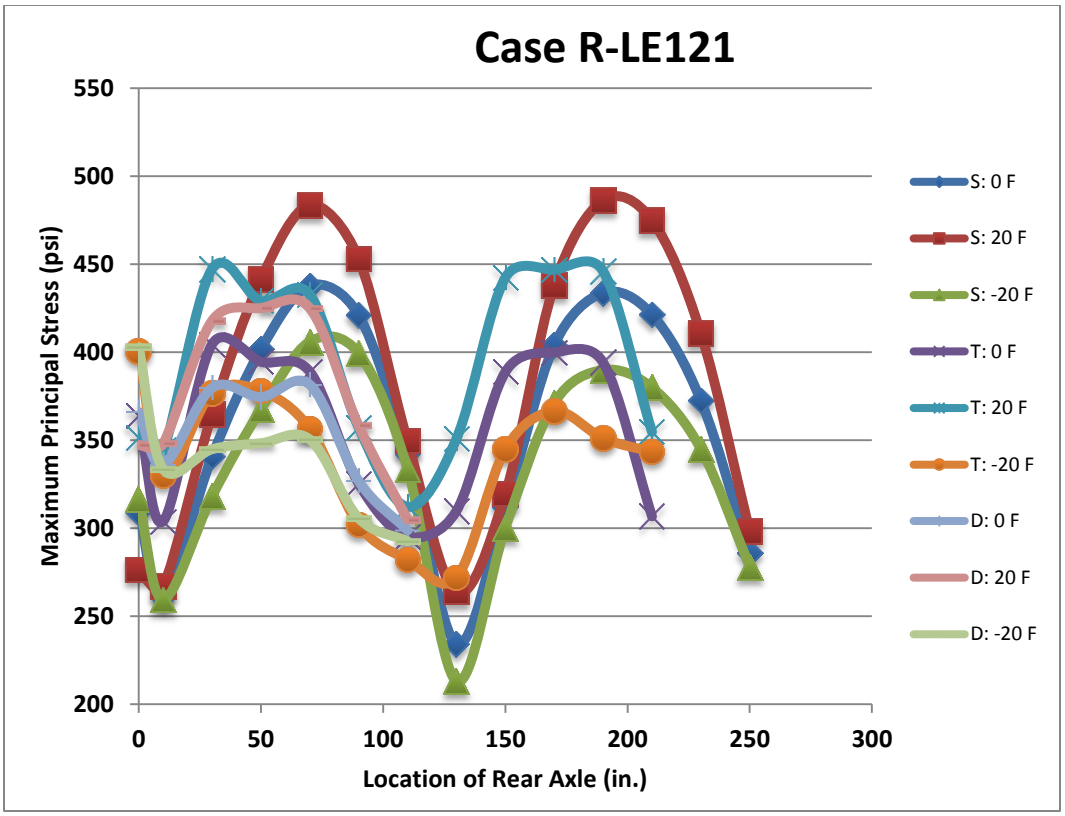

Figure B10: Maximum principal (tensile) stress for Case R-LE121 versus axle position

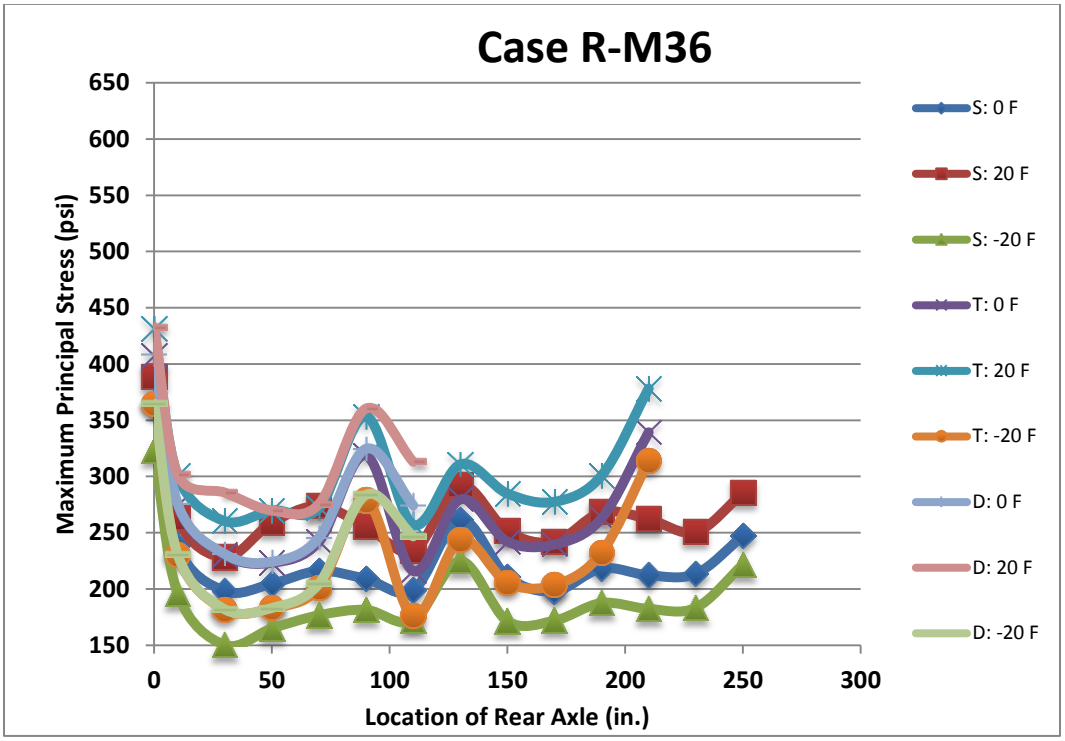

Figure B11: Maximum principal (tensile) stress for Case R-M36 versus axle position

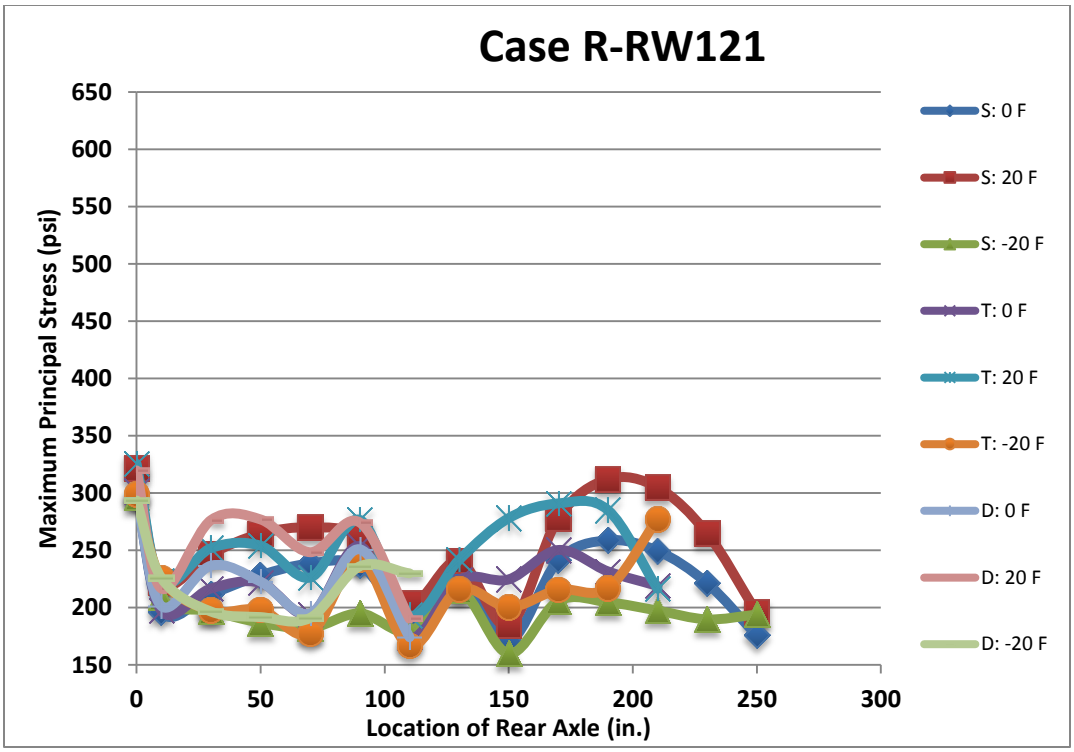

Figure B12: Maximum principal (tensile) stress for Case R-RW121 versus axle position

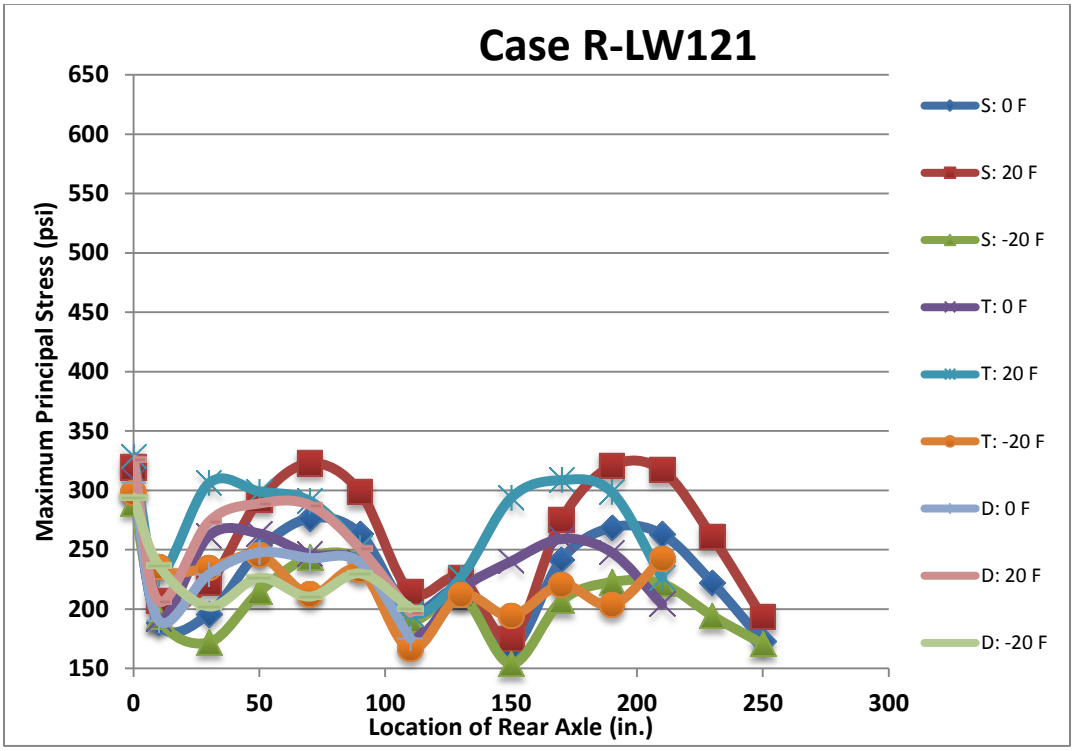

Figure B13: Maximum principal (tensile) stress for Case R-LW121 versus axle position

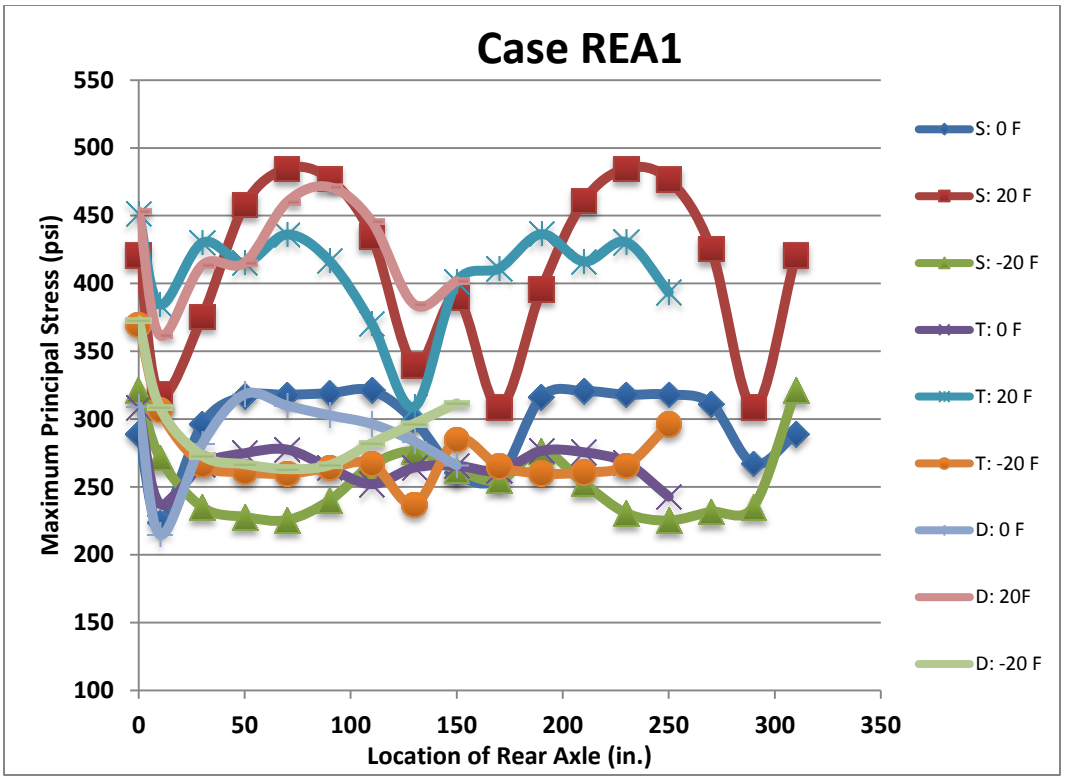

Figure B14: Maximum principal (tensile) stress for Case REA1 versus axle Position

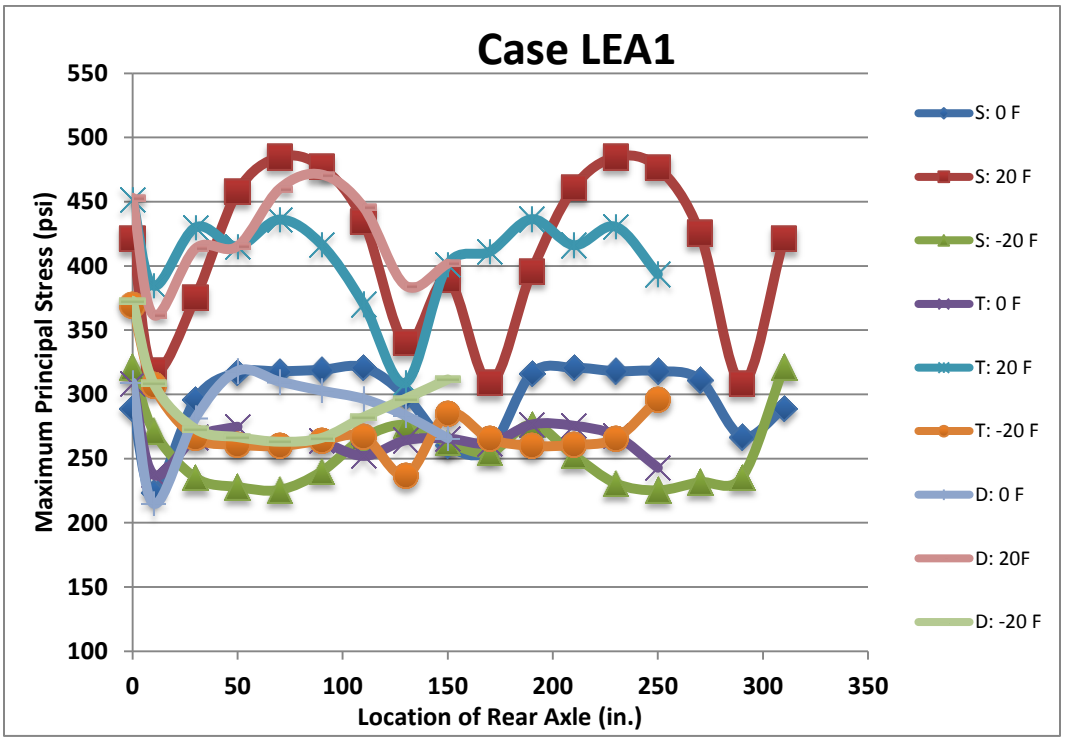

Figure B15: Maximum principal (tensile) stress for Case LEA1 versus axle Position

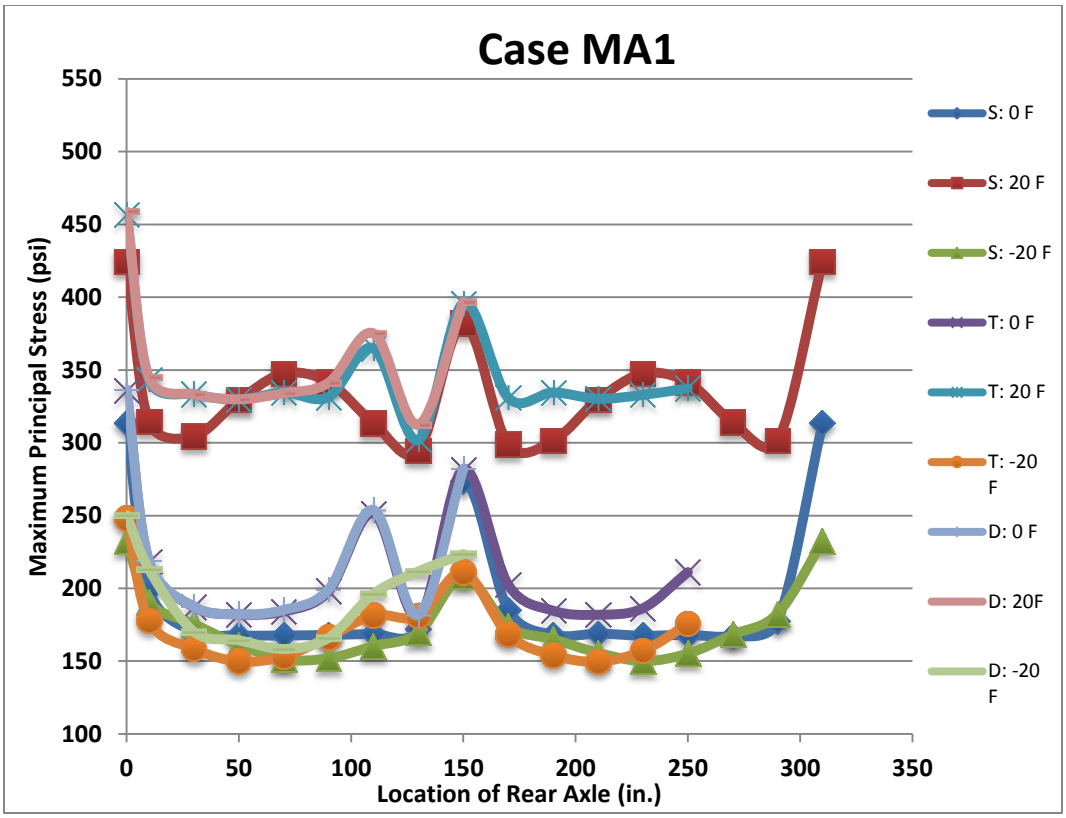

Figure B16: Maximum principal (tensile) stress for Case MA1 versus axle Position